Development of Electrophoretic Methods for Monitoring Small Molecule Neuroactive Compounds in Brain Microdialysis Samples

By

© 2022

Galina Bulgakova
Specialist, Lomonosov Moscow State University, 2015

Submitted to the graduate degree program in Chemistry and the Graduate Faculty of the University of Kansas in partial fulfillment of the requirements for the degree of Doctor of Philosophy.

_____

Chair: Dr. Susan M. Lunte

_____

Dr. Robert C. Dunn

_____

Dr. Meredith D. Hartley

_____

Dr. Cindy L. Berrie

_____

Dr. Karen J. Nordheden

Date Defended: 5 May, 2022

The dissertation committee for Galina Bulgakova certifies that this is the approved version of the following dissertation:

Development of Electrophoretic Methods for Monitoring Small Molecule Neuroactive Compounds in Brain Microdialysis Samples

Chair: Dr. Susan M. Lunte

Date Approved: 9 May, 2022

Abstract

The burden of neurological disorders has been increasing across the United States over the last thirty years with stroke, neurodegenerative diseases such as Alzheimer's and migraine contributing the most to the number of disability adjusted life years. As the population continues to age, the need for targeted therapies for these conditions grows. However, even today, the available treatments are aimed at symptom management and not the root cause of the disease. Development of new pharmacological interventions requires a detailed understanding of the underlying biological processes, and in the case of the disorders affecting the nervous system, these are notoriously complex. Therefore, there is a high demand for analytical tools capable of providing insight into *in vivo* neurochemical dynamics.

Microdialysis (**MD**) is a powerful technique that makes it possible to perform continuous sampling from living tissues for long periods of time. The composition of the obtained sample is reflective of all small molecules present in the MD probe surroundings (*e.g.* tissues), which means that with an appropriate analytical method it is possible to quantify multiple compounds simultaneously. To this end, separation-based techniques such as capillary and microchip electrophoresis (known as CE and ME respectively) can be used in tandem with MD to monitor neurochemical concentration changes in biological systems. By direct coupling of MD with ME (**MD-ME**) we are able to produce a separation-based biosensor for near real-time on-line *in vivo* and *in vitro* monitoring of the species of interest in continuous sample flow.

This thesis focuses on the development of ME and CE methods for the monitoring of neurotransmitters, ascorbic acid (**AA**), and adenosine energy metabolites. First, the development of a ME separation and electrochemical detection (**EC**) of four monoamine neurotransmitters, two

dopamine metabolites DOPAC and HVA, and AA is described and evaluated by the analysis of a rat brain homogenate sample. Next, the composition of the background electrolyte (**BGE**) used for the ME separation was further reoptimized to ensure compatibility with MD perfusates containing physiological concentrations of Ca^{2+} and Mg^{2+}. This required a switch of the buffering system from phosphate to an organic buffer, MES, and the addition of EDTA to prevent precipitation of the metal cations with the surfactant present in the BGE.

The effect of MD perfusate NaCl content on the dialysate ionic composition and *in vivo* recovery of monoamine neurotransmitter metabolites was also studied using CE with capacitively coupled contactless conductivity detection and liquid chromatography with EC detection. It was shown that to reliably evaluate the effect of sodium content on the recovery of analytes, the post-surgery rest time must be longer than 1 hour. Evaluation of Na^{+} recovery from tissues showed that at 40% of physiological concentration of NaCl there was no significant flux of sodium into the perfusate. It was also determined that, given sufficient post-surgery rest time, the recoveries of both the metabolites (DOPAC, HVA, and 5-HIAA) and sodium did not vary following initial equilibration of the probe during 90–100 min of sampling.

A small-scale animal study was carried out to investigate the effect of glutamate content in perfusate on the signal of AA in dialysates obtained from rat brain using *in vivo* on-line MD-ME-EC analysis. A non-physiological effect of decreased ascorbate recovery during MD sampling with glutamate-containing solutions was observed, although ultimately it appeared to be an artifact of the MD probe batch used in the experiments.

Finally, a robust reproducible CE-UV separation was developed for adenosine triphosphate, diphosphate, and monophosphate. It was shown to be compatible with a previously developed transient isotachoforesis method for on-line preconcentration of these analytes from MD samples.

Acknowledgements

My 6 years of graduate school at the University of Kansas have been shaped into the wonderful experience by the incredible people who have been around me throughout these 6 years full of both the routine and the unexpected (so much of the unexpected!).

First and foremost, I would like to express my gratitude to my mentor and advisor Dr. Susan Lunte. In the Summer of 2014, I tagged along with my then-boyfriend-now-husband Sasha on a visit to KU Physics & Astronomy Department where he was planning to do research in Dr. Dave Besson's lab. Trying to make the most of the trip, I found Sue's group on the Chemistry Department website, and Dave reached out to her asking if she'd let me into her lab for a few weeks to learn about the group's research. Anyone who knows Sue will not be surprised to learn that she said yes to this out of the blue proposition. The several weeks I spent shadowing the future Dr. Nate Oborny, trying to run some experiments on microchips (which I had not even seen before coming to KU!), and just being part of the Lunte group led to an application to KU's graduate program. This experience changed the course of my life, and I have not regretted the decision for one second. Sue is the kind of mentor who lifts you up, guides you, and lets you explore. If things are not working or making sense – a meeting with Sue always clears the fog, shows the path forward, and lifts the spirits. I know my experience with this is very much universal for all of us Lunte group members. Sue's also given me so many opportunities to share my research with the larger scientific community and become part of it by participating in conferences, workshops, and social gatherings. During my time in the group I also got ample chances to mentor undergraduate students and grow in the process. Through all of the challenges life threw her way during the last few years, Sue always made sure that we knew our well-being and success were important to her. I cannot imagine a better mentor, and I will forever be grateful!

The second year of my graduate school experience was “a bit” unusual – a trip home to Russia over the holidays turned into a 7-month long waiting game with the visa office. I would like to sincerely thank the Department of Chemistry for their unyielding support during this time. I was still able to take my class with Prof. Soper, pay rent, and be part of the KU Chemistry community even from an ocean away. I am grateful for every word of support, every letter written to government officials, and every accommodation. The amount of care I received from the department is unbelievable and sets a high bar for how the community should treat its members.

A special thanks goes to my Lunte lab family. Dr. Nate Oborny and Dr. Shamal Ungawel Durayalage spent hours in lab and in the clean room teaching me microchip electrophoresis 101. With such brilliant scientists as my mentors it was a joy to try new things, fail, and try again and again until the goal was reached. I will always be inspired by how full of new exciting ideas Nate can be, and Shamal’s endless positivity and dedication to everything he does. I am lucky to call you my friends.

I would also like to thank Dr. Kelci Schilly for the comradery during the hours spent working on mass-spectrometry class projects, lab organizing, chip troubleshooting, all the frustrations and joys that came from being a graduate student. Every coffee break and post-lab dinner made it possible to keep on going forward when things got tough. I cannot wait to be colleagues again!

To Dr. Sara Thomas – thank you for teaching me everything I know about animal work, the long *in vivo* experiment days, and spending weeks and weeks on wrangling the LC equipment into submission. I would be lost without you!

I thank Emily Kurfman for teaching me new things about CE and sharing your C^4D expertise, our baking and movie nights, and chats about books. To Dhanushka Weerasekara and Indika

Warnakula– thank you for the company during those long late nights in the lab, always being willing to help with everything microfabrication-related, and cheering me up when I needed it.

I am very grateful to have had the opportunity to mentor Anton Barybin and Riley Stegmaier. I owe Shamal and Kelci a lot for training them when they first joined the group, and thank both Anton and Riley for the dedication and enthusiasm with which you approached your projects. Good luck with your studies and research! I am excited to see your bright futures unfold.

Of course, I cannot forget to thank Cady Bush for all the help with scheduling conundrums, travel planning, purchasing advice, and endless kind words. Cady, you are the greatest of all time.

Outside of the Lune group, I have many-many people to thank. Dr. Zeke Piskulich – a wonderful friend and one of my most vocal advocates for me during the time when I was stuck outside of the U.S. Those senators/congressmen/mayors did not know what hit them! To my fellow KU Chemistry graduate students – thank you for the time spent sharing our science, successes and frustrations, and all of the fun times in between.

I want to thank my family – for being there for me and pushing me to be better from another continent for the last few years. Knowing that my mom and brother are always in my corner to both support me and encourage me means the world. They know me better than anyone, and help me be my best self at always. Without you I would not be where I am today.

Finally, I thank my husband Sasha for bringing me to Kansas in the first place, encouraging me and helping me grow. Thank you for making the career choices that kept you close during my time in graduate school and working with me towards our future. The best is yet to come!

Table of contents

1. Dissertation overview

1.1. Research objectives

The growing incidence of noncommunicable neurological disorders ranging from stroke to various dementias to epilepsy increases the demand for effective therapeutic options for these disorders. Due to the lack of sufficient understanding of the biochemical processes involved in their development and progression, treatments have so far focused on symptom management. To fill in gaps in the knowledge, analytical tools that allow to track changes in concentrations of neurochemicals in disease states are needed. Availability of techniques for on-line monitoring of neuroactive compounds can also provide valuable information for correlating their dynamics with behavior and observable symptoms while enabling better timing of pharmacological interventions. Microdialysis (**MD**) is a technique commonly used to sample from living tissues (including the brain) for extended periods of time. When MD is coupled to a separation-based analytical method, multiple analytes of interest can be monitored simultaneously, expanding the amount of information gained from each experiment.

The main goal of the studies described in this thesis is the development of microchip electrophoresis with electrochemical detection (**ME-EC**) and microdialysis methods for the monitoring of neurochemicals that play important roles in neurological disorders. Coupling MD with ME-EC produces a separation-based sensor for on-line analysis with near real-time temporal resolution that can be miniaturized for on-site applications. A chapter is also dedicated to the development of a capillary electrophoresis (**CE-UV**) method that is compatible with on-line sample preconcentration for the quantification of adenosine energy metabolites in microdialysis samples. Thus, the overall objective of this dissertation is to progress the development of analytical approaches to investigating the molecular mechanisms contributing to the development of neurological disorders.

1.2. Chapter summaries

1.2.1. *Chapter 2: Role of monoamine and amino acid neurotransmitters in neurodegeneration and introduction to microdialysis sampling coupled to microchip electrophoresis*

A review of the involvement of two classes of neurotransmitters – monoamines and amino acids – in neurodegeneration is provided, highlighting their roles in such conditions as stroke, Parkinson's and Alzheimer's diseases. Pharmacological strategies targeting these neurotransmitter pathways are noted. Additionally, an overview of the basic principles behind microdialysis sampling and microchip electrophoresis is given, concluding with the available configurations for the combination of the two to create separation-based sensors for on-line monitoring of biological systems. Examples of *in vitro* and *in vivo* applications of such devices to the studies of neurochemical processes are given.

1.2.2. *Chapter 3: Microchip electrophoresis separation method for the monitoring of biogenic monoamine neurotransmitters and endogenous interferences*

To enable simultaneous monitoring of four monoamine neurotransmitters, namely dopamine, epinephrine, norepinephrine, and serotonin, a ME-EC method was developed to ensure their resolution from each other and from two dopamine metabolites DOPAC and HVA and ascorbic acid. Optimization of the separation was carried out by changing the composition of the background electrolyte (**BGE**) components including phosphate buffer at pH 7.4, sodium dodecyl sulfate (**SDS**), boric acid, and the organic solvent additive dimethyl sulfoxide (**DMSO**). The resulting ME-EC method provided sub-micromolar limits of detection for the neurotransmitters of interest and was used for off-line analysis of a rat brain homogenate sample.

1.2.3. *Chapter 4: Coupling in vivo microdialysis sampling with microchip electrophoresis: compatibility of the separation with Ca^{2+}-containing perfusates*

The composition of the perfusate used for MD sampling has a strong effect on the concentration of analytes determined in the dialysates. Previous *in vivo* studies have shown that the basal dopamine levels are negatively affected by the removal of calcium ions from perfusate, therefore any analytical method coupled to MD sampling aiming to quantify this neurotransmitter must be compatible with the presence of calcium ions in the sample matrix. To prevent precipitation of BGE components in the presence of Ca^{2+}, the BGE composition was modified to substitute phosphate buffer pH 7.4 with MES, and EDTA was added to prevent an interaction between calcium and SDS. All component concentrations were reoptimized, and the organic additive was changed from DMSO to acetonitrile.

1.2.4. *Chapter 5: Coupling in vivo microdialysis sampling with microchip electrophoresis: optimization of perfusate composition*

Electrophoresis separations suffer from poor compatibility with samples containing high amounts of salts. The most common perfusate used for MD sampling from the brain is artificial cerebrospinal fluid (**aCSF**), which contains ~150 mM of NaCl and low millimolar concentrations of Ca^{2+}. Mg^{2+}, and K^{+}. The off-line MD-CE study described in this chapter investigated both the effects of NaCl content in perfusate and the duration of sampling on the recovery of Na^{+} ions from the brain. The perfusates that were evaluated mimicked the ionic composition of aCSF but contained sub-physiological concentrations of NaCl. The goal of these experiments was to determine the optimal concentration of NaCl for perfusates used in future on-line MD-ME-EC experiments. The obtained MD samples were also analyzed via liquid chromatography with EC

detection (**LC-EC**) to study the effects of perfusate composition changes and sampling duration on the *in vivo* recovery of neurotransmitter metabolites.

1.2.5. *Chapter 6: ME-EC detection of ascorbate recovered during microdialysis sampling with perfusates containing glutamate*

Ascorbic acid has many functions in the central nervous system. Its relationship with glutamate neurotransmission has been of interest for some time as there is evidence of heteroexchange between ascorbate and glutamate. However, the exact mechanism of this interaction has not been confirmed. A series of on-line MD-ME-EC experiments was carried out both *in vivo* and *in vitro* to evaluate the potential of this analytical platform to investigate the effect of Glu on ascorbate extracellular concentration dynamics. A non-physiological effect of reduced ascorbate recovery in the presence of 0.1–1 mM glutamate in the perfusate used for microdialysis was observed and ultimately found to be an artifact of the probe batch used in the experiments.

1.2.6. *Chapter 7: Separation method for on-line tITP preconcentration and quantification of ATP, ADP, and AMP with capillary electrophoresis with UV absorption detection*

The development of a robust and reproducible CE-UV separation for adenosine energy metabolites ATP, ADP, and AMP is described. The resulting method is performed using reverse polarity and utilizes a complex BGE that contains high concentrations of surfactant, a chelating metal ion, a cyclodextrin, and an organic solvent additive. The final separation was compatible with an on-line preconcentration protocol for transient isotachophoresis previously developed in our laboratory for these analytes.

1.2.7. *Chapter 8: Future directions*

Short and long-term future directions for the projects detailed in this dissertation are discussed.

2. Role of monoamine and amino acid neurotransmitters in neurodegeneration and introduction to microdialysis sampling coupled to microchip electrophoresis

2.1. Introduction

Complexity is a descriptor that applies to all diseases of the brain. The structure of the organ itself is very intricate, and the relationships between brain biochemistry and observable behavior and cognition are still under-studied. This leads to the lack of full comprehension of all the links between the fundamental cause of a disease to its pathology and symptoms for any given neurological disorder. A variety of interconnected processes can contribute to a disease state, including protein misfolding[1], inflammation[2], oxidative stress[3] and dysregulation[4] of cell-to-cell signaling to name a few. This in turn means that the development of effective treatments that exhibit minimal side effects is extremely challenging.

Neurotransmitters (NTs) are signaling molecules that allow neurons to communicate with each other or other cell types such as muscle cells[5], which means that they are involved in any process in the body that requires innervation. NTs can be classified as amino acids, monoamines, acetylcholine, peptides, soluble gases as well as other molecule types. (Figure 2.1). This chapter discusses the role of monoamine and amino acid neurotransmitters in neurodegenerative disorders. It also provides details on a promising experimental approach for studies of the mechanisms contributing to diseases of the brain – microdialysis sampling combined with microchip electrophoresis.

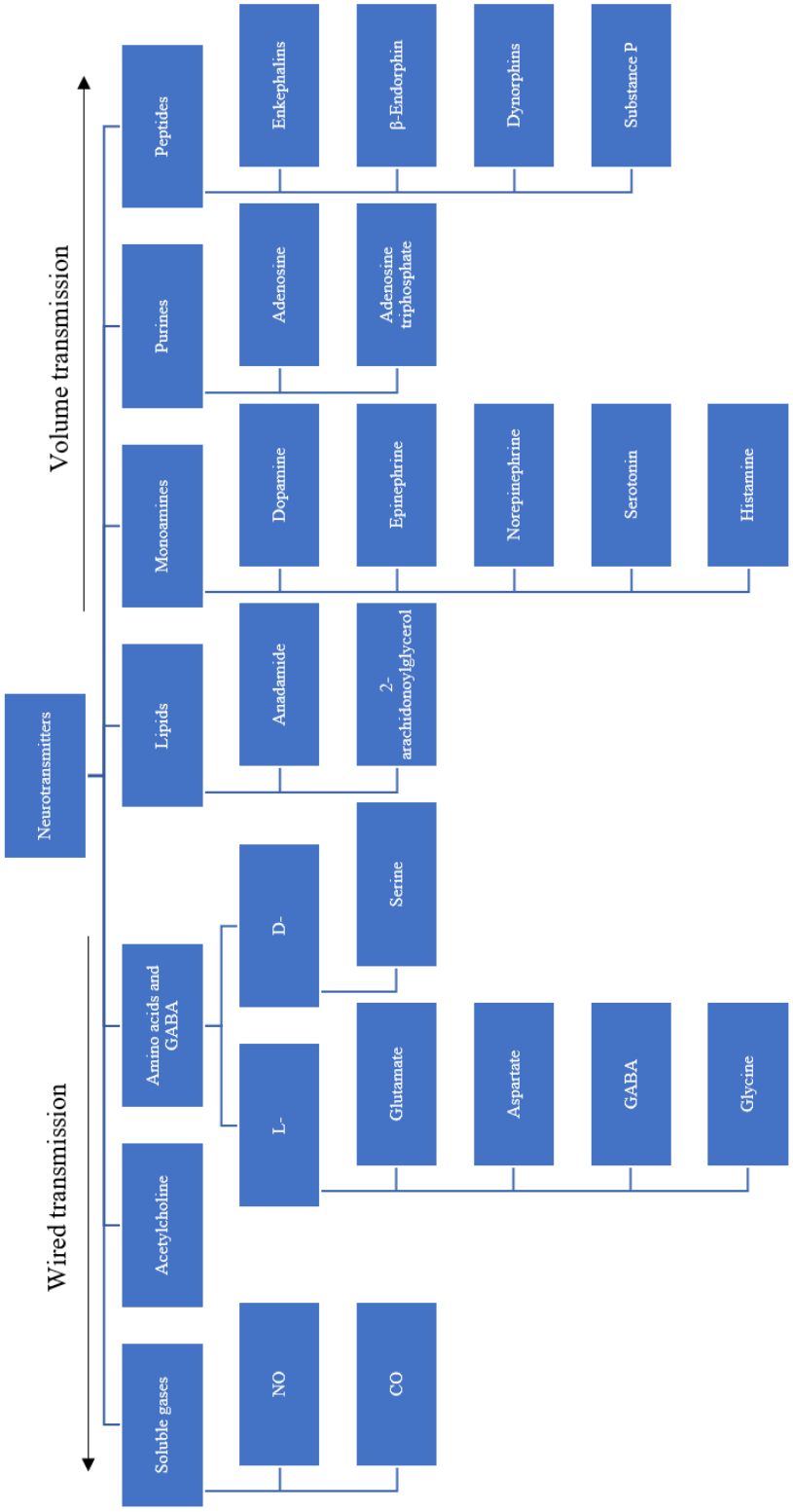

Figure 2.1. Classification of neurotransmitters in order of transition from wired transmission to volume transmission, with examples[5,6].

2.2. Monoamine neurotransmitters in neurodegeneration

2.2.1. *Dopamine*

Neurotransmitters that fall into the category of monoamines include dopamine (**DA**), epinephrine (**EPI**), norepinephrine (**NE**), serotonin (**5-HT**), and histamine. The most common member of this class considered in the discussions of neurodegenerative diseases is DA – 3,4-dihydroxyphenethylamine – the most ubiquitous catecholamine neurotransmitter in the midbrain. It is involved in a number of processes including regulation of locomotor activity, cognition, memory, emotion, and positive reinforcement. The dopaminergic neurons populate four major pathways – nigrostriatal, mesocortical, mesolimbic, and tuberoinfundibular. They are mainly located in the substantia nigra pars compacta (**SNpr**), ventral tegmental area (**VTA**), and arcuate nuclei[7,8]. Optimal concentrations of DA, both intracellular, extracellular, and in vesicles, are critical for efficient cognition and behavior, and dysfunction of DA systems is implicated in such disorders as Parkinson's disease (**PD**)[7,9–13], Alzheimer's disease (**AD**)[12], Huntington's disease (**HD**), attention deficit disorder[7], and Asperger syndrome[14].

Parkinson's disease and Huntington's disease are two of the most common neurodegenerative disorders that present with abnormal movement[7]. Therefore the involvement of DA neurotransmission in the development of these conditions is unsurprising due to DA's role in regulating locomotor activity. Loss of dopamine receptors (mostly D_2 in PD, and both D_1 and D_2 in HD) has been confirmed in clinical and preclinical studies, even in the early stages of these disorders[7]. Subsequently, DA replacement therapy using its precursor L-3,4-dihydroxyphenylalanine (**L-DOPA**) is the standard for treatment of PD symptoms[15]. At the same time, investigations focusing on the neurotransmitter itself provide a more complex picture. For instance, early-stage HD patients have been shown to have elevated levels of DA, suggesting that

pharmacological interventions focusing on reduction of its levels early in the disease could prove beneficial for the patient outcome. On the other hand, late-stage HD is characterized by decreased levels of DA, indicating that dopamine release dynamics change throughout the course of the disease in a time-dependent manner[7].

Data obtained via animal models of PD show both increased and decreased levels of the neurotransmitter depending on the model used: Parkin exon 3 knockout mice exhibit an increase of striatal DA, exon 2 deletion does not alter DA levels, overexpression of α-synuclein results in depletion of DA[16], and DJ-1 null mice show increased DA concentrations in tissues[17]. Animal models of HD, which have been genetically engineered to express human huntingtin protein, also show variability in DA concentrations: R6/2 and YAC 128 mice are characterized by decreased levels of DA and its metabolites in striatum, while the tgHD rats have increased DA in SNpr and VTA. Finally, chemically induced animal models of PD (obtained using 1-methyl-4-phenyl-1,2,3,6-tetrahydropyridine, rotenone, and 6-hydroxydopamine) show increased levels of DA and metabolites, as opposed to chemically-induced HD models (achieved through administration of 3-nitropropionic acid and quinolinic acid), which show decreased levels of these compounds[7]. The lack of agreement between different animal models for both diseases highlights the need for further investigations of the mechanisms and time-dependence of DA level changes in Parkinson's and Huntington's diseases.

Frequently, the discussion of dopamine's role in neurodegeneration focuses on the loss of dopaminergic (**DAergic**) neurons in SNpr observed in PD patients and the decreased levels of DA in both PD and late-stage HD. At the same time, excess of dopamine and its metabolites is known to exhibit neurotoxicity due to their involvement in production of reactive oxygen species (H_2O_2, O_2^-, and •OH) and highly toxic quinones[7,8,10–12,15]. For instance, a study using *C. elegans* showed

that the neurotoxic effect of Mn^{2+} – an environmental toxin associated with earlier onset and higher prevalence of PD – is caused by the Mn-mediated conversion of extracellular DA into toxic metabolites, followed by re-uptake of those metabolites into neurons using dopamine transporter DAT-1. The presence of these compounds inside the cell results in oxidative stress, which in turn causes degeneration of DAergic neurons[6]. Another study showed that elevated cytosolic concentrations of DA itself caused necrotic neurodegeneration in a transgenic mouse model with overexpression of dopamine transporters in striatal neurons[15]. A similar effect has been implicated in cell death during ischemic stroke. An increase of extracellular concentration of DA (up to 2 mM) is observed during ischemia in gerbils; however, depletion of endogenous DA through removal of nigrostriatal pathway neurons mediates cell damage following ischemia[8].

DA-associated oxidative stress is not only implicated in the progression of several neurodegenerative disorders, but also in the decline of dopamine-dependent functions of the brain (locomotion, memory, learning, *etc*.) during normal aging. Age-related decline of DA neurotransmission in the frontal cortex along with loss of D_2 receptors have been reported for humans and are thought to be responsible for the decline of cognitive and motor functions. This deterioration is believed to be caused by DA-related oxidative stress inducing apoptosis in aged brains. This conclusion was initially corroborated through studies that show both age-related accumulation of DA oxidation products in DA-enriched brain areas like SN and the presence of apoptotic neurons in SN of aged monkeys[8]. Later, *in vitro* and *in vivo* studies demonstrated that introduction of high amounts of DA caused DNA laddering – a specific pattern of DNA fragmentation associated with apoptosis through activation of transcription factor AP-1 and NF-κB pathways. This effect could be duplicated using D_2 receptor agonists and was counteracted by the addition of antioxidants such as glutathione. Interestingly, a continuation of these studies using

astrocyte cell cultures determined that instead of neurotoxicity, DA addition resulted in glial cell mitogenesis and expression of glial fibrillary acidic protein, indicating reactive gliosis, which could be indicative of either a neuroprotective or neuroinflammatory role of astrocytes during DA-induced oxidative stress[8]. To summarize, DA dysregulation can lead to apoptosis of neurons and activation of astrocytes that contribute to loss of brain functions in neurodegenerative disorders and aging.

Finally, *o*-quinones produced from DA have been shown to conjugate cysteine moieties of proteins. In the case of parkin this results in the inhibition of its neuroprotective function, with catechol modification of the protein exclusively localized to SN. When it comes to α-synuclein (α-SN) (the protein which makes up Lewy bodies, the hallmark abnormal protein aggregates observed in PD and some dementias), a modification with DA *o*-quinone results in stabilization of toxic protofibrils and decrease of fibril formation, while aminochrome (the most stable *o*-quinone product of DA oxidation) promotes α-SN oligomerization. These are only two examples of proteins that can be affected by DA-derived quinones, and the outcomes of such interactions span from protein degradation impairment to disruption of monoaminergic vesicle axonal transport and overall progressive neuronal dysfunction[10]. Aminochrome can also initiate redox cycling where it utilizes NADH or NADPH to be reduced to leukoaminochrome-*o*-semiquinone, which spontaneously oxidizes back into aminochrome in the presence of O_2. As a result, normal energy metabolism is impeded by depleting the supplies of NADH and oxygen required for mitochondrial synthesis of ATP[10].

2.2.2. *Norepinephrine*

Norepinephrine is another neurotransmitter with well-established direct involvement in PD and AD[12]. Locus coeruleus (**LoC**) is a nucleus in the brain stem primarily responsible for the synthesis

of NE in the brain with projections into forebrain, brainstem, cerebellum and spinal cord[18,19]. With connections to a high variety of brain structures, NE's involvement spans from memory and learning to arousal and vigilance, circadian rhythm and sleep. Very importantly for PD, NE affects the release of DA in projections to the striatum by influencing the activity of SNpc and VTA[19].

Loss of NE innervation in LoC in the central nervous system (**CNS**)[19,20] and sympathetic ganglia in the peripheral nervous system (**PNS**)[19] has been shown to precede loss of DAergic neurons in PD by several years, with the extent of neurodegeneration and Lewy body pathology in the remaining LoC and PNS neurons very similar[20] to or even exceeding[19] that observed in SNpc. It is also notable that aggregation of α-SN and loss of sympathetic norepinephrinergic (**NEergic**) innervation in the myocardium precede CNS changes in PD, serving as evidence that the progression of the disease begins in the PNS. Recently, animal models that follow the progressive ascending pattern of neurodegeneration (LoC → SN → primary motor cortex and hippocampus) that is observed in PD patients have been obtained for the first time by first depleting brain NE either using lipopolysaccharide or neurotoxin N-(2-chloroethyl)-N-ethyl-2-bromobenzylamine[21].

NEergic and DAergic neurons share several features, including the accumulation of neuromelanin and the expression of enzymes for catecholamine synthesis and catabolism. This enables a common mechanism for the involvement of these cell populations in the development of PD and other neurodegenerative disorders, that is metabolism-related oxidative stress and auto-oxidation product toxicity[12,19,20]. On the other hand, the role of NE in the inhibition of pro-inflammatory cytokine production and in the reduction of oxidative stress, mitochondria membrane depolarization, and caspase activation serve as evidence of the protective function of NE. When PD patient brains were studied post-mortem, the regions rich in NE were seen to experience a smaller degree of DAergic neuron loss[19]. In animal models where PD pathology was induced

chemically, lesioning of LoC enhanced the loss of DAergic neurons, while increased synthesis of NE lessened their degeneration[19,20].

As a pharmacological target, NE has shown promise in improving both motor and cognitive symptoms of Parkinsonism. Antagonists of adrenoreceptors used to increase release of NE from the surviving neurons have been shown to reduce tremors when used on their own; they also diminish L-DOPA-induced dyskinesia without counteracting L-DOPA's anti-Parkinsonian action[19,20]. Similarly to L-DOPA, a NE prodrug called L-*threo*-3,4-dihydroxyphenylserine (L-DOPS) is used to treat orthostatic hypotension and has been successfully tested as treatment for the freezing of gait, both symptoms of PD[19,20]. As LoC projects to the frontal cortex, several small studies have successfully targeted NE neurotransmission for the improvement of cognitive symptoms of PD, such as attention deficits and poor spatial working performance[15]. Similarly, due to LoC projections to limbic structures, NE has been used as a target for improving symptoms of depression in PD patients. Several NE uptake inhibitors have performed successfully in both small open-label studies and larger-scale double-blinded studies, although no improvement of motor symptoms was observed[19,20]. All of the above makes NE a promising target for the investigation and treatment of motor, cognitive, and autonomic dysfunctions in PD. When it comes to AD, a popular therapeutic approach to targeting the toxicity of both DA and NE metabolites is to improve axonal transport and thus prevent their accumulation inside the cells[12].

2.2.3. *Serotonin*

5-hydroxytryptamine, commonly referred to as serotonin, is an aromatic monoamine that is mainly synthesized from tryptophan in the human GI tract (95%)[22]. In the gut, 5-HT is involved in assimilation and absorption, regulation of particle transport and fluid discharge, and has been implicated in the development of such digestion disorders as irritable bowel syndrome[23]. After

being released into the bloodstream, serotonin can also be taken up by platelets, taking part in their aggregation, maintenance of vascular tone, and hypertension[22].

Serotonin is found in the central nervous systems of all animals and has been shown to regulate body temperature and circadian rhythms, mood and emotions, cognition, motor behavior, energy balance, and other processes in the brain[22,24]. The 18 types of serotonin receptors identified so far in vertebrates are classified into 7 families[22]. While serotonergic neurons are found throughout the brain, most of them, including those responsible for synthesis of this transmitter, are located in the raphe nuclei of the brain stem. The extracellular concentration of 5-HT is regulated by release from vesicles at the synapses and active uptake by serotonin transporters (**SERT**) and organic cation transporters[22,24].

In humans, age-related changes of the serotonergic system have been identified, including decreased 5-HT release in specific brain regions, decreased expression and binding affinity of receptors, increased SERT expression. Animal models have also shown decreased gene expression for tryptophan hydroxylase – the enzyme responsible for the first and rate-limiting step of 5-HT synthesis from tryptophan. This and some other evidence suggests an important role of serotonin in aging[22]. Furthermore, serotonin has been implicated in multiple psychological conditions like depression and anxiety disorders, and neurodegenerative disorders such as AD[22,25], PD[22,24,26,27], HD[28], and multiple sclerosis (**MS**)[29].

In Parkinson's disease, loss of serotonergic neurons has been confirmed in both the striatum (where the DA pathology develops) and outside of it. Lewy body pathology has been found in the median raphe nuclei prior to affecting dopaminergic neurons in the midbrain. A tomography-based study of patients at various stages of PD progression showed that the loss of SERT happens in a nonlinear manner and is not related to the disease duration, disability, or duration of dopamine replacement

therapy. At the same time, the intensity of tremor, which appears to be independent of DA terminal capacity or receptor availability, was correlated with the loss of 5-HT1A serotonin receptor binding. Loss of SERT binding in several brain regions, including the caudate, putamen, raphe nuclei, and thalamus was also shown to be more significant in patients with tremor-dominant PD than in akinetic-rigid PD and normal controls. Finally, both animal and human studies have shown that striatal serotonergic terminals play an important role in the development of L-DOPA-induced dyskinesia via aberrant processing of L-DOPA and release of DA in a non-physiological manner as they lack autoregulatory feedback for this neurotransmitter, and use of agonists for type 1A 5-HT receptors can modulate this side effect of DA replacement therapy[24].

When it comes AD, most studies focus on the involvement of serotonin either in cognition and memory or in depression[25,30,31]. Animal studies have shown that by targeting SERT with selective serotonin reuptake inhibitors (**SSRI**), production and chronic accumulation of toxic amyloid β (**Aβ**) proteins could be reduced. Clinical studies using imaging of Aβ showed lower cortical amyloid levels for participants who have taken SSRI within 5 years prior to the study. It was also shown that citalopram, an SSRI marketed under the name Celexa, lowered CSF levels of the protein in healthy volunteers.[31] Interestingly, another common SSRI escitalopram did not reduce Aβ levels in mice, but did show reduction of tau protein hyperphosphorylation in rat hippocampal cultures treated with $A\beta_{1-42}$[25]. Serotonin receptor 5-HT4R agonists have also been shown to reduce amyloid plaque formation and neuroinflammation through induction of α-secretase cleavage of amyloid precursor protein. In addition antagonists of 5-HT6R have shown improvement of cognition through stimulation of glutamate, acetylcholine, and catecholamine cortical and limbic pathways both in animal models and in a clinical trial as part of combination therapy[31]. Overall, as it is the Aβ oligomers that are currently thought to be the toxic agent in the development of AD

pathology, reducing production of Aβ through serotonin pathways is a promising strategy for achieving neuroprotection, although clinical studies have shown that this approach needs to be implemented at the early stages of the disease to effectively slow its progression[25,31].

Targeting of serotonin pathways, most commonly via SSRIs, has been used for treatment of most neuropsychiatric disorders, although the specific mechanisms responsible for symptom improvement are not always fully understood due to the overall complexity of the interactions in question[22].

2.3. Amino acid neurotransmitters in neurodegeneration

Involvement of amino acids in neurotransmission has been established since 1960s when L-glutamate (**L-Glu**) and L-aspartate (**L-Asp**) were classified as excitatory neurotransmitters and γ-aminobutyric acid (**GABA**) and glycine (**Gly**) were classified as inhibitory neurotransmitters[32]. Later, neurotransmitter functions of other amino acids including β-alanine and D-serine were discovered[33–35], broadening the scope of possible participation of these compounds in neurodegeneration. While amino acid profiling has been used as an approach to finding biomarkers for neurological disorders[36], it is the current convention that L-Glu has one of the most important roles in neurodegeneration due to its excitatory function and overall ubiquity in the brain (90% of all synapses contain it, with the total content in the brain ~ 10 mM[37,38] or 5–15 mmol/kg of brain tissue[39]).

2.3.1. *L-Glutamate*

While L-Glu is the most common free amino acid in mammalian diet, it is nearly quantitatively metabolized (mostly to carbon dioxide) during digestion and is synthesized *in vivo* from either α-ketoglutarate or from amino acids in the "glutamate family" (glutamine, arginine, proline and

histidine). In the brain, L-Glu concentrations vary from ~1 μM in the cerebrospinal fluid (**CSF**) to 100 mM in the nerve terminal vesicles. Excitatory action of Glu is carried out through two receptor types – ionotropic (*e.g.* NMDAr, AMPAr, KAr) and metabotropic, both of which activate ion channels either by direct binding with Glu or through secondary messenger pathways[37] following exocytosis of Glu-containing vesicles from the pre-synaptic neuron. As there are no enzymes responsible for metabolizing extracellular glutamate, termination of the glutaminergic neurotransmission is carried out through removal of Glu from the synaptic cleft via transporters present in astroglia and neurons[39,40]. Disruption of glutamate removal causes excessive excitation of neurons that may result in cell damage and death – a phenomenon commonly referred to as excitotoxicity. This disruption may occur for a variety of reasons, such as an energy deficit inhibiting the ATP-dependent Glu reuptake; cell injury resulting in release of the intracellular metabolic Glu pool into extracellular space; presence of exogenous agonists of glutamate receptors[40]. Furthermore, as one specific type of Glu transporter – excitatory amino acid transporter 2 (**EAAT2**) – is responsible for the uptake of 90% of the neurotransmitters released during neuron excitation, its dysfunction inevitably leads to excitotoxic cell damage and has been experimentally shown to be involved in the progression of several neurodegenerative disorders including AD.[41] Another critical aspect of Glu-related excitotoxicity is related to the self-propagating nature of tissue damage ("glutamatergic loop") resulting from the fact that when neurons die, their stores of glutamate are released into the extracellular space, causing depolarization of the surrounding neurons and exacerbating the excess of the neurotransmitter and demand for its removal[40].

The first observed effect of prolonged exposure to increased glutamate concentrations is neuronal swelling due to influx of Na^+, Cl^-, and water through AMPA and KA receptors. While this swelling

of neuronal structures can be mediated by eliminating the ion excess from the cells, the main cause for neurodegeneration during excitotoxic events is thought to be mediated by NMDA receptors, which are highly permeable to Ca^{2+} ions. Influx of calcium into neurons disturbs the intracellular homeostasis of this ion, causing stress on the endoplasmic reticulum (**ER**), mitochondrial calcium overload, and oxidative stress. In the case of ER, the disruption results in inhibition of protein synthesis and has been suggested to induce neuronal apoptosis. In mitochondria, excess Ca^{2+} lead to the disruption of electron transport chain and inhibition of ATP formation. This in turn leads to mitochondrial permeability transition pore opening and rupture of the organelle accompanied by release of caspase-activating proteins, which also triggers apoptosis. Finally, oxidative stress caused by imbalance in the production of reactive nitrogen and oxygen species results in damage to proteins, nucleic acids, and lipids, which culminates in disruption of cellular functions and integrity. To summarize, the initial rapid neuronal death due to excitotoxicity of Glu is thought to be due to cell necrosis caused by cell and organelle swelling, which is followed by eventual clearance of Glu and death of the surviving cells due to delayed apoptosis[40].

Involvement of excitotoxicity in neuronal damage is well-established in acute CNS insults such as stroke and traumatic brain injury. High glutamate concentrations have been detected in microdialysis samples obtained from animal models of ischemia and traumatic brain injury patients. Although neuroprotection has been achieved with use of Glu receptor antagonists and release inhibitors in animal models and *in vitro*, the results of clinical trials of these drugs in humans so far have been disappointing. In some cases, side effects like agitation, hallucinations, and confusion have been observed due to the need to use high concentrations of antagonists to produce the desired physiological changes. In others, the compounds that performed successfully in animal trials were not effective in humans. Also, timing of treatment has proven to be critical

as, for example, the glutamate release inhibitor BW 619C89 showed neuroprotective function when administered during induced ischemia but did not reduce tissue damage if administration was carried out 5 min after reperfusion. Overall, NMDA receptor antagonists so far have proven ineffective in mitigating stroke and trauma-related cell damage in human patients; however, AMPA receptor agonists, glutamate release inhibitors, and selective agents for the NR2B subunit of NMDAr responsible for glutamate recognition are more likely to produce positive patient outcomes, especially if used in combination with each other[40].

Several chronic diseases, such as Huntington's disease, Alzheimer's disease, Parkinson's disease, amyotrophic lateral sclerosis (**ALS**), MS, and HIV dementia have been shown to be affected by glutamate induced excitotoxicity. Most of these conclusions were made based on similarity of neuronal loss patterns in patients and animal models where lesions either in the brain or in the spinal cord were caused by excitotoxicity. Supporting evidence includes attenuation of damage with use of NMDA and AMPA receptor antagonists, glutamate release blockers, and lesioning of the glutamatergic pathways. As mentioned above, loss of EAAT2 transporters in AD and ALS also strongly indicates glutamate's involvement in these disorders. A moderate affinity NMDA receptor antagonist memantine was shown to have a neuroprotective function for AD patients and animal models of MS and HIV dementia, but not in HD patients. A glutamate release inhibitor rilutek (marketed as Riluzole) was shown to be effective in extending survival in ALS patients. To summarize, targeting L-Glu neurotransmission via ionotropic receptors is a promising approach to slowing down the progress of neurodegeneration in chronic neurological disorders.[40]

It is important to add that therapeutic targeting of glutamatergic pathways has not been limited to the ionotropic receptors. While metabotropic receptors respond to stimuli slower and are mostly thought to play a role in neuromodulation and not transmission, their antagonists (for post-synaptic

receptors) and agonists (for pre-synaptic receptors) have been showing promise for managing both neurodegenerative and neurologic disorders with fewer side effects than, for example, NMDAr blockers. While only one clinical trial has been successful so far (improvement of cognitive symptoms in schizophrenia with a metabotropic receptor agonist LY2140023), further investigations in this direction, especially combining multiple subtypes of these receptors, must be evaluated[42].

2.3.2. *D-Serine*

As was stated above, NMDA receptors play a critical role in glutamate-induced excitotoxicity. However, L-Glu is not the only amino acid involved in the activation of NMDA receptors as they require a co-agonist to operate. While glycine was originally identified at as a co-agonist which binds to the NR1 subunit of the receptor, it was more recently discovered that an "unusual" amino acid D-serine (**D-Ser**) is present in the brain in fairly large amounts and has the affinity to the NMDAr co-agonist binding site three times greater than that of glycine[34,43]. Studies of the crystal structure of the binding core of the NR1 subunit show that D-Ser forms three more hydrogen bonds when compared to glycine and displaces a molecule of water from the binding pocket[43].

Even though D-Ser was discovered in the mammalian brain quite recently, its decreased levels have already been implicated in the hypofunction of NMDA receptors leading to the positive, negative, and cognitive symptoms in schizophrenia. When it comes to neurodegeneration, it is thought that inhibition of serine racemase (the enzyme responsible for conversion of L-Ser into the D- isomer of the amino acid) may modulate the activation of NMDA receptors during acute and chronic insults and may result in neuroprotection without the risk of significant side effects seen with NMDAr inhibitors. Overproduction of L-Ser may also play a role in neurodegenerative disorders. For instance, the spinal cord of ALS patients contains elevated levels of both D-Ser and

serine racemase, which, according to experiments carried out with animal models of the disease, is caused by dysfunction of glial cells[43].

2.3.3. *γ-Aminobutyric acid*

A major inhibitory neurotransmitter of the CNS, GABA is involved in maintenance of equivalent neurotransmission and modulation of neuronal migration, differentiation, proliferation, *etc*. Synthesized from glutamate by glutamic acid decarboxylase, GABA is stored in synaptic vesicles, released into the synaptic cleft, and removed by membrane-bound GABA transporters (**GAT**) of pre- and post-synaptic neurons and glial cells[44].

Similarly to glutamate, two types of receptors – postsynaptic ionotropic and both pre- and postsynaptic metabotropic – mediate GABAergic transmission. Fast synaptic inhibition is carried out through activation of the chloride channels of the ionotropic receptors, pharmacological targeting of which with barbiturates, benzodiazepines and steroid anesthetics has been shown to have anti-convulsant, anxiolytic, and sedative effects[44,45]. A G protein coupled metabotropic receptor is thought to be involved in the development of neurological and psychiatric disorders[44].

As overactivation of the excitatory glutamatergic neurotransmission plays an important role in neurodegeneration, it comes as no surprise that dysregulation of the inhibitory GABAergic systems also contributes to this process. For example, various mouse models of AD demonstrate alterations of GABA neurotransmission and even neurodegeneration of the GABAergic neurons. GABA insufficiency has also been shown in MS patients with the secondary progressive form of the disease, indicating a link between GABA levels and degradation of motor functions[44].

In PD, degradation of the DA neurons in the SNpc which project to the striatal GABAergic neurons results in overactive output nuclei of the basal ganglia causing inhibition of the thalamic output to

the cortex. Decreased levels of GABA are detected in postmortem brains of PD patients, especially in the regions of significant degeneration of dopaminergic neurons. Binding of the ionotropic receptors was also shown, but was limited to SN, globus pallidus, and caudate putamen and was not seen in the cortex[45]. Decreased levels of GABA have also been observed in the CSF of PD patients[44]. While current treatments focus on compensating the loss of DA neurotransmission, therapies targeting GABA production, release, and neurotransmission may provide new avenues for alleviating the burden of this disorder.

GABAergic motor neurons in the striatum are the first to degenerate in HD patients, with the entire cortico-striato-pallidal circuit being destroyed as the disease progresses. Receptor-binding studies show that neurodegeneration starts at the neuron terminals, with cell bodies dying later. In contrast to PD, degeneration of the GABAergic neurons first results in overactive thalamic outputs to the cortex causing chorea, and later progression inhibits the thalamic output resulting in akinesia. Due to the loss of GABAergic neurons, increasing GABA production and release is unlikely to yield improvement of the symptoms; however, use of uptake inhibitors (especially for the glial transporters) may be able to enhance the activity of the remaining neurotransmitter. Transplantation of GABAergic neurons is also being investigated as a treatment of the HD pathology[45].

In conclusion, loss of GABAergic neurons contributes to the excitatory/inhibitory imbalance known to play a critical role in the development of many neurodegenerative diseases. Therefore, maintenance of GABA neurotransmission offers a promising target for the development of neuroprotective and therapeutic agents.

2.4. Microdialysis sampling coupled to microchip electrophoresis for studies of the brain

The absolute incidence of neurological and neurodegenerative disorders continues to grow in the U.S. with its aging population[46], costing $655 billion in direct medical and non-medical costs, indirect costs from lost productivity, and uncompensated caregiving hours in 2020[47]. Despite the urgent need for therapeutics there are still many conditions that lack cures and for which treatments provide only symptom management. The cause of this is the lack of detailed understanding of the molecular mechanisms resulting in the development of these disorders.

Availability of analytical methods that allow *in vivo* monitoring of dynamic changes in the concentrations of neuroactive compounds in brain tissues is key to unveiling the complexities of the underlying processes in neurological diseases. Quantification of individual compounds with high spatial and temporal resolution has so far been enabled through use of microelectrode-based biosensors and fast scan cyclic voltammetry[48–51]. *In situ* simultaneous monitoring of multiple compounds has been achieved with sensor arrays[52–54], however the data for each analyte in this case is obtained from different locations in the tissue. This means that to correlate change of concentrations for different species with each other one must assume relative homogeneity of the tissues in question. Microdialysis (**MD**) is a technique that makes it possible to combine sampling from living tissues with separations[50,55–57], thus expanding the number and nature of the detected compounds based on the capabilities of the analytical method used. Furthermore, the possibility of pairing with continuous sample flow eliminates the need of sample handling and improves temporal resolution when microdialysis sampling is directly coupled to liquid chromatography[57–59], capillary electrophoresis[60,61], and microchip electrophoresis[62–64] instruments.

Microchip electrophoresis (**ME**) is a promising technique that can be used in tandem with MD sampling: it requires very low sample volumes, separations typically take < 100 s, and the microfluidic devices and electronics are easily miniaturized. ME analytical systems can be placed on backs of larger laboratory animals to minimize restriction of their movements and thus perform studies where animals can truly be considered feely-roaming[65] or used for near-patient analysis of microdialysis samples[66]. In this section, fundamentals of microdialysis sampling and microchip electrophoresis are discussed, with the focus on applying the combined MD-ME approach to on-line *in vivo* studies of the brain.

2.4.1. *Fundamentals of microdialysis sampling*

Sampling via microdialysis is performed by placing a probe containing a semi-permeable membrane into an environment of interest (*e.g.*, tissues and tissue homogenates) and flowing a sampling solution, referred to as perfusate, through the probe using a syringe pump. When perfusate is in contact with the membrane, any compound with molecular weight below the membrane molecular weight cut-off (**MWCO**) diffuses from the probe surroundings into the solution inside the probe based on the concentration gradient between the two media, creating a dialysate sample. Composition of this solution is representative of all species present in the extracellular fluid of tissues that are small enough to cross the membrane, and the lack of proteins in it prevents enzymatic degradation of the analytes and enables immediate analysis of these samples without clean-up. Since no fluid is removed from the sampling environment during this process, MD can be performed for extended periods of time with minimal effects on the surrounding tissue beyond implantation damage, especially if strategies to minimize the immune response are employed[67]. The above factors make MD a powerful technique for long-term

sampling from living tissues and monitoring of dynamic changes of extracellular concentrations of multiple small molecules and peptides simultaneously.

For any microdialysis-based experiment, several parameters must be considered. Optimal probe design depends on the tissue type from which one wants to perform sampling: linear probes are best suited for homogenous tissues such as skin and liver[63], while sampling from the brain is typically performed with rigid cannula probes[5,68,69]. Available membrane materials vary in hydrophobicity and charge, affecting the transport of species during sampling. The MWCO of the membrane can also be selected in order to influence sampling selectivity. Finally, the size of the probe membrane may be changed based on the animal species and spatial resolution desired. Commercially available CNS probes are available with a variety of membrane materials (cuprophan, polyethylsulfone, polyarylethersulfone, polyacrylonitrule, cellulose), MWCO (20–2000 kDa), and membrane lengths (0.5–10 mm) and outer diameters (0.180–0.5 mm)[70–72]. When it comes to perfusate, the general approach is to match its composition as closely as possible to the extracellular fluid (**ECF**) of the tissue of interest. Typically, Ringer's solution or artificial cerebrospinal fluid (**aCSF**) are utilized as perfusates in cerebral MD[5,69], with the occasional addition of such compounds as ascorbic acid[73,74] (to avoid depletion of this antioxidant from the extracellular space) and dexamethasone[67] (anti-inflammatory agent) for basal measurements. When the effect of a pharmaceutical agent on the concentration of an endogenous analyte needs to be evaluated, the agent of interest can be added to the perfusate and delivered directly to the sampling site via retrodialysis.

Once the MD parameters discussed above have been selected, one critical variable remains – perfusion flow rate. This easily adjustable instrumental setting is tightly connected to two criteria important for the *in vivo* studies of neurochemical dynamics – efficiency of analyte recovery and

temporal resolution of the collected data. Analyte recovery from tissues can be evaluated as relative (extraction efficiency calculated as *c*(perfusate)/*c*(tissue) when the initial concentration of analyte in perfusate is zero[63]) and absolute (mass of analyte retained in perfusate). Due to passive diffusion being the primary mechanism of analyte transfer across the membrane, relative analyte recovery is inversely related to the probe perfusion flow rate, while absolute recovery increases together with the increased flow. At the typical microdialysis flow rates of 0.3–2.0 μL/min, the relative recovery often does not exceed 20% based on analyte species[5]. This in turn means that for quantification of these compounds either the analytical method limits of detection (**LOD**) must be significantly below ECF tissue concentrations, or large sample volumes must be used to ensure collection of detectable analyte mass.

This ties recovery to the question of temporal resolution: for the compounds present in the brain at relatively high endogenous concentrations in the micromolar-millimolar range (ascorbate, glucose, glutamate, etc.), even at very low MD recoveries quantification presents no issue if the analytical technique is sufficiently sensitive. This means that the temporal resolution of analysis is restricted by (1) the sample volume requirements during both off-line and on-line analysis with conventional instrumentation and (2) the analytical method run time during on-line analysis using microseparation techniques. However, in the case of compounds with concentrations in the nanomolar range, the resolution is determined by the MD sampling process since either the relative recovery needs to be maximized by using very low flow rates or the absolute recovery must be increased by collecting for longer periods of time – both options which negatively affect temporal resolution. It should be noted that there are other parameters, such as microdialysis membrane material, MWCO, and dimensions, analyte species properties, Taylor diffusion of the sample zones, and diffusion resistance of the tissues that also play a role in analyte recovery. Overall, the

balance of perfusate flow rate, analyte recovery, sample volume requirements, and temporal resolution must be considered when designing studies using microdialysis sampling for monitoring of neurochemical processes[5,63,68].

2.4.2. *Fundamentals of microchip electrophoresis*

Microchip electrophoresis (**ME**) uses the same separation principles as capillary electrophoresis, where analytes are separated based on their electrophoretic mobility. The transition from conventional instrumentation to a microfluidic platform yields miniaturized devices that enable fast efficient separations; it also allows to utilize microchannel geometries for integration of continuous sample flow, on-line sample derivatization and preconcentration, and on-chip detection[57,75–78]. This makes ME a favorable candidate for pairing with MD sampling for on-line *in vivo* monitoring of neuroactive species in the brain.

A microchip electrophoresis separation is carried out in a microchannel (usually < 15 cm long) fabricated from glass, plastic, or polymer material[79] filled with a background electrolyte solution (**BGE**). To perform the separation, a small plug of sample is introduced into the channel and a constant voltage is applied to initiate migration of analytes. The innate electrophoretic mobility (μ_{ep}) of each specie is proportional to the absolute value of its charge (q) and inversely related to its hydrodynamic radius (r) as shown in Equation 1:

$$\mu_{ep} = \frac{q}{6\pi\eta r} \qquad \text{(Equation 1)},$$

where η indicates the viscosity of the medium (BGE). The direction of μ_{ep} is determined by the sign of the charge. During the so-called "normal polarity" separations, where a positive voltage is applied at the channel inlet and grounded at the outlet, the mobility of cations is directed towards the ground serving at cathode, while anions are attracted to the anode at the inlet. In isolation, this

would mean that only the positively charged species would travel the entire length of the microchannel, reaching the detection point. However, another physical phenomenon takes place in the system, enabling the detection of the negatively charged and neutral analytes as well.

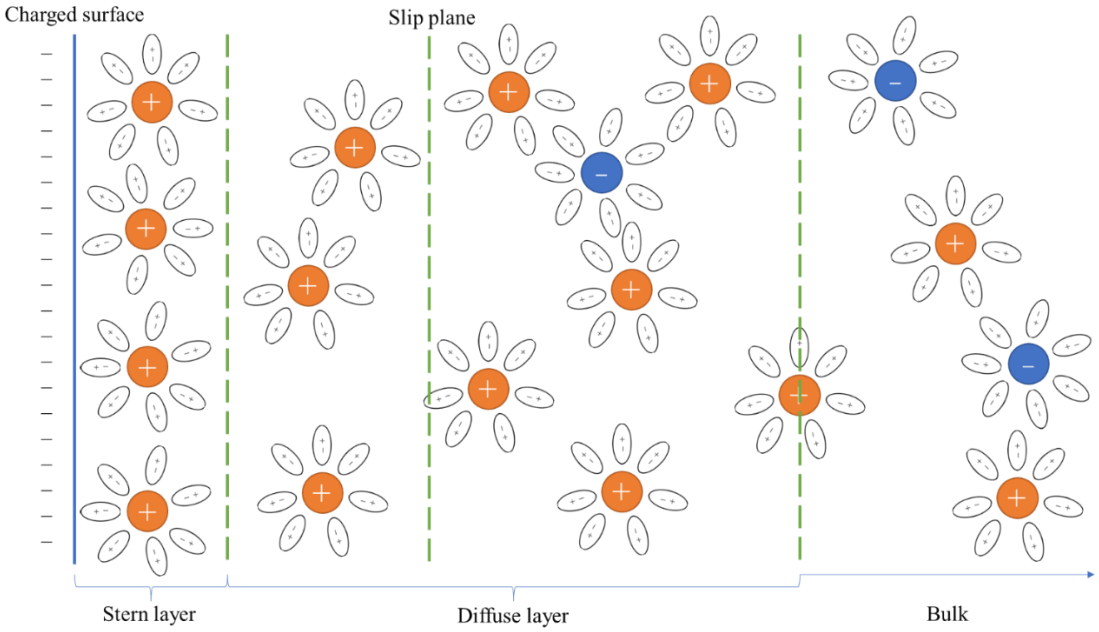

Figure 2.2. Structure of an electric double layer at a charged surface.

Electrophoretic separations are generally performed on devices that carry a charge on the channel surfaces. Most often this is ensured by using silicon oxide-based materials (fused silica, glass, or quartz) or by modifying the surface with oxidizing plasma or chemical reagents (ionic polymers, surfactants, *etc*.). When an electrolyte solution (*e.g.*, BGE) comes in contact with such channels, an electric double layer is created due to the electrostatic attraction of the solution ions to the surface charges of the opposite sign (Figure 2.2). Spatial distribution of these solution counterions and the magnitude of their attraction to the charged surface change with the distance from the channel wall, and while those closest to it are fixed in the so-called Stern layer, the ions in the diffuse layer are more mobile. When an external electric field is applied to this system, the hydrated ions beyond the slip plane of the diffuse layer migrate according to their electrophoretic mobility,

creating a bulk flow in the channel referred to as electroosmotic flow (**EOF**). If the channel walls are negatively charged (for instance in fused silica devices), it is the BGE cations that are responsible for the creation of the EOF, and in normal polarity separations this bulk flow is directed towards the cathode and the detection point, contributing to the overall observed mobility ($\mu_{observed}$) of the analyte species (Equation 2). If the magnitude of the EOF mobility (μ_{EOF}) is sufficiently high, even anions with high negative μ_{ep} will have a positive $\mu_{observed}$ and will be detected. Overall, the analytes will be separated and detected with the smallest highly charged cations migrating first, followed by larger less positive cations, all neutral species, large anions, and finally small highly charged anions.[80]

$$\mu_{observed} = \mu_{ep} + \mu_{EOF} \qquad \text{(Equation 2)}$$

One of the strengths of electrophoretic separations lies in the shape of the resulting flow profile – as an electric field is used to create the flow, its profile is uniform throughout the channel with the exception of the narrow zones immediately adjacent to the channel walls. This prevents broadening of the sample plug observed with parabolic pressure-driven flows (*e.g.*, during chromatographic separations), resulting in efficient separations. It should also be noted that if the polarity of the separation needs to be reversed to switch the analyte migration order and have the anions reach the detector first, the channel surface charge needs to be positive so that the EOF is directed towards the anode. This can also be accomplished by using surface modifying agents mentioned above.

Detection during ME experiments is most commonly performed using fluorescence (**LIF**) or electrochemical (**EC**) detection [81], although use of capacitively coupled contactless conductivity detection is also gaining popularity[82,83]. While LIF detection is more sensitive than EC detection,

most analytes must be derivatized to be detected using this technique. For on-line analyses, the derivatization step can be accomplished on the microchip by adding inlets for the reagents and a mixing structure to the device[75]. This approach requires the derivatization reaction to yield high amounts of fluorescent products over comparatively short periods of time, otherwise Taylor dispersion, due to the addition of long mixing and reaction channels, would result in decreased temporal resolution. Miniaturization of the instrumental setups necessary to carry out ME-LIF experiments (laser, objective, filters, alignment system, etc.) poses a challenge as well, although our group has made progress in this direction in the recent years[66].

On the other hand, EC detection allows the monitoring of many biomolecules without prior derivatization. In the case of neuroactive compounds, the list of naturally electrochemically active species includes neurotransmitters and neuromodulators, antioxidants, nucleobases, and reactive nitrogen and oxygen species. The most common mode of EC detection used with ME is oxidative amperometry, where a constant voltage is applied to the working electrode (**WE**) placed near the end of the separation channel. Oxidation of the analyte species happens as they pass by the WE, generating current, which serves as the signal. By selecting the WE material and applied potential, detection sensitivity and selectivity can be adjusted. Common material options include metals (platinum, gold, palladium, *etc*.) and carbon (carbon fiber, pyrolyzed photoresist film, carbon paste and ink). The latter tends to provide good analyte responses for biologically relevant organic compounds, such as catecholamines[63,84]. It should be noted that compatibility between the choice of the working electrode material and the microchip substrate also plays an important role in the experiment design.

Care must be taken when deciding on the placement of the working electrode relative to the separation channel. While putting the electrode directly inside the channel (in-channel detection)

allows to minimize sample zone broadening due to diffusion, this configuration exposes the WE and the potentiostat used to apply the detection voltage to the high electric field driving the separation, causing high noise and requiring use of an isolated potentiostat. During end-channel detection, the electrode is placed in the waste well several microns away from the channel outlet, protecting the potentiostat and working electrode from the separation field but leading to sample zone diffusion as it leaves the channel, lowering separation efficiency and analyte resolution. Electrode alignment where the gap between the end of the channel and WE is minimal (3–5 μm) is sometimes referred to as pseudo in-channel. Finally, off-channel detection serves as an intermediate option: the working electrode is placed inside the separation channel, but a more massive decoupler electrode is placed further in-channel upstream from the WE to ground the separation voltage thus isolating the potentiostat from it. While this approach has the advantage of lower noise and minimal sample diffusion, it is complicated by the need to select a decoupler electrode material which would adsorb the gas generated at the ground and thus prevent formation of bubbles in the channel (Pt and Pd have been used for normal polarity separations as they adsorb H_2)[85].

2.4.3. *Combining microdialysis sampling with microchip electrophoresis – progress towards compact separation-bases sensors for studies of the central nervous system*

As was briefly mentioned above, the continuous pressure-driven flow of sample obtained via microdialysis may be directly connected to a microchip electrophoresis device of appropriate geometry. Small-bore tubing is used to make the connection while the length is kept as short as possible to minimize Taylor diffusion and lag time between sampling and analysis. It is critical that the bonding between the microchip layers is strong enough to withstand the backpressure created by the pumping of the sample into the device[63].

The small sample volumes used for ME injections ensure near real-time monitoring of biological events via on-line MD-ME, with temporal resolution determined mainly by the duration of the analysis run. Introduction of the sample plug into the separation channel is typically carried out via one of the three strategies: flow gated injection, injection using pneumatically controlled valves, or injection from segmented flow.

Flow gated sample injection is the easiest one to implement in terms of instrumentation as it does not require any additional components other than a microchip, the syringe pump for MD sampling, and a high voltage power supply to enable the ME separation. For this approach, a "double t" microchip with a wide top channel is needed (see Figure 2.3). The flow of MD sample fills the top channel and is driven towards the separation channel by pressure from the pump. The high voltage applied to the buffer well establishes an electrokinetic gate, diverting the sample flow into waste. If this voltage is floated, the pressure from the pump pushes the sample into the separation channel, and once the voltage is reestablished, the buffer flow cuts off a small plug of dialysate and initiates the separation of analytes. The relative simplicity and minimal instrumentation requirements make this strategy optimal for utilization in miniaturized portable detection systems[63].

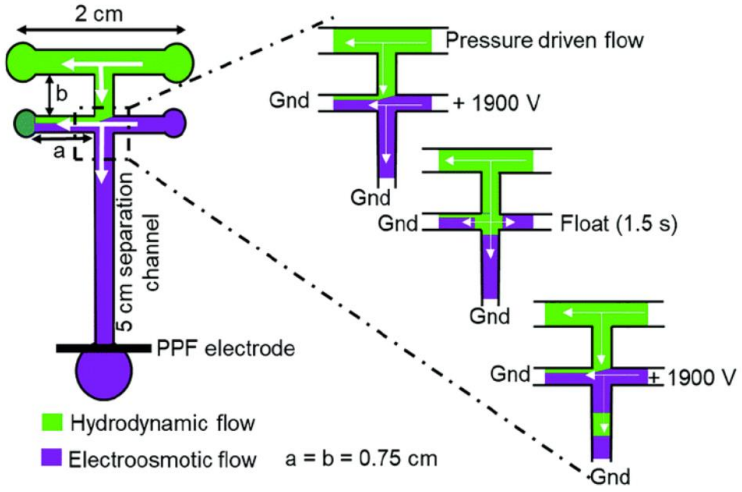

Figure 2.3. Flow gated injection of sample. Adapted from Gunawardhana et al.[86]

Injection of sample using pneumatic valves is another widely used approach. Microchip construction in this case requires use of a flexible material, such as polydimethyl siloxane (**PDMS**), to create two feature-containing layers (flow and control). Pressure driven sample flow is isolated from the separation channel by a closed valve, which is opened for a short period of time to inject the sample and is closed again for the duration of the analysis run. Compared to flow gated devices, fabrication of the chip is more challenging, and valve actuators and a gas tank are added to the list of necessary instrumentation. While this approach allows for more flexibility when selecting the separation voltage, the necessity to use compressed gas for valve operation stands in the way of miniaturization and using this MD-ME integration strategy for near-patient and on-animal analysis[63].

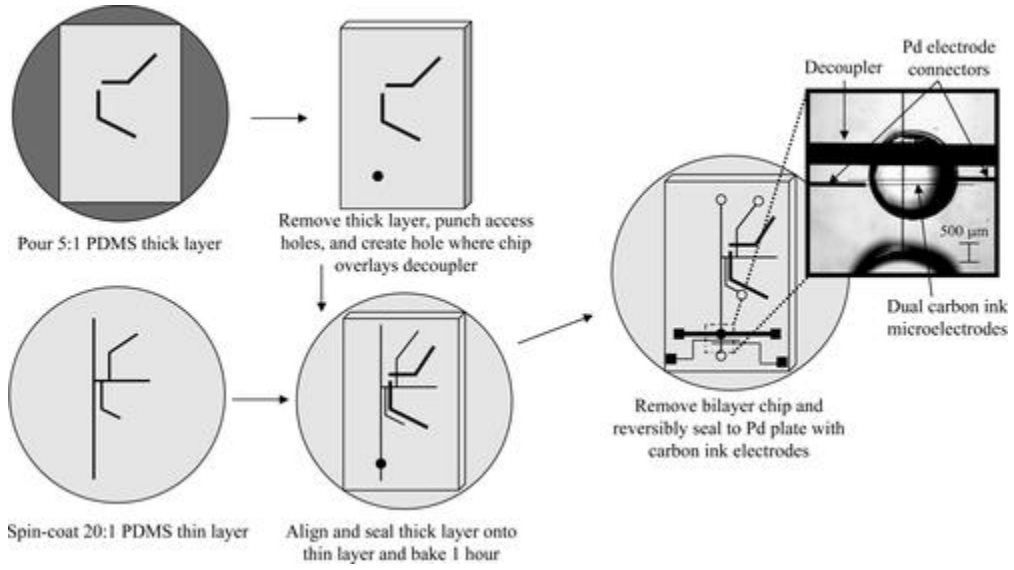

Figure 2.4. Microchip electrophoresis chip with pneumatic valves for sample injection. Reproduced from Mecker *et al.*[87] with permission.

Lastly, segmentation of MD sample flow can be used prior to ME analysis to preserve temporal resolution of the analysis. Splitting of the sample into nanoliter volume droplets by introducing immiscible oil zones into the flow prevents diffusion of analytes while the sample undergoes

derivatization for LIF detection and travels in the connecting tubing. Prior to ME analysis, the sample is desegmented and injected into the separation channel[88]. For on-line MD-ME-LIF, the temporal resolution of the method is determined by the duration of the ME run, while off-line sample collection and segmentation allows to achieve temporal resolution of 2 s limited by mass transport effects in the MD probe[89]. On-line implementation of this MD-ME configuration requires pairing of two microchip devices – one for flow segmentation followed by analyte derivatization and the other for desegmentation and separation, along with pumps required to drive oil and derivatization reagent flows.

2.4.4. *Application of MD-ME to monitoring of neurochemicals*

Development and improvement of the on-line MD-ME analysis platforms for studies of neurochemical processes is still an ongoing process. The Martin group at St. Louis University has focused on the pneumatically controlled devices and have been able to use them for the monitoring of dopamine release from PC12 neuroblastoma cell cultures due to exposure to elevated K^+ and Ca^{2+} concentrations[87]. More recently, the group has also developed the methodology for fabricating microchips for these experiments entirely through 3D printing[90]. Such advancement towards mass production of the devices expands the pool of investigators who can now get involved in this area of research but would otherwise lack the facilities (clean rooms and photolithography equipment) required to obtain necessary instrumentation.

A research group at the University of Michigan led by R. Kennedy pioneered the approach for coupling MD sample flow segmentation to microchip electrophoresis separations. Using on-line MD-ME-LIF with both flow gated[91] and later segmented flow[88] configurations, they were able to observe an increase of extracellular Glu (and in the case of segmented flow Asp as well) following administration of a glutamate uptake inhibitor. The more recent efforts have been focused on

improving the temporal resolution of off-line analysis of MD samples with ME-LIF, allowing to obtain values limited by the performance of the sampling method itself[89] and monitor K^+ induced changes of Glu, Asp, Gly, GABA, and taurine with 10 s resolution[92].

Finally, the Lunte group at the University of Kansas was the first to demonstrate on-line coupling of MD sampling and ME separations using the flow gated interface in 2004[93]. Since then, the group has demonstrated the ability of this approach to monitor various classes of neuroactive compounds both *in vitro* and *in vivo*. Devices for on-line monitoring of amino acid neurotransmitters via MD-ME-LIF were described by Nandi *et al.* and used to monitor aspartate and glutamate *in vivo*[62]. The device was also used to evaluate blood-brain barrier permeability following peripheral injection of fluorescein and observe its clearance from the brain over 90 min. The microchip design for such experiments was later optimized by Nandi *et al.*[75] and Oborny[94] to minimize signal rise time, analysis lag time, and yield of the derivatization reaction. A portable instrument for ME experiments with LIF detection was also developed in order to advance utilization of this method in clinical settings[66].

On-line MD-ME coupled to EC detection has been used in our group for monitoring of L-DOPA pathway metabolism both *in vitro* with brain homogenate[86] and *in vivo* in the striatum[95]. By delivering high K^+ to the brain via retrodialysis, we were able to observe *in vivo* dopamine release due to neuron depolarization[86], although it must be noted that limits of detection were not sufficiently low to enable monitoring of basal neurotransmitter concentrations. A method for the monitoring of adenosine metabolism was also developed and tested *in vitro* during enzymatic conversion of adenosine to inosine over 3 hours[96].

MD-ME-EC instrumentation has also been miniaturized and employed for on-animal monitoring of subcutaneous conversion of nitroglycerin to nitrite[65]. This study serves as proof of concept for

future experiments focusing on correlating changes of neuroactive compound concentrations with behavior and physiological state of freely roaming animals.

1.1. Concluding remarks

The growing prevalence of neurological disorders highlights the need for deeper understanding of the biological processes involved in their development and progression and adds urgency to the demand for analytical tools which can aid their investigation. This review shows that while the involvement of neurotransmitters in the diseases of the brain is undeniable, the exact molecular mechanisms and pharmacological treatment approaches require further research. Microdialysis sampling coupled to microchip electrophoresis is a promising tool for the on-line *in vivo* and *in vitro* studies of neurological conditions. The separation-based sensor can be customized to monitor a variety of species of interest and can be used beyond the laboratory setting for near-patient and on-animal analysis.

2.5. References

(1) Agorogiannis, E. I.; Agorogiannis, G. I.; Papadimitriou, A.; Hadjigeorgiou, G. M. Protein Misfolding in Neurodegenerative Diseases. *Neuropathol. Appl. Neurobiol.* **2004**, *30* (3), 215–224.

(2) Cervellati, C.; Trentini, A.; Pecorelli, A.; Valacchi, G.; Valacchi, G.; Valacchi, G. Inflammation in Neurological Disorders: The Thin Boundary Between Brain and Periphery. *Antioxid. Redox Signal.* **2020**, *33* (3), 191–210.

(3) Singh, A.; Kukreti, R.; Saso, L.; Kukreti, S. Oxidative Stress: A Key Modulator in Neurodegenerative Diseases. *Mol. 2019, Vol. 24, Page 1583* **2019**, *24* (8), 1583.

(4) Bozzi, Y.; Dunleavy, M.; Henshall, D. C. Cell Signaling Underlying Epileptic Behavior. *Front. Behav. Neurosci.* **2011**, *5*, 45.

(5) Anderzhanova, E.; Wotjak, C. T. Brain Microdialysis and Its Applications in Experimental Neurochemistry. *Cell Tissue Res.* **2013**, *354* (1), 27–39.

(6) Hyman, S. E. Neurotransmitters. *Curr. Biol.* **2005**, *15* (5).

(7) Jamwal, S.; Kumar, P. Insight Into the Emerging Role of Striatal Neurotransmitters in the Pathophysiology of Parkinson's Disease and Huntington's Disease: A Review. *Curr. Neuropharmacol.* **2019**, *17* (2), 165–175.

(8) Luo, Y.; Roth, G. S. The Roles of Dopamine Oxidative Stress and Dopamine Receptor Signaling in Aging and Age-Related Neurodegeneration. *Antioxid. Redox Signal.* **2000**, *2* (3), 449–460.

(9) Hunter, R. L.; Dragicevic, N.; Seifert, K.; Choi, D. Y.; Liu, M.; Kim, H.; Cass, W. A.; Sullivan, P. G.; Bing, G. Inflammation Induces Mitochondrial Dysfunction and Dopaminergic Neurodegeneration in the Nigrostriatal System. *J. Neurochem.* **2007**, *100*, 1375–1386.

(10) Zhang, S.; Wang, R.; Wang, G. Impact of Dopamine Oxidation on Dopaminergic Neurodegeneration. *ACS Chem. Neurosci.* **2019**, *10*, 945–953.

(11) Benedetto, A.; Au, C.; Avila, D. S.; Milatovic, D.; Aschner, M. Extracellular Dopamine Potentiates Mn-Induced Oxidative Stress, Lifespan Reduction, and Dopaminergic Neurodegeneration in a BLI-3-Dependent Manner in Caenorhabditis Elegans. *PLoS Genet.* **2010**, *6* (8).

(12) Burke, W. J.; Li, S. W.; Chung, H. D.; Ruggiero, D. A.; Kristal, B. S.; Johnson, E. M.; Lampe, P.; Kumar, V. B.; Franko, M.; Williams, E. A.; Zahm, D. S. Neurotoxicity of MAO Metabolites of Catecholamine Neurotransmitters: Role in Neurodegenerative Diseases. *Neurotoxicology* **2004**, *25* (1–2), 101–115.

(13) Xiong, Y.; Neifert, S.; Karuppagounder, S. S.; Liu, Q.; Stankowski, J. N.; Lee, B. D.; Ko, H. S.; Lee, Y.; Grima, J. C.; Mao, X.; Jiang, H.; Kang, S. U.; Swing, D. A.; Iacovitti, L.; Tessarollo, L.; Dawson, T. M.; Dawson, V. L. Robust Kinase- and Age-Dependent Dopaminergic and Norepinephrine Neurodegeneration in LRRK2 G2019S Transgenic Mice. *Proc. Natl. Acad. Sci. U. S. A.* **2018**, *115* (7), 1635–1640.

(14) Nieminen-von Wendt, T. S.; Metsähonkala, L.; Kulomäki, T. A.; Aalto, S.; Autti, T. H.; Vanhala, R.; Eskola, O.; Bergman, J.; Hietala, J. A.; von Wendt, L. O. Increased Presynaptic Dopamine Function in Asperger Syndrome. *Neuroreport* **2004**, *15* (5), 757–760.

(15) Chen, L.; Ding, Y.; Cagniard, B.; Laar, A. D. Van; Mortimer, A.; Chi, W.; Hastings, T. G.; Kang, U. J.; Zhuang, X. Unregulated Cytosolic Dopamine Causes Neurodegeneration Associated with Oxidative Stress in Mice. *J. Neurosci.* **2008**, *28* (2), 425–433.

(16) Fleming, S. M.; Fernagut, P.-O.; Chesselet, M.-F. Genetic Mouse Models of Parkinsonism: Strengths and Limitations. *NeuroRx J. Am. Soc. Exp. Neurother.* **2005**, *2*, 495–503.

(17) Chen, L.; Cagniard, B.; Mathews, T.; Jones, S.; Koh, H. C.; Ding, Y.; Carvey, P. M.; Ling, Z.; Kang, U. J.; Zhuang, X. Age-Dependent Motor Deficits and Dopaminergic Dysfunction in DJ-1 Null Mice *. *J. Biol. Chem.* **2005**, *280* (22), 21418–21426.

(18) Poe, G. R.; Foote, S.; Eschenko, O.; Johansen, J. P.; Bouret, S.; Aston-Jones, G.; Harley, C. W.; Manahan-Vaughan, D.; Weinshenker, D.; Valentino, R.; Berridge, C.; Chandler, D. J.; Waterhouse, B.; Sara, S. J. Locus Coeruleus: A New Look at the Blue Spot. *Nat. Rev. Neurosci. 2020 2111* **2020**, *21* (11), 644–659.

(19) Espay, A. J.; Lewitt, P. A.; Kaufmann, H. Norepinephrine Deficiency in Parkinson's Disease: The Case for Noradrenergic Enhancement. *Mov. Disord.* **2014**, *29* (14), 1710–1719.

(20) LeWitt, P. A. Norepinephrine: The next Therapeutics Frontier for Parkinson's Disease. *Transl. Neurodegener.* **2012**, *1* (1), 1–4.

(21) Song, S.; Jiang, L.; Oyarzabal, E. A.; Wilson, B.; Li, Z.; Shih, Y. Y. I.; Wang, Q.; Hong, J. S. Loss of Brain Norepinephrine Elicits Neuroinflammation-Mediated Oxidative Injury and Selective Caudo-Rostral Neurodegeneration. *Mol. Neurobiol.* **2019**, *56* (4), 2653–2669.

(22) Fidalgo, S.; Ivanov, D. K.; Wood, S. H. Serotonin: From Top to Bottom. *Biogerontology 2012 141* **2012**, *14* (1), 21–45.

(23) Bruta, K.; Vanshika; Bhasin, K.; Bhawana. The Role of Serotonin and Diet in the Prevalence of Irritable Bowel Syndrome: A Systematic Review. *Transl. Med. Commun. 2021 61* **2021**, *6* (1), 1–9.

(24) Politis, M.; Niccolini, F. Serotonin in Parkinson's Disease. *Behav. Brain Res.* **2015**, *277*, 136–145.

(25) Mdawar, B.; Ghossoub, E.; Khoury, R. Selective Serotonin Reuptake Inhibitors and Alzheimer's Disease. *Neural Regen. Res.* **2020**, *15* (1), 41.

(26) Pagano, G.; Niccolini, F.; Fusar-Poli, P.; Politis, M. Serotonin Transporter in Parkinson's Disease: A Meta-Analysis of Positron Emission Tomography Studies. *Ann. Neurol.* **2017**, *81* (2), 171–180.

(27) Miyazaki, I.; Asanuma, M. Serotonin 1A Receptors on Astrocytes as a Potential Target for the Treatment of Parkinson's Disease. *Curr. Med. Chem.* **2016**, *23* (7), 686–700.

(28) Haffenden, V.; Patel, A. Serotonin Syndrome in Asymptomatic Huntington's Disease. *Prog. Neurol. Psychiatry* **2018**, *22* (1), 21–23.

(29) Hernandez, A. M. S.; Singh, C.; Valero, D. J.; Nisar, J.; Ramirez, J. I. T.; Kothari, K. K.; Isola, S.; Gordon, D. K. Multiple Sclerosis and Serotonin: Potential Therapeutic Applications. *Cureus* **2020**,

12 (11), e11293.

(30) Geldenhuys, W. J.; Van Der Schyf, C. J. Role of Serotonin in Alzheimer's Disease. *CNS Drugs 2011 259* **2012**, *25* (9), 765–781.

(31) Claeysen, S.; Bockaert, J.; Giannoni, P. Serotonin: A New Hope in Alzheimer's Disease? *ACS Chem. Neurosci.* **2015**, *6* (7), 940–943.

(32) Fagg, G. E.; Foster, A. C. Amino Acid Neurotransmitters and Their Pathways in the Mammalian Central Nervous System. *Neuroscience* **1983**, *9* (4), 701–719.

(33) Tiedje, K. E.; Stevens, K.; Barnes, S.; Weaver, D. F. β-Alanine as a Small Molecule Neurotransmitter. *Neurochem. Int.* **2010**, *57* (3), 177–188.

(34) Snyder, S. H.; Kim, P. M. D-Amino Acids as Putative Neurotransmitters: Focus on D-Serine. *Neurochem. Res. 2000 255* **2000**, *25* (5), 553–560.

(35) Snyder, S. H.; Ferris, C. D. Novel Neurotransmitters and Their Neuropsychiatric Relevance. *Am. J. Psychiatry* **2000**, *157* (11), 1738–1751.

(36) Socha, E.; Koba, M.; Kośliński, P. Amino Acid Profiling as a Method of Discovering Biomarkers for Diagnosis of Neurodegenerative Diseases. *Amino Acids* **2019**, *51* (3), 367–371.

(37) Brosnan, J. T.; Brosnan, M. E. Glutamate: A Truly Functional Amino Acid. *Amino Acids* **2013**, *45* (3), 413–418.

(38) Mehta, A.; Prabhakar, M.; Kumar, P.; Deshmukh, R.; Sharma, P. L. Excitotoxicity: Bridge to Various Triggers in Neurodegenerative Disorders. *Eur. J. Pharmacol.* **2013**, *698* (1–3), 6–18.

(39) Zhou, Y.; Danbolt, N. C. Glutamate as a Neurotransmitter in the Healthy Brain. *J. Neural Transm.* **2014**, *121* (8), 799.

(40) Salińska, E.; Danysz, W.; Łazarewicz, J. W. The Role of Excitotoxicity in Neurodegeneration. *Folia Neuropathol.* **2005**, *43* (4), 322–339.

(41) Kim, K.; Lee, S. G.; Kegelman, T. P.; Su, Z. Z.; Das, S. K.; Dash, R.; Dasgupta, S.; Barral, P. M.; Hedvat, M.; Diaz, P.; Reed, J. C.; Stebbins, J. L.; Pellecchia, M.; Sarkar, D.; Fisher, P. B. Role of Excitatory Amino Acid Transporter-2 (EAAT2) and Glutamate in Neurodegeneration: Opportunities for Developing Novel Therapeutics. *J. Cell. Physiol.* **2011**, *226* (10), 2484–2493.

(42) Crupi, R.; Impellizzeri, D.; Cuzzocrea, S. Role of Metabotropic Glutamate Receptors in Neurological Disorders. *Front. Mol. Neurosci.* **2019**, *12*, 20.

(43) Wolosker, H.; Dumin, E.; Balan, L.; Foltyn, V. N. D-Amino Acids in the Brain: D-Serine in Neurotransmission and Neurodegeneration. *FEBS J.* **2008**, *275* (14), 3514–3526.

(44) Kim, J.; Lee, S.; Kang, S.; Kim, S. H.; Kim, J. C.; Yang, M.; Moon, C. Brain-Derived Neurotropic Factor and GABAergic Transmission in Neurodegeneration and Neuroregeneration. *Neural Regen. Res.* **2017**, *12* (10), 1733.

(45) Kleppner, S. R.; Tobin, A. J. GABA Signalling: Therapeutic Targets for Epilepsy, Parkinson's Disease and Huntington's Disease. *https://doi.org/10.1517/14728222.5.2.219* **2005**, *5* (2), 219–239.

(46) Feigin, V. L.; Nichols, E.; Alam, T.; Bannick, M. S.; Beghi, E.; Blake, N.; Culpepper, W. J.; Dorsey, E. R.; Elbaz, A.; Ellenbogen, R. G.; Fisher, J. L.; Fitzmaurice, C.; Giussani, G.; Glennie, L.; James, S. L.; Johnson, C. O.; Kassebaum, N. J.; Logroscino, G.; Marin, B.; Mountjoy-Venning, W. C.; Nguyen, M.; Ofori-Asenso, R.; Patel, A. P.; Piccininni, M.; Roth, G. A.; Steiner, T. J.; Stovner, L. J.; Szoeke, C. E. I.; Theadom, A.; Vollset, S. E.; Wallin, M. T.; Wright, C.; Zunt, J. R.; Abbasi, N.; Abd-Allah, F.; Abdelalim, A.; Abdollahpour, I.; Aboyans, V.; Abraha, H. N.; Acharya, D.; Adamu, A. A.; Adebayo, O. M.; Adeoye, A. M.; Adsuar, J. C.; Afarideh, M.; Agrawal, S.; Ahmadi, A.; Ahmed, M. B.; Aichour, A. N.; Aichour, I.; Aichour, M. T. E.; Akinyemi, R. O.; Akseer, N.; Al-Eyadhy, A.; Al-Shahi Salman, R.; Alahdab, F.; Alene, K. A.; Aljunid, S. M.; Altirkawi, K.; Alvis-Guzman, N.; Anber, N. H.; Antonio, C. A. T.; Arabloo, J.; Aremu, O.; Ärnlöv, J.; Asayesh, H.; Asghar, R. J.; Atalay, H. T.; Awasthi, A.; Ayala Quintanilla, B. P.; Ayuk, T. B.; Badawi, A.; Banach, M.; Banoub, J. A. M.; Barboza, M. A.; Barker-Collo, S. L.; Bärnighausen, T. W.; Baune, B. T.; Bedi, N.; Behzadifar, M.; Behzadifar, M.; Béjot, Y.; Bekele, B. B.; Belachew, A. B.; Bennett, D. A.; Bensenor, I. M.; Berhane, A.; Beuran, M.; Bhattacharyya, K.; Bhutta, Z. A.; Biadgo, B.; Bijani, A.; Bililign, N.; Bin Sayeed, M. S.; Blazes, C. K.; Brayne, C.; Butt, Z. A.; Campos-Nonato, I. R.; Cantu-Brito, C.; Car, M.; Cárdenas, R.; Carrero, J. J.; Carvalho, F.; Castañeda-Orjuela, C. A.; Castro, F.; Catalá-López, F.; Cerin, E.; Chaiah, Y.; Chang, J. C.; Chatziralli, I.; Chiang, P. P. C.; Christensen, H.; Christopher, D. J.; Cooper, C.; Cortesi, P. A.; Costa, V. M.; Criqui, M. H.; Crowe, C. S.; Damasceno, A. A. M.; Daryani, A.; De la Cruz-Góngora, V.; De La Hoz, F. P.; De Leo, D.; Degefa, M. G.; Demoz, G. T.; Deribe, K.; Dharmaratne, S. D.; Diaz, D.; Dinberu, M. T.; Djalalinia, S.; Doku, D. T.; Dubey, M.; Dubljanin, E.; Duken, E. E.; Edvardsson, D.; El-Khatib, Z.; Endres, M.; Endries, A. Y.; Eskandarieh, S.; Esteghamati, A.; Esteghamati, S.; Farhadi, F.; Faro, A.; Farzadfar, F.; Farzaei, M. H.; Fatima, B.; Fereshtehnejad, S. M.; Fernandes, E.; Feyissa, G. T.; Filip, I.; Fischer, F.; Fukumoto, T.; Ganji, M.; Gankpe, F. G.; Garcia-Gordillo, M. A.; Gebre, A. K.; Gebremichael, T. G.; Gelaw, B. K.; Geleijnse, J. M.; Geremew, D.; Gezae, K. E.; Ghasemi-Kasman, M.; Gidey, M. Y.; Gill, P. S.; Gill, T. K.; Gnedovskaya, E. V.; Goulart, A. C.; Grada, A.; Grosso,

G.; Guo, Y.; Gupta, R.; Gupta, R.; Haagsma, J. A.; Hagos, T. B.; Haj-Mirzaian, A.; Haj-Mirzaian, A.; Hamadeh, R. R.; Hamidi, S.; Hankey, G. J.; Hao, Y.; Haro, J. M.; Hassankhani, H.; Hassen, H. Y.; Havmoeller, R.; Hay, S. I.; Hegazy, M. I.; Heidari, B.; Henok, A.; Heydarpour, F.; Hoang, C. L.; Hole, M. K.; Homaie Rad, E.; Hosseini, S. M.; Hu, G.; Igumbor, E. U.; Ilesanmi, O. S.; Irvani, S. S. N.; Islam, S. M. S.; Jakovljevic, M.; Javanbakht, M.; Jha, R. P.; Jobanputra, Y. B.; Jonas, J. B.; Józwiak, J. J.; Jürisson, M.; Kahsay, A.; Kalani, R.; Kalkonde, Y.; Kamil, T. A.; Kanchan, T.; Karami, M.; Karch, A.; Karimi, N.; Kasaeian, A.; Kassa, T. D.; Kassa, Z. Y.; Kaul, A.; Kefale, A. T.; Keiyoro, P. N.; Khader, Y. S.; Khafaie, M. A.; Khalil, I. A.; Khan, E. A.; Khang, Y. H.; Khazaie, H.; Kiadaliri, A. A.; Kiirithio, D. N.; Kim, A. S.; Kim, D.; Kim, Y. E.; Kim, Y. J.; Kisa, A.; Kokubo, Y.; Koyanagi, A.; Krishnamurthi, R. V.; Kuate Defo, B.; Kucuk Bicer, B.; Kumar, M.; Lacey, B.; Lafranconi, A.; Lansingh, V. C.; Latifi, A.; Leshargie, C. T.; Li, S.; Liao, Y.; Linn, S.; Lo, W. D.; Lopez, J. C. F.; Lorkowski, S.; Lotufo, P. A.; Lucas, R. M.; Lunevicius, R.; Mackay, M. T.; Mahotra, N. B.; Majdan, M.; Majdzadeh, R.; Majeed, A.; Malekzadeh, R.; Malta, D. C.; Manafi, N.; Mansournia, M. A.; Mantovani, L. G.; März, W.; Mashamba-Thompson, T. P.; Massenburg, B. B.; Mate, K. K. V.; McAlinden, C.; McGrath, J. J.; Mehta, V.; Meier, T.; Meles, H. G.; Melese, A.; Memiah, P. T. N.; Memish, Z. A.; Mendoza, W.; Mengistu, D. T.; Mengistu, G.; Meretoja, A.; Meretoja, T. J.; Mestrovic, T.; Miazgowski, B.; Miazgowski, T.; Miller, T. R.; Mini, G. K.; Mirrakhimov, E. M.; Moazen, B.; Mohajer, B.; Mohammad Gholi Mezerji, N.; Mohammadi, M.; Mohammadi-Khanaposhtani, M.; Mohammadibakhsh, R.; Mohammadnia-Afrouzi, M.; Mohammed, S.; Mohebi, F.; Mokdad, A. H.; Monasta, L.; Mondello, S.; Moodley, Y.; Moosazadeh, M.; Moradi, G.; Moradi-Lakeh, M.; Moradinazar, M.; Moraga, P.; Moreno Velásquez, I.; Morrison, S. D.; Mousavi, S. M.; Muhammed, O. S.; Muruet, W.; Musa, K. I.; Mustafa, G.; Naderi, M.; Nagel, G.; Naheed, A.; Naik, G.; Najafi, F.; Nangia, V.; Negoi, I.; Negoi, R. I.; Newton, C. R. J.; Ngunjiri, J. W.; Nguyen, C. T.; Nguyen, L. H.; Ningrum, D. N. A.; Nirayo, Y. L.; Nixon, M. R.; Norrving, B.; Noubiap, J. J.; Nourollahpour Shiadeh, M.; Nyasulu, P. S.; Ogbo, F. A.; Oh, I. H.; Olagunju, A. T.; Olagunju, T. O.; Olivares, P. R.; Onwujekwe, O. E.; Oren, E.; Owolabi, M. O.; A, M. P.; Pakpour, A. H.; Pan, W. H.; Panda-Jonas, S.; Pandian, J. D.; Patel, S. K.; Pereira, D. M.; Petzold, M.; Pillay, J. D.; Piradov, M. A.; Polanczyk, G. V.; Polinder, S.; Postma, M. J.; Poulton, R.; Poustchi, H.; Prakash, S.; Prakash, V.; Qorbani, M.; Radfar, A.; Rafay, A.; Rafiei, A.; Rahim, F.; Rahimi-Movaghar, V.; Rahman, M.; Rahman, M. H. U.; Rahman, M. A.; Rajati, F.; Ram, U.; Ranta, A.; Rawaf, D. L.; Rawaf, S.; Reinig, N.; Reis, C.; Renzaho, A. M. N.; Resnikoff, S.; Rezaeian, S.; Rezai, M. S.; Rios González, C. M.; Roberts, N. L. S.; Roever, L.; Ronfani, L.; Roro, E. M.; Roshandel, G.; Rostami, A.; Sabbagh, P.; Sacco, R. L.; Sachdev, P. S.; Saddik, B.; Safari, H.; Safari-Faramani, R.; Safi, S.; Safiri, S.; Sagar, R.; Sahathevan, R.; Sahebkar, A.; Sahraian, M. A.; Salamati,

P.; Salehi Zahabi, S.; Salimi, Y.; Samy, A. M.; Sanabria, J.; Santos, I. S.; Santric Milicevic, M. M.; Sarrafzadegan, N.; Sartorius, B.; Sarvi, S.; Sathian, B.; Satpathy, M.; Sawant, A. R.; Sawhney, M.; Schneider, I. J. C.; Schöttker, B.; Schwebel, D. C.; Seedat, S.; Sepanlou, S. G.; Shabaninejad, H.; Shafieesabet, A.; Shaikh, M. A.; Shakir, R. A.; Shams-Beyranvand, M.; Shamsizadeh, M.; Sharif, M.; Sharif-Alhoseini, M.; She, J.; Sheikh, A.; Sheth, K. N.; Shigematsu, M.; Shiri, R.; Shirkoohi, R.; Shiue, I.; Siabani, S.; Siddiqi, T. J.; Sigfusdottir, I. D.; Sigurvinsdottir, R.; Silberberg, D. H.; Silva, J. P.; Silveira, D. G. A.; Singh, J. A.; Sinha, D. N.; Skiadaresi, E.; Smith, M.; Sobaih, B. H.; Sobhani, S.; Soofi, M.; Soyiri, I. N.; Sposato, L. A.; Stein, D. J.; Stein, M. B.; Stokes, M. A.; Sufiyan, M. B.; Sykes, B. L.; Sylaja, P.; Tabarés-Seisdedos, R.; Te Ao, B. J.; Tehrani-Banihashemi, A.; Temsah, M. H.; Temsah, O.; Thakur, J. S.; Thrift, A. G.; Topor-Madry, R.; Tortajada-Girbés, M.; Tovani-Palone, M. R.; Tran, B. X.; Tran, K. B.; Truelsen, T. C.; Tsadik, A. G.; Tudor Car, L.; Ukwaja, K. N.; Ullah, I.; Usman, M. S.; Uthman, O. A.; Valdez, P. R.; Vasankari, T. J.; Vasanthan, R.; Veisani, Y.; Venketasubramanian, N.; Violante, F. S.; Vlassov, V.; Vosoughi, K.; Vu, G. T.; Vujcic, I. S.; Wagnew, F. S.; Waheed, Y.; Wang, Y. P.; Weiderpass, E.; Weiss, J.; Whiteford, H. A.; Wijeratne, T.; Winkler, A. S.; Wiysonge, C. S.; Wolfe, C. D. A.; Xu, G.; Yadollahpour, A.; Yamada, T.; Yano, Y.; Yaseri, M.; Yatsuya, H.; Yimer, E. M.; Yip, P.; Yisma, E.; Yonemoto, N.; Yousefifard, M.; Yu, C.; Zaidi, Z.; Zaman, S. Bin; Zamani, M.; Zandian, H.; Zare, Z.; Zhang, Y.; Zodpey, S.; Naghavi, M.; Murray, C. J. L.; Vos, T. Global, Regional, and National Burden of Neurological Disorders, 1990–2016: A Systematic Analysis for the Global Burden of Disease Study 2016. *Lancet. Neurol.* **2019**, *18* (5), 459.

(47) Thorpe, K. E.; Levey, A. I.; Thomas, J. *U.S. Burden of Neurodegenerative Disease: Literature Review Summary*; 2021.

(48) Liu, Z.; Tian, Y. Recent Advances in Development of Devices and Probes for Sensing and Imaging in the Brain. *Sci. China Chem. 2021 646* **2021**, *64* (6), 915–931.

(49) Chatard, C.; Meiller, A.; Marinesco, S. Microelectrode Biosensors for in Vivo Analysis of Brain Interstitial Fluid. *Electroanalysis* **2018**, *30* (6), 977–998.

(50) Su, Y.; Bian, S.; Sawan, M. Real-Time in Vivo Detection Techniques for Neurotransmitters: A Review. *Analyst* **2020**, *145* (19), 6193–6210.

(51) Tan, C.; Robbins, E. M.; Wu, B.; Cui, X. T. Recent Advances in In Vivo Neurochemical Monitoring. *Micromachines 2021, Vol. 12, Page 208* **2021**, *12* (2), 208.

(52) Ferreira, N. R.; Ledo, A.; Laranjinha, J.; Gerhardt, G. A.; Barbosa, R. M. Simultaneous

Measurements of Ascorbate and Glutamate in Vivo in the Rat Brain Using Carbon Fiber Nanocomposite Sensors and Microbiosensor Arrays. *Bioelectrochemistry* **2018**, *121*, 142–150.

(53) Kucherenko, D. Y.; Kucherenko, I. S.; Soldatkin, O. O.; Topolnikova, Y. V.; Dzyadevych, S. V.; Soldatkin, A. P. A Highly Selective Amperometric Biosensor Array for the Simultaneous Determination of Glutamate, Glucose, Choline, Acetylcholine, Lactate and Pyruvate. *Bioelectrochemistry* **2019**, *128*, 100–108.

(54) Doughty, P. T.; Hossain, I.; Gong, C.; Ponder, K. A.; Pati, S.; Arumugam, P. U.; Murray, T. A. Novel Microwire-Based Biosensor Probe for Simultaneous Real-Time Measurement of Glutamate and GABA Dynamics in Vitro and in Vivo. *Sci. Reports 2020 101* **2020**, *10* (1), 1–19.

(55) Guihen, E.; O'Connor, W. T. Current Separation and Detection Methods in Microdialysis the Drive towards Sensitivity and Speed. *Electrophoresis* **2009**, *30* (12), 2062–2075.

(56) Nandi, P.; Lunte, S. M. Recent Trends in Microdialysis Sampling Integrated with Conventional and Microanalytical Systems for Monitoring Biological Events: A Review. *Anal. Chim. Acta* **2009**, *651* (1), 1–14.

(57) Zestos, A. G.; Kennedy, R. T. Microdialysis Coupled with LC-MS/MS for In Vivo Neurochemical Monitoring. *AAPS J. 2017 195* **2017**, *19* (5), 1284–1293.

(58) Ngo, K. T.; Varner, E. L.; Michael, A. C.; Weber, S. G. Monitoring Dopamine Responses to Potassium Ion and Nomifensine by in Vivo Microdialysis with Online Liquid Chromatography at One-Minute Resolution. *ACS Chem. Neurosci.* **2017**, *8* (2), 329–338.

(59) Hamilton, E. M.; Young, S. D.; Bailey, E. H.; Humphrey, O. S.; Watts, M. J. Online Microdialysis-High-Performance Liquid Chromatography- Inductively Coupled Plasma Mass Spectrometry (MD-HPLC-ICP-MS) as a Novel Tool for Sampling Hexavalent Chromium in Soil Solution. *Environ. Sci. Technol.* **2021**, *55* (4), 2422–2429.

(60) Horstkotte, B.; Cerdà, V. Coupling of Flow Techniques with Capillary Electrophoresis: Review of Operation Principles, Challenges, Potentials, and Applications. *J. Chromatogr. Sci.* **2009**, *47* (8), 636–647.

(61) Gong, M.; Zhang, N.; Maddukuri, N. Flow-Gated Capillary Electrophoresis: A Powerful Technique for Rapid and Efficient Chemical Separation. *Anal. Methods* **2018**, *10* (26), 3131–3143.

(62) Nandi, P.; Desai, D. P.; Lunte, S. M. Development of a PDMS-Based Microchip Electrophoresis Device for Continuous Online in Vivo Monitoring of Microdialysis Samples. *Electrophoresis* **2010**,

31 (8), 1414–1422.

(63) Saylor, R. A.; Lunte, S. M. A Review of Microdialysis Coupled to Microchip Electrophoresis for Monitoring Biological Events. *J. Chromatogr. A* **2015**, *1382*, 48–64.

(64) Karlinsey, J. M. Sample Introduction Techniques for Microchip Electrophoresis: A Review. *Anal. Chim. Acta* **2012**, *725*, 1–13.

(65) E. Scott, D.; D. Willis, S.; Seth Gabbert; David Johnson; Erik Naylor; M. Janle, E.; E. Krichevsky, J.; E. Lunte, C.; M. Lunte, S. Development of an On-Animal Separation-Based Sensor for Monitoring Drug Metabolism in Freely Roaming Sheep. *Analyst* **2015**, *140* (11), 3820–3829.

(66) Oborny, N. J.; Costa, E. E. M.; Suntornsuk, L.; Abreu, F. C.; Lunte, S. M. Evaluation of a Portable Microchip Electrophoresis Fluorescence Detection System for the Analysis of Amino Acid Neurotransmitters in Brain Dialysis Samples. *Anal. Sci.* **2016**, *32* (1), 35–40.

(67) Jaquins-Gerstl, A.; Michael, A. C. Dexamethasone-Enhanced Microdialysis and Penetration Injury. *Front. Bioeng. Biotechnol.* **2020**, *8*, 1386.

(68) Tisdall, M. M.; Smith, M. Cerebral Microdialysis: Research Technique or Clinical Tool. *BJA Br. J. Anaesth.* **2006**, *97* (1), 18–25.

(69) Chefer, V. I.; Thompson, A. C.; Zapata, A.; Shippenberg, T. S. Overview of Brain Microdialysis. *Curr. Protoc. Neurosci.* **2009**, *47* (1), 7.1.1-7.1.28.

(70) CMA Probes & Guides for Microdialysis https://microdialysis.com/products/probes-guides.html (accessed 2022 -04 -04).

(71) BASi® | Microdialysis Probes https://www.basinc.com/microdialysis-probes (accessed 2022 -04 -04).

(72) Eicom Microdialysis Catalog https://eicomusa.com/Eicom_MD_Catalog/#page=1 (accessed 2022 -04 -04).

(73) Lai, Y. J.; Shen, E. Y.; Pan, W. H. T. Effects of Ascorbate in Microdialysis Perfusion Medium on the Extracellular Basal Concentration of Glutamate in Rat's Striatum. *Neurosci. Lett.* **2000**, *279* (3), 145–148.

(74) de Lange, E. C. M.; Danhof, M.; de Boer, A. G.; Breimer, D. D. Critical Factors of Intracerebral Microdialysis as a Technique to Determined the Pharmacokinetics of Drugs in Rat Brain. *Brain Res.* **1994**, *666* (1), 1–8.

(75) Nandi, P.; Scott, D. E.; Desai, D.; Lunte, S. M. Development and Optimization of an Integrated PDMS Based-Microdialysis Microchip Electrophoresis Device with on-Chip Derivatization for Continuous Monitoring of Primary Amines. *Electrophoresis* **2013**, *34* (6), 895–902.

(76) John, A. S.; Sidek, M. M.; Thang, L. Y.; Sami, S.; Tey, H. Y.; See, H. H. Online Sample Preconcentration Techniques in Nonaqueous Capillary and Microchip Electrophoresis. *J. Chromatogr. A* **2021**, *1638*, 461868.

(77) Wu, M.; Chen, W.; Wang, G.; He, P.; Wang, Q. Analysis of Acrylamide in Food Products by Microchip Electrophoresis with On-Line Multiple-Preconcentration Techniques. *Food Chem.* **2016**, *209*, 154–161.

(78) Kitagawa, F.; Kawai, T.; Sueyoshi, K.; Otsuka, K. Recent Progress of On-Line Sample Preconcentration Techniques in Microchip Electrophoresis. *Anal. Sci.* **2012**, *28* (2), 85–85.

(79) Castro, E. R.; Manz, A. Present State of Microchip Electrophoresis: State of the Art and Routine Applications. *J. Chromatogr. A* **2015**, *1382*, 66–85.

(80) *Handbook of Capillary and Microchip Electrophoresis and Associated Microtechniques*, 3rd ed.; Landers, J. P., Ed.; CRC Press, 2008.

(81) Saylor, R. A.; Reid, E. A.; Lunte, S. M. Microchip Electrophoresis with Electrochemical Detection for the Determination of Analytes in the Dopamine Metabolic Pathway. *Electrophoresis* **2015**, *36* (16), 1912–1919.

(82) Coltro, W. K. T.; Lima, R. S.; Segato, T. P.; Carrilho, E.; De Jesus, D. P.; Do Lago, C. L.; Da Silva, J. A. F. Capacitively Coupled Contactless Conductivity Detection on Microfluidic Systems—Ten Years of Development. *Anal. Methods* **2012**, *4* (1), 25–33.

(83) Hauser, P. C.; Kubáň, P. Capacitively Coupled Contactless Conductivity Detection for Analytical Techniques – Developments from 2018 to 2020. *J. Chromatogr. A* **2020**, *1632*, 461616.

(84) Schilly, K. M.; Gunawardhana, S. M.; Wijesinghe, M. B.; Lunte, S. M. Biological Applications of Microchip Electrophoresis with Amperometric Detection: In Vivo Monitoring and Cell Analysis. *Anal. Bioanal. Chem. 2020 41224* **2020**, *412* (24), 6101–6119.

(85) Gunasekara, D. B.; Wijesinghe, M. B.; Saylor, R. A.; Lunte, S. M. Principles and Strategies for Microchip Electrophoresis with Amperometric Detection. In *Electrochemical Strategies in Detection Science*; Arrigan, D. W. M., Ed.; Royal Society of Chemistry, 2015; pp 85–124.

(86) M. Gunawardhana, S.; A. Bulgakova, G.; M. Barybin, A.; R. Thomas, S.; M. Lunte, S. Progress toward the Development of a Microchip Electrophoresis Separation-Based Sensor with Electrochemical Detection for on-Line in Vivo Monitoring of Catecholamines. *Analyst* **2020**, *145* (5), 1768–1776.

(87) Mecker, L. C.; Martin, R. S. Integration of Microdialysis Sampling and Microchip Electrophoresis with Electrochemical Detection. *Anal. Chem.* **2008**, *80* (23), 9257–9264.

(88) Wang, M.; Roman, G. T.; Perry, M. L.; Kennedy, R. T. Microfluidic Chip for High Efficiency Electrophoretic Analysis of Segmented Flow from a Microdialysis Probe and in Vivo Chemical Monitoring. *Anal. Chem.* **2009**, *81* (21), 9072–9078.

(89) Wang, M.; Slaney, T.; Mabrouk, O.; Kennedy, R. T. Collection of Nanoliter Microdialysate Fractions in Plugs for Off-Line in Vivo Chemical Monitoring with up to 2 s Temporal Resolution. *J. Neurosci. Methods* **2010**, *190* (1), 39–48.

(90) Castiaux, A. D.; Selemani, M. A.; Ward, M. A.; Martin, R. S. Fully 3D Printed Fluidic Devices with Integrated Valves and Pumps for Flow Injection Analysis. *Anal. Methods* **2021**, *13* (42), 5017–5024.

(91) Sandlin, Z. D.; Shou, M.; Shackman, J. G.; Kennedy, R. T. Microfluidic Electrophoresis Chip Coupled to Microdialysis for in Vivo Monitoring of Amino Acid Neurotransmitters. *Anal. Chem.* **2005**, *77* (23), 7702–7708.

(92) Wang, M.; Hershey, N. D.; Mabrouk, O. S.; Kennedy, R. T. Collection, Storage, and Electrophoretic Analysis of Nanoliter Microdialysis Samples Collected from Awake Animals in Vivo. *Anal. Bioanal. Chem.* **2011**, *400* (7), 2013–2023.

(93) Huynh, B. H.; Fogarty, B. A.; Martin, R. S.; Lunte, S. M. On-Line Coupling of Microdialysis Sampling with Microchip-Based Capillary Electrophoresis. *Anal. Chem.* **2004**, *76* (21), 6440–6447.

(94) Oborny, N. J. Development of a Microfluidic Based Portable Analyzer for Continuous Monitoring of Glutamate and Other Amino Acid Neurotransmitters, University of Kansas, 2017.

(95) Saylor, R. A.; Lunte, S. M. PDMS/Glass Hybrid Device with a Reusable Carbon Electrode for on-Line Monitoring of Catecholamines Using Microdialysis Sampling Coupled to Microchip Electrophoresis with Electrochemical Detection. *Electrophoresis* **2018**, *39* (3), 462–469.

(96) Gunawardhana, S. M.; Lunte, S. M. Continuous Monitoring of Adenosine and Its Metabolites Using Microdialysis Coupled to Microchip Electrophoresis with Amperometric Detection. *Anal. Methods* **2018**, *10* (30), 3737–3744.

3. Microchip electrophoresis separation method for the monitoring of biogenic monoamine neurotransmitters and endogenous interferences

3.1. Introduction

The involvement of monoamine neurotransmitters in processes ranging from metabolism to memory and behavior has been widely recognized for decades[1–4], and more narrowly focused investigations into the specific function mechanisms for these compounds are still being conducted today[5–12]. Some of such studies, especially those dealing with behavior and cognition, require analysis of samples collected from animal brain tissues *in vivo*, commonly using surgically implanted microdialysis (**MD**) probes[13–16]. This technique makes it possible to perform continuous sampling from awake freely moving animals for extended periods of time, providing solutions representative of the small molecule composition of the extracellular fluid of tissues and uncontaminated with proteins. Its main shortcoming is the necessity to use low sample flow rates (typically 1 μL/min and below) to obtain high analyte recoveries because analyte transport from the tissue into the sampling solution (perfusate) is driven by diffusion, and most neurotransmitters are present in the extracellular space at very low concentrations (nM–low μM). This significantly limits the temporal resolution that can be obtained when quantification is carried out using conventional separation-based methods as they require comparatively large sample volumes, and high sample recoveries are crucial for determination of analytes with low extracellular concentrations.

On-line integration of MD sample collection and separation techniques such as liquid chromatography (**LC**) and capillary (**CE**) and microchip electrophoresis (**ME**) has been widely adopted as the approach to bypassing the need for sample handling and off-line collection of large sample volumes[14,15,17–23]. In this case, the temporal resolution of the analysis is determined by the duration of the separation method run, unless sample flow segmentation is implemented. This

analysis format also allows minimizes the interactions between the researcher and the animal model, which is critical for studies of behavior.

Use of conventional instrumentation as in the case of LC and CE, results in the need to limit the animal's mobility usually in a bowl with a swivel, which may affect experimental outcomes of behavioral studies. On the other hand, a miniaturized analytical system such as ME, especially when paired with electrochemical detection (**EC**), makes it possible to place all the analytical instrumentation on the back of a large laboratory animal (e.g., a sheep), resulting in experimental conditions where the subject can truly be considered "freely-roaming"[23]. Thanks to the possibility of incorporating continuous sample flow, low sample volume requirements, and run times significantly shorter than those of conventional CE (typically < 120 s), ME also makes it possible to carry out on-line analysis of MD samples with improved temporal resolution when compared to the conventional techniques.

The combination of microdialysis sampling with microchip electrophoresis with electrochemical detection (**MD-ME-EC**) results in a selective separation-based sensor for small molecule electroactive analytes. This instrumentation can be optimized in terms of microchip dimensions (separation channel length, etc.), materials (glass, polydimethylsiloxane (**PDMS**), plastic, or hybrid material devices), and EC detection working electrode material. While microfabricated metal electrodes are frequently used for the amperometric detection in ME experiments, a variety of carbon-based electrodes (carbon fiber, paste or ink, pyrolyzed photoresist film (**PPF**)) are also available when the analytes of interest are more easily oxidized on a carbon surface, as is the case with catecholamine neurotransmitters.[24]

Our group has successfully utilized MD-ME-EC to monitor the dopamine (**DA**) metabolic pathway compounds (Figure 3.1*a*) both *in vitro* (Figure 3.1*b,* conversion of L-3,4-dihydroxyphenylalanine

(**L-DOPA**) to DA in rat brain tissue homogenate) and *in vivo* (Figure 3.1*c*, release of DA due to neuron depolarization as a result of perfusion of a potassium-containing solution though a probe placed in rat striatum)[9]. In these studies, the microchannels had three walls of PDMS and one wall of glass, and a carbon PPF working electrode was used for amperometric detection at 1.0 V vs Ag/AgCl. The background electrolyte (**BGE**) used in these experiments consisted of 15 mM phosphate buffer pH 7.4, 2.5 mM boric acid, and 15 mM SDS. While we were able to observe *in vitro* synthesis of DA from L-DOPA and its *in vivo* release due to stimulation of neuron depolarization with K^+ solution, it must be noted that basal levels of the neurotransmitter could not be detected due to both low analyte recovery and insufficiently low limits of detection. Nonetheless, this study supports the suitability of MD-ME-EC for the *in vivo* monitoring of small molecule neuroactive compounds in MD samples.

The purpose of the present study is to expand the scope of our earlier efforts and develop a ME-EC separation method to simultaneously monitor four key monoamine neurotransmitters – dopamine, epinephrine (**EPI**), norepinephrine (**NEPI**), and serotonin (**5-HT**). Applicability of this methods to studies of biological samples is exhibited with analysis of a rat brain homogenate sample.

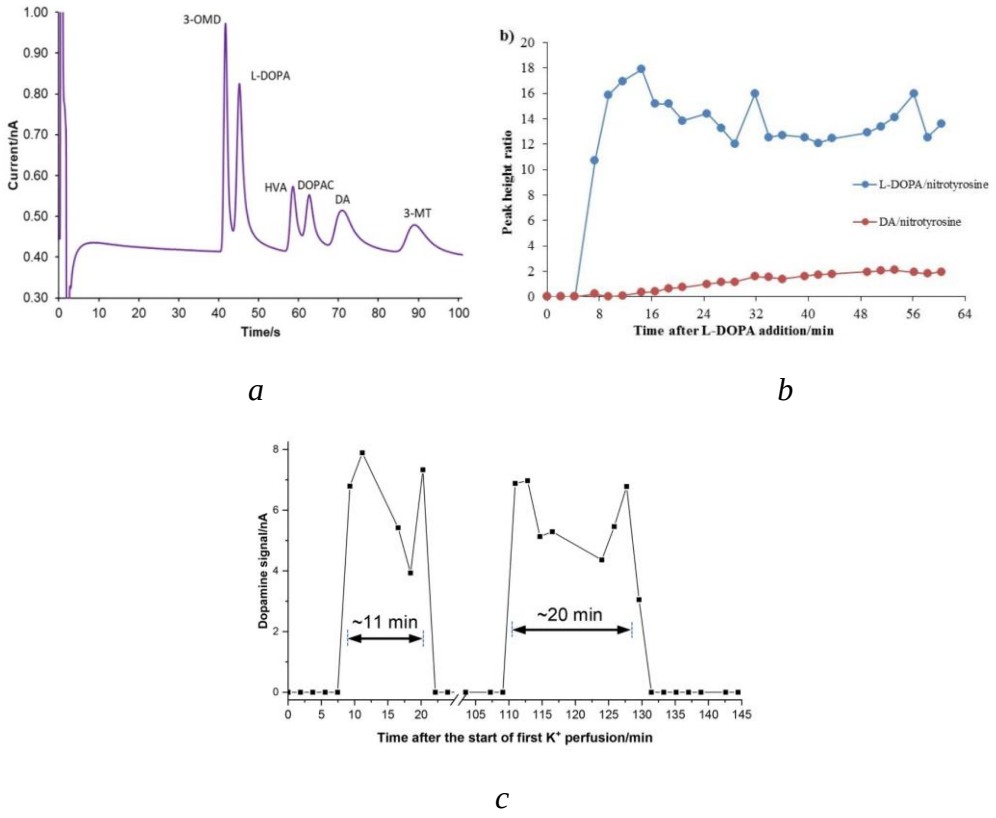

a *b*

c

Figure 3.1. (*a*) Electropherogram of an ME-EC separation of compounds in the dopamine metabolic pathway. (*b*) Production of DA from added L-DOPA in rat brain homogenate sample as a function of time. (*c*) Release of DA in rat striatum following perfusion of solution containing 100 mM K^+. All figures reproduced from Gunawardhana *et al.*[25]

3.2. Materials and methods

3.2.1. *Chemicals and reagents*

Dopamine hydrochloride, (±)-norepinephrine bitartrate salt, hydroquinone (**HQ**), sodium phosphate monobasic, sodium phosphate dibasic, boric acid, and 70% perchloric acid solution were obtained from Sigma-Aldrich (St. Louis, MO, USA). 3,4-Dihydroxyphenylacetic acid (**DOPAC**), L-(+)-ascorbic acid (**AA**), serotonin hydrochloride, and homovanillic acid (**HVA**) were purchased from Alfa Aesar (Ward Hill, MA, USA). L-(-)-epinephrine was supplied by Acros

Organics (Geel, Belgium), sodium dodecyl sulfate (**SDS**) – by Thermo Scientific (Waltham, MA, USA), and ethylenediaminetetraacetic acid disodium salt dihydrate (**EDTA**), hydrochloric acid, sodium hydroxide, sodium chloride, potassium chloride, isopropyl alcohol (**IPA**), and dimethyl sulfoxide (**DMSO**) were purchased from Fisher Scientific (Fairlawn, NJ, USA). All chemicals were used as received. Solutions were prepared using 18.2 MΩ water (Millipore, Kansas City, MO, USA).

Device fabrication was carried out using the following reagents and materials: AZ 1518 positive photoresist and AZ 300 MIF developer (AZ Electronic Materials, Sommerville, NJ, USA); SU-8 10 photoresist and SU-8 developer (Micro-Chem, Newton, MA, USA), polydimethylsiloxane resin and curing agent (Sylgard 184 silicon elastomer base and curing agent, Dow Corning Corp., Midland, MI, USA), quartz glass plates (5 in × 5 in × 0.085 in, Glass Fab, Rochester, NY, USA), copper wire (22 gage, Westlake Hardware, Lawrence, KS, USA), and colloidal silver liquid (Ted Pella, Inc., Redding, CA, USA). 0.5 mm diameter platinum wires (Goodfellow, Huntingdon, England) and Ag/AgCl reference electrodes (Bioanalytical Systems, West Lafayette, IN, USA) were also used in the experiments.

3.2.2. *PPF electrode fabrication*

30 μm-wide PPF electrodes were fabricated on quartz plates according to a previously published procedure[25]. In short, a bare quartz plate cut to 4 in × 2.5 in × 0.085 in was spin coated (Brewer Science Cee 200CBX Programmable Spin Coater) with AZ 1518 positive photoresist and prebaked at 100°C for 3 minutes. The coated plate was then allowed to cool to room temperature and exposed to a UV flood source at 20 mW/cm^2 for 10 s through a photomask. Following the exposure, the plate was baked at 100°C for 10 min and developed using AZ 300 MIF developer. After complete removal of the exposed photoresist, the plate was rinsed with reverse osmosis water, dried with N_2

flow, and post-baked at 100°C for 10 min. The quartz plate containing an electrode photofilm feature was then placed into a tube furnace and pyrolyzed at 925°C for 1 hour in N_2 atmosphere. This resulted in formation of a PPF carbon electrode that was 35 μm wide and approximately 500 nm tall. A copper lead was then attached to the plate with thin (~1 mm) bands of lab tape and hot glue and connected to the PPF electrode using colloidal silver liquid.

3.2.3. *Hybrid PDMS/glass chip fabrication*

Microchips with three walls of PDMS and one wall of quartz glass were fabricated using previously published procedure using soft lithography techniques[26]. Silicon masters with 15 μm high and 40 μm wide raised features (see chip geometry and dimensions in Figure 3.2*a*) were produced using SU-8 negative photoresist. Chips were cast from 10:1 elastomer:curing agent mixture and cured at 70 °C for at least 3 hours. A 4 mm biopsy punch was used to create buffer, buffer waste, sample solution, and sample waste wells. The chip was then aligned on a PPF electrode plate using pseudo in-channel alignment (Figure 3.2*b*).

3.2.4. *Microchip separation conditions*

Prior to analysis, all microchips were conditioned with IPA for 1 minute, 0.1 M NaOH for 3 minutes, and BGE for 3 minutes using pressure. Platinum leads were then placed in the sample and buffer wells for the application of buffer and sample potentials. Platinum grounds were placed in the sample waste and buffer waste reservoirs. Detection of analytes was carried out at 0.8 V vs. Ag/AgCl unless specified otherwise with a Pt counter electrode placed in the buffer waste reservoir. Two Spellman CZE 1000R (Hauppauge, NY, USA) high voltage power supplies were used to apply the buffer and sample potentials, electrochemical detection was carried out using a BAS 4C-LC Epsilon potentiostat (Bioanalytical Systems, West Lafayette, IN, USA) and in-house

written LabView software (National Instruments, Austin, TX, USA). Data analysis was carried out using Origin 2020 (OriginLab Corporation, Northampton, MA, USA) and Microsoft Excel (Redmond, WA, USA).

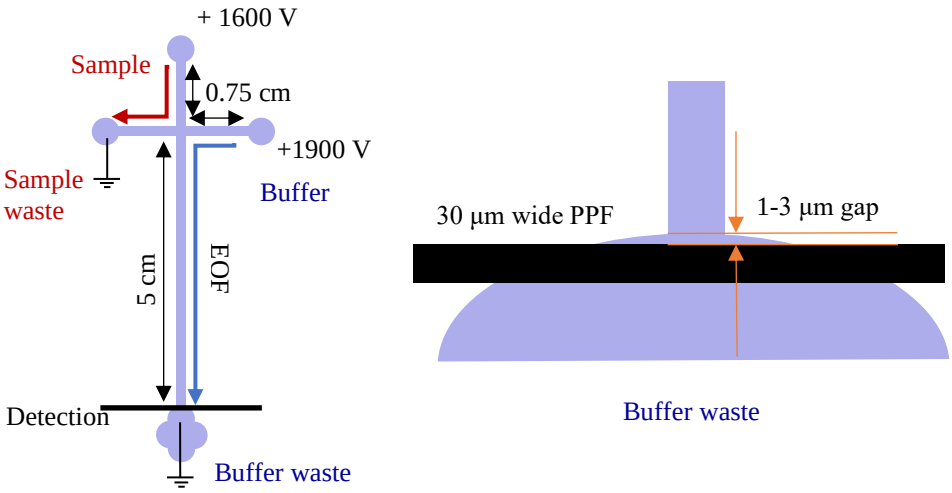

Figure 3.2. (*a*) Geometry and dimensions of a 5 cm ME device. (*b*) Pseudo in-channel alignment of the working electrode of a ME-EC device.

3.2.5. *Animal experiments*

Male Sprague Dawley rats (Charles River, Wilmington, MA, USA) were used to collect animal MD sample and brain tissues. All procedures were carried out in accordance with an Animal Use Statement approved by the Institutional Animal Care and Use Committee at the University of Kansas and meet the standards set by the Association for Assessment and Accreditation of Laboratory Animal Care.

3.2.5.1. Probe implantation procedure and brain microdialysis sample collection

Rat was anesthetized by isoflurane inhalation followed by i.p. injection of 100 mg/kg ketamine and 10 mg/kg xylazine diluted in saline. Anesthesia was maintained throughout probe implantation

surgery and MD sampling by constant flow of isoflurane (0.5–2%) supplied via nose cone. Surgery was performed using a stereotaxic instrument with the probe guide cannula placed into the striatum at the following coordinates from bregma: A/P +0.7, M/L −2.7 and V/D −3.4. The cannula was fixed to the skull with metal screw ankers and dental cement. Once the CMA 12 Elite CNS microdialysis probe with a 4 mm PAES 20 kDA MWCO membrane (CMA Microdialysis, Kista, Sweden) was placed into the cannula, it was constantly perfused with 15 mM sodium phosphate buffer solution at pH 7.4 at 1 μL/min with a CMA/102 microdialysis pump. Following 1 h post-surgery recovery a MD sample was collected for off-line analysis.

3.2.5.2. Rat brain tissue collection and preparation of brain homogenate sample for off-line analysis

Brain tissue was provided by the Johnson lab. They were collected from a male Sprague Dawley rat. Animal was anesthetized by isoflurane inhalation and euthanized via decapitation. The brain was split into hemispheres, one of which was flash frozen in liquid nitrogen and stored at –80°C prior to preparation of homogenate sample.

The collected brain tissue was thawed in ice-cold artificial cerebral spinal fluid (**aCSF**) for 10–15 min immediately prior to homogenization. Thawed tissue was weighed, and homogenization solution (0.2 M $HClO_4$ and 0.1% EDTA disodium salt) was added in the ration of 2 mL of solution per 1 g of tissue. Homogenization was carried out using bead mill homogenizer (Bead Ruptor Elite, Omni International, Kennesaw, GA, USA) in 7 mL vials using 6 beads per brain hemisphere and agitating for two consecutive rounds of two 20 s cycles at 3.1 m/s with 1 s dwell time between cycles. The resulting tissue homogenate was centrifuged (VWR International, Radnor, PA, USA) in a 2.0 mL Eppendorf tube at 4°C and 14,000 rpm for 15 min. The supernatant was collected and

centrifuged again according to the same program in a filtration tube with a 30 kDa cut-off filter (MilliporeSigma, Burlington, MA, USA).

3.3. Results and discussion

3.3.1. *Off-line analysis of a rat brain microdialysis sample*

A preliminary study determined that four biogenic neurotransmitters of interest (DA, EPI, NEPI, and 5-HT) can be separated on a PDMS-glass microchip with 5 cm long separation channel using BGE consisting of 15 mM phosphate buffer pH 7.4 and 15 mM SDS (Figure 3.3).

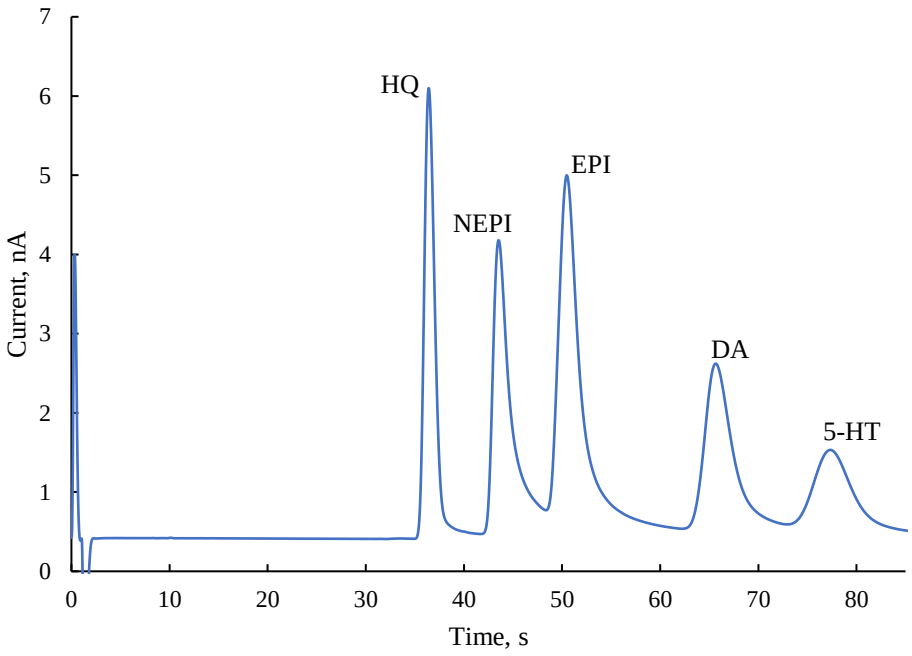

Figure 3.3. Electrophoretic separation of 4 biogenic amine neurotransmitters. BGE: 15 mM phosphate buffer pH 7.4 and 15 mM SDS. 5 cm separation channel, 220 V/cm. Detection using a 30 μm PPF working electrode at 0.8 V vs Ag/AgCl.

To evaluate the performance of this separation, off-line analysis of a rat brain MD sample was performed. The results are shown in Figure 3.4. Spiking of the sample with individual standards

of neurotransmitters suggested that one of the peaks (from here on identified as “peak X”) could correspond to the signal of EPI. However, the height of this peak was almost ½ of that of the AA peak, suggesting concentrations for these compounds in the same order of magnitudes. While ascorbate is very prevalent in the extracellular space, with concentrations around 400 μM[27], the endogenous concentrations of EPI in the brain extracellular space tend to be in the nanomolar range[28], which was below the limits of detection for this neurotransmitter in our system.

To verify the identity of peak X, the analyte standards, unspiked MD sample, and MD sample spiked with EPI were all analyzed at a lower detection potential (0.55 V vs Ag/AgCl) at the PPF working electrode. Then, peak heights ($I_{0.80}$ and $I_{0.55}$) for the EPI standard, peak X, and peak X + EPI were determined and used to calculate current ratios $I_{0.55}/I_{0.80}$. This ratio is characteristic of the electrochemical properties of each analyte and thus can be used to confirm peak identity in tandem with analyte migration time. According to the calculated values (Table 3.1), the current ratio for peak X is significantly lower than that of the EPI standard, and the ratio for the mixed peak X + EPI lies between their values, as can be expected for a signal originating from a mixture of two different compounds. This data confirms that the species contributing the most to the response obtained for peak X is not EPI.

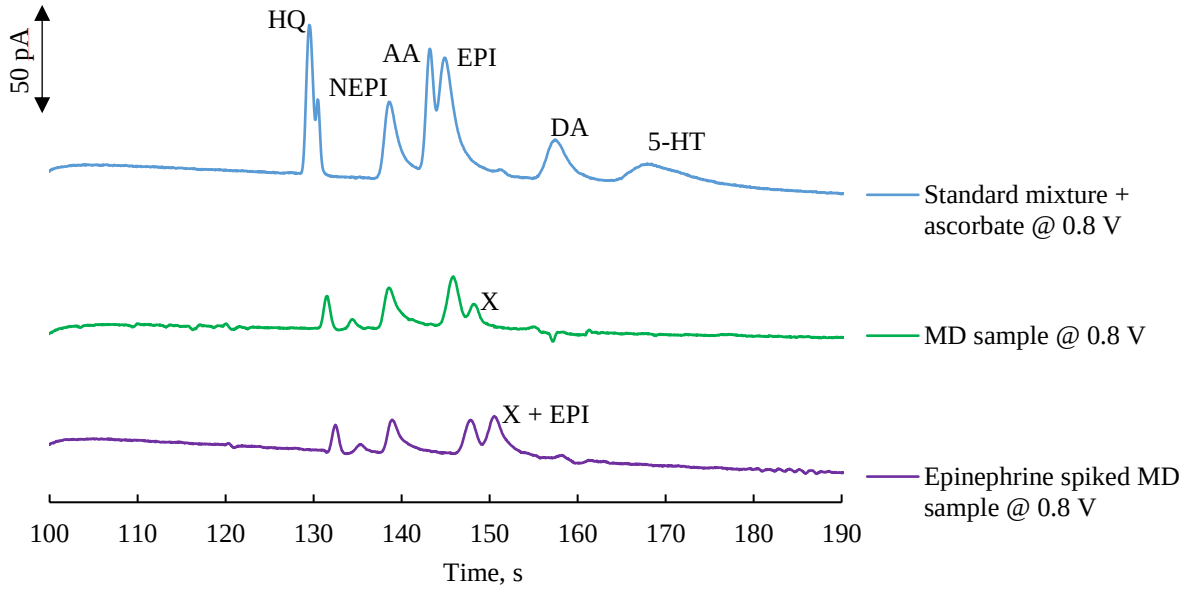

Figure 3.4. Electropherograms of biogenic amine neurotransmitter standard mixture with an addition of ascorbic acid, rat brain microdialysis sample, and the same sample spiked with EPI standard. BGE: 15 mM phosphate buffer pH 7.4 and 15 mM SDS. 5 cm separation channel, 220 V/cm. Detection using a 30 μm PPF working electrode at 0.8 V vs Ag/AgCl.

In order to determine the identity of the endogenous interference migrating at the same time as EPI, two major metabolites of dopamine – HVA and DOPAC – were investigated. It was determined that in the BGE used for the MD sample analysis these compounds both compounds comigrate with EPI, making them likely candidates for the identity of peak X. The current ratios calculated for these species (Table 3.1) indicated that while HVA exhibits $I_{0.55}/I_{0.80}$ too low for it to be considered the major constituent of the unknown peak, the ratio of DOPAC matches that of peak X. This in turn suggests that the unknown peak X is mostly made up by DOPAC. This also means that for any further study of MD samples targeting biogenic amine neurotransmitters, it is crucial to develop a separation method where the metabolites of DA and AA are fully resolved from the peaks of NEPI, EPI, DA, and 5-HT.

Table 3.1. Peak current ratios for EPI standard, unknown peak X, peak X spiked with EPI standard, and dopamine metabolites HVA and DOPAC for working electrode potentials of 0.55 V and 0.80 V. N = 3.

Species	$I_{0.55}/I_{0.80}$
EPI standard	0.98 ± 0.01
Peak X (MD sample)	0.70 ± 0.02
Peak X + EPI (spiked MD sample)	0.82 ± 0.03
DOPAC standard	0.66 ± 0.02
HVA standard	0.15 ± 0.01

3.3.2. *Separation optimization*

Optimization of the separation conditions was carried out using the analyte standard mixture containing DA, EPI, NEPI, 5-HT, DOPAC, HVA, and AA at 100 μM each in 15 mM sodium phosphate buffer pH 7.4.

3.3.2.1. Effect of boric acid on analyte resolution

The addition of boric acid to the BGE is used for these separations due to the ability of borate ions to complex with *cis*-diols present in the structures of several of the analytes of interest. The complexation alters the electrophoretic mobilities of the *cis*-diols in the sample leading to improved resolution. When the concentration of added boric acid was varied from 0 to 15 mM in 5 mM increments, the best resolution was observed at the extremes: 5 mM and 15 mM (Figure 3.5). In order to minimize the overall ionic strength of the BGE and the current generated in the separation channel, 5 mM boric acid was selected for further optimization.

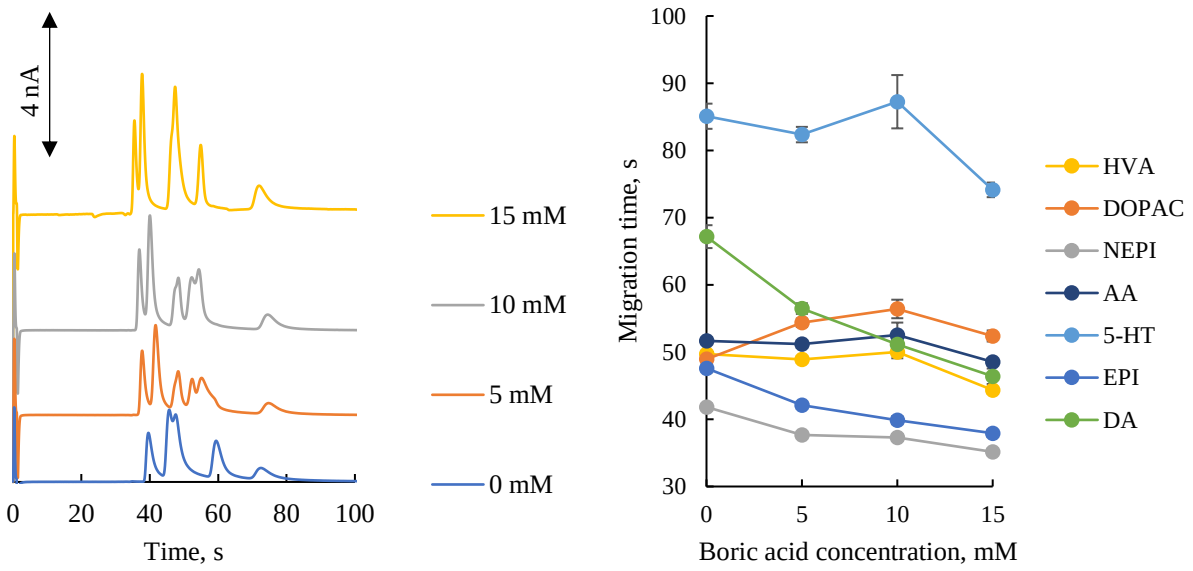

a *b*

Figure 3.5. (*a*) Electropherograms of standard analyte mixtures obtained with BGE containing 15 mM phosphate at pH 7.4, 15 mM SDS, and various concentrations of boric acid. (*b*) Analyte migration times in BGE with various boric acid content. 5 cm separation channel, 220 V/cm. Detection using a 35 μm PPF working electrode at 0.8 V vs Ag/AgCl. Each point corresponds to N = 3 injections.

3.3.2.2. Optimization of SDS content in BGE

Surfactants play an important role in separations using microchip electrophoresis. For devices constructed using polymer materials, such as PDMS, their presence is critical to create a stable charged surface in the channel necessary for maintaining constant electroosmotic flow (**EOF**). At concentrations above critical micelle concentration (**CMC**) these compounds form micelles, which can serve as a pseudo stationary phase. This creates an additional mechanism of analyte separation, micellar electrokinetic chromatography (**MEKC**), where analytes are separated based on their hydrophobicity. Thus, the more hydrophobic a compound is, the more time it will spend migrating

inside the micelles, and vice versa. The micelles are also typically highly charged thanks to their ionic hydrophilic head group, meaning that electrostatic interactions between them and the analytes of the opposite charge can be very strong, also affecting analyte migration rate.

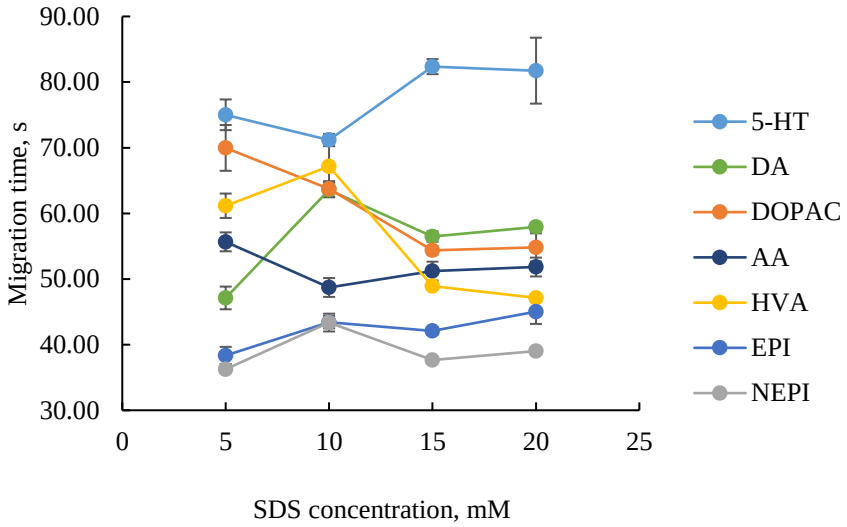

Figure 3.6. Migration times of analytes in the BGE containing 15 mM phosphate at pH 7.4, 5 mM boric acid, and various SDS concentrations. Each point corresponds to N = 3 injections.

In this study, the SDS content in the BGE was varied from 5 to 20 mM, while the concentrations of the rest of the constituents were kept constant (15 mM phosphate at pH 7.4, 5 mM boric acid). Only the lowest SDS concentration in the tested range (5 mM) was below the CMC (8 mM) of this surfactant. Two sets of conditions – 5 mM and 20 mM SDS – resulted in near-baseline resolution of the analytes of interest (Figure 3.6). However, the BGE containing the lowest SDS concentration resulted in poor day-to-day reproducibility, most likely due to the inability of such low SDS concentration to maintain a stable charged surface at the three PDMS walls of the hybrid device. Therefore, 20 mM SDS (along with 5 mM boric acid) was selected for the continued optimization of the separation conditions.

3.3.2.3. Buffer concentration effect

A number of properties make phosphate a suitable buffering agent for BGEs used for on-line MD-ME-EC separations. As it is capable of maintaining the mammalian physiological pH of 7.4, separation conditions can be selected in such a manner where there is not a pH mismatch between the BGE and the microdialysis sample solution. It is also electrochemically stable at the typical working electrode potentials (-1 V – 1.4 V) used for EC detection, enabling low electrochemical background signal.

The ionic strength of the BGE has a direct effect on any electrophoretic separation as it affects the thickness of the electrical double layer (**EDL**) near the charged surface of the channel and therefore the value of the ζ potential – the electric potential of the slip plane of the EDL. Increased concentrations of the so-called "indifferent" electrolytes (ones that do not make up the structure of the charged surface and do not have specific adsorption to it) shrink the EDL and decrease its ζ value, which in turn results in the decreased EOF. Decreasing the EOF can be beneficial as it decreases the observed (overall) mobilities of analytes and therefore increases the relative differences between analyte migration times improving resolution. On the other hand, very high electrolyte concentrations in the BGE can lead to high separation currents in the channel and Joule heating. This can then lead to changes in BGE properties including viscosity and pH, formation of gas bubbles in the microchannels, and causes higher background noise of the EC detection. Therefore, a balance must be found to ensure maximum analyte separation at reasonable separation current values.

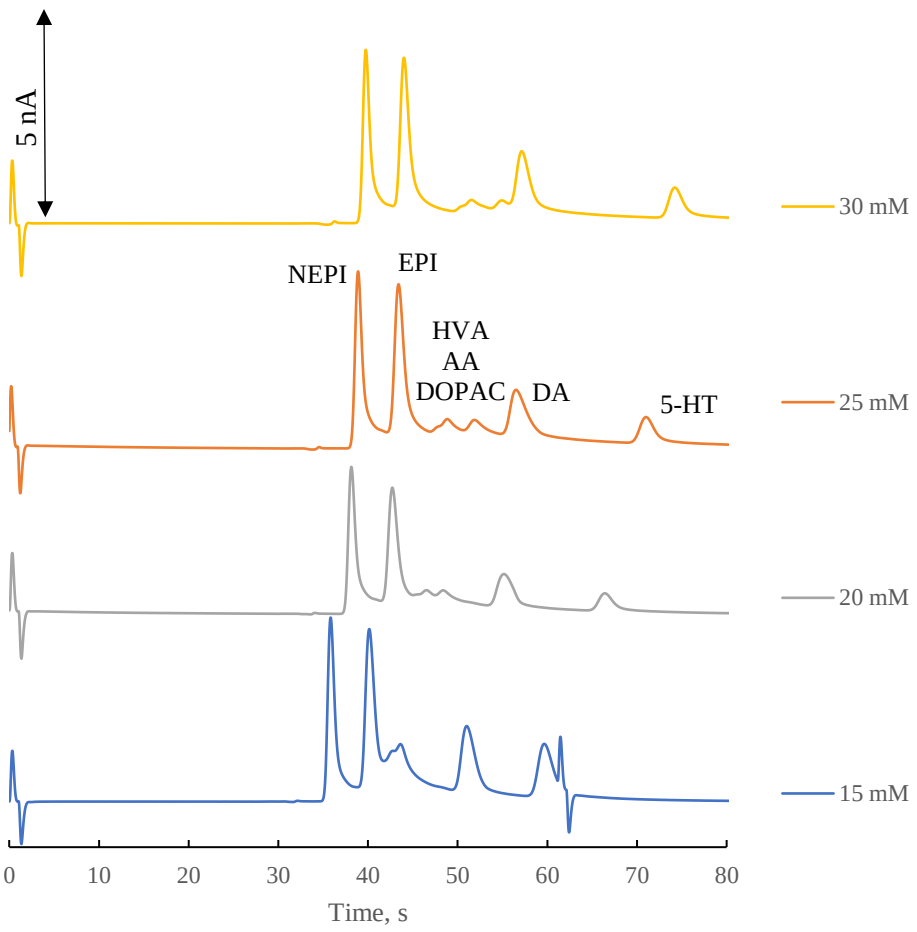

Figure 3.7. Electropherograms of standard mixture separations using BGE containing various concentrations of phosphate at pH 7.4, 5 mM boric acid, and 20 mM SDS. 5 cm separation channel, 220 V/cm. Detection using a 35 μm PPF working electrode at 0.8 V vs Ag/AgCl.

Phosphate buffer concentrations ranging from 15 mM to 30 mM were selected for the separation optimization (Figure 3.7). It was determined that increasing the concentration of the buffer made it possible to resolve the negatively charged analytes (DOPAC, HVA, and AA) from EPI. These analytes were shifted to a later migration time and closer to the DA peak. While 25 mM phosphate in the BGE showed the best resolution of HVA, DOPAC and AA from both EPI and DA, further optimization was performed using the 30 mM phosphate instead of 25 mM. This choice was made in view of the next step of BGE modification – addition of an organic solvent – that would lower

the dielectric constant of the BGE, increase its resistance, and thus lower the generated separation current, allowing to use a higher electrolyte concentration without the risk of overheating.

3.3.2.4. Addition of an organic solvent (DMSO)

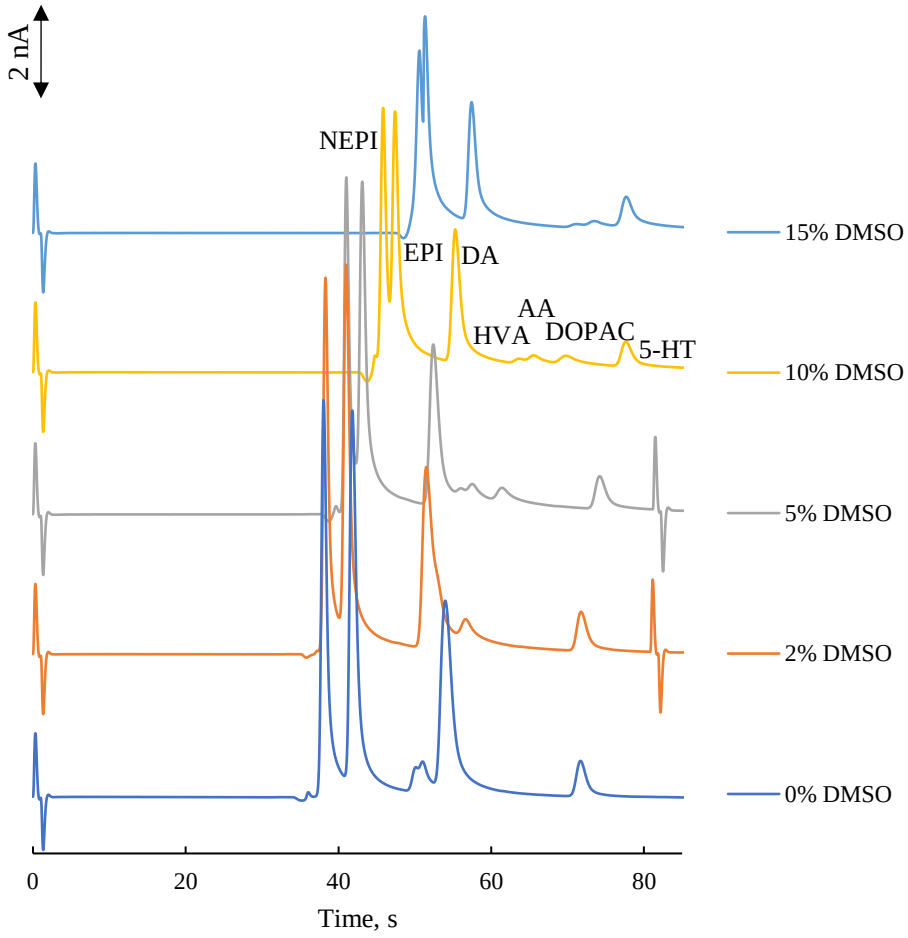

Figure 3.8. Electropherograms of standard mixture separations using BGE containing 30 mM phosphate at pH 7.4, 5 mM boric acid, 20 mM SDS, and various v/v additions of DMSO. Peaks labeled for the 10% DMSO trace. 5 cm separation channel, 220 V/cm. Detection using a 35 μm PPF working electrode at 0.8 V vs Ag/AgCl.

Organic solvents are often used to improve electrophoretic separations as they can affect the EOF by lowering the dielectric constant of the BGE and the ζ potential, and also alter the interactions

between the components of the BGE and the analytes of interest by increasing the hydrophobicity of the pseudo "mobile phase" in the MEKC based separation. In the case of the separation conditions undergoing optimization in this study, the presence of organic solvents can also affect the structure of SDS micelles, thus affecting their interactions with hydrophobic analytes.

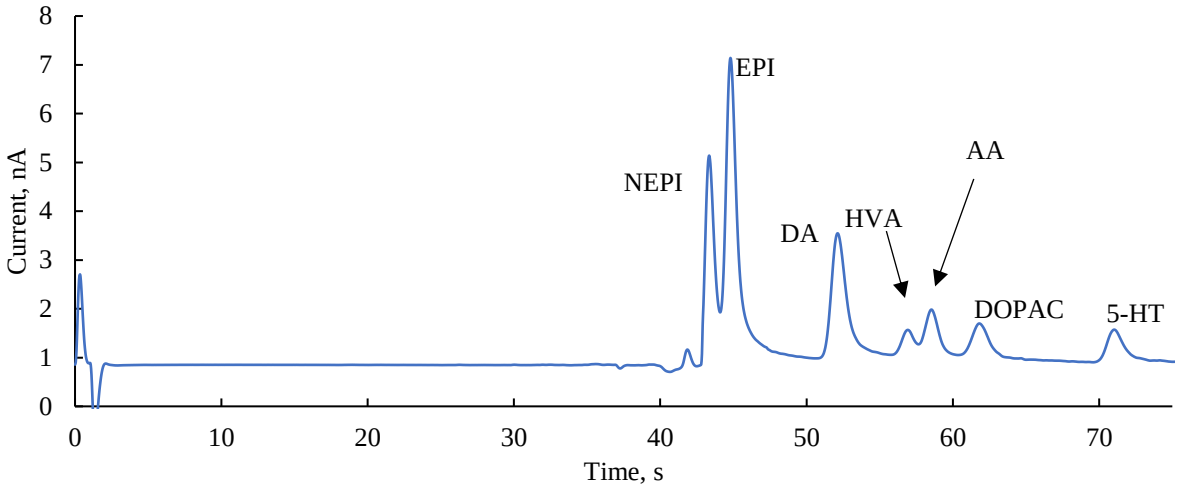

Figure 3.9. Optimized separation of the 100 µM analyte standard mixture of monoamine neurotransmitters, dopamine metabolites, and ascorbic acid in 15 mM phosphate at pH 7.4. BGE: 30 mM phosphate at pH 7.4, 5 mM boric acid, 20 mM SDS, and 10% v/v DMSO. 5 cm separation channel, 220 V/cm. Detection using a 35 µm PPF working electrode at 0.8 V vs Ag/AgCl.

Several v/v additions of dimethyl sulfoxide (**DMSO**) were tested in order to improve the separation. As can be seen in Figure 3.8, the presence of DMSO mostly affected the mobilities of the group of negatively charged analytes (DOPAC, HVA, and AA). At 0% they partially comigrated with the front of the DA peak, then shifted towards the tail of the DA peak when the DMSO concentrations were increased to 2% and 5%. At 10% DMSO they were fully resolved from all four positively charged neurotransmitters, while increasing the concentration to 15% resulted in one of these peaks (DOPAC) comigrating with 5-HT. Therefore, the BGE consisting

of 30 mM phosphate at pH 7.4, 5 mM boric acid, 20 mM SDS, and 10% v/v DMSO resulted in the best separation for these seven analytes (Figure 3.9). Interestingly, the migration order in this separation is the same as was observed for the BGE with the following composition during optimization of SDS content: 15 mM phosphate at pH 7.4, 5 mM boric acid, 5 mM SDS. This suggests that the addition of 10% of DMSO results in an increase of CMC of SDS and destruction of the micelles[29], and the high SDS concentration serves to ensure the stability of the charged surface of the microchannel.

3.3.3. *Analytical figures of merit*

Calibration curves with coefficients of determination R^2 above 0.99 were constructed for all analytes of interest (Figure 3.10). Limits of detection (LOD) were estimated as 400 nM for AA, HVA, and DOPAC, 300 nM for 5-HT, 200 nM for DA, and 100 nM for EPI and NEPI (S/N = 3). The higher LOD values for the negatively charged analytes are likely due to the inefficiency of their electrokinetic injection into the separation channel. It is also possible that a higher working electrode potential is necessary for more efficient oxidation of the analytes in the new BGE.

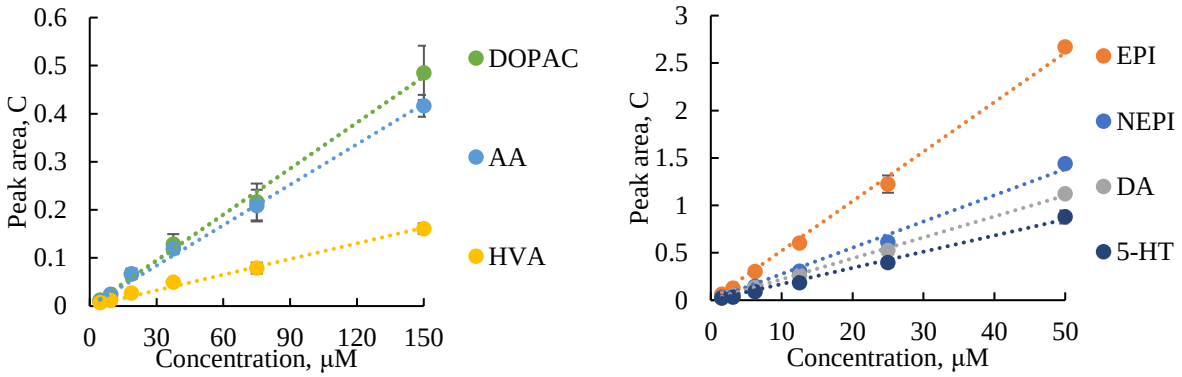

Figure 3.10. Calibration curves for the analytes of interest. All R^2 values above 0.99.

3.3.4. *Off-line analysis of a rat brain homogenate sample*

Analysis of a rat brain homogenate sample was carried out following its dilution with deionized water in 1:1 ratio by volume. This made it possible to maintain an electrophoretic current in the sample channel that was similar to that observed for analyte standard mixtures prepared in 15 mM phosphate pH 7.4. Eleven peaks were observed in the electropherogram of the tissue homogenate (Figure 3.11), eight of which are above the LOD.

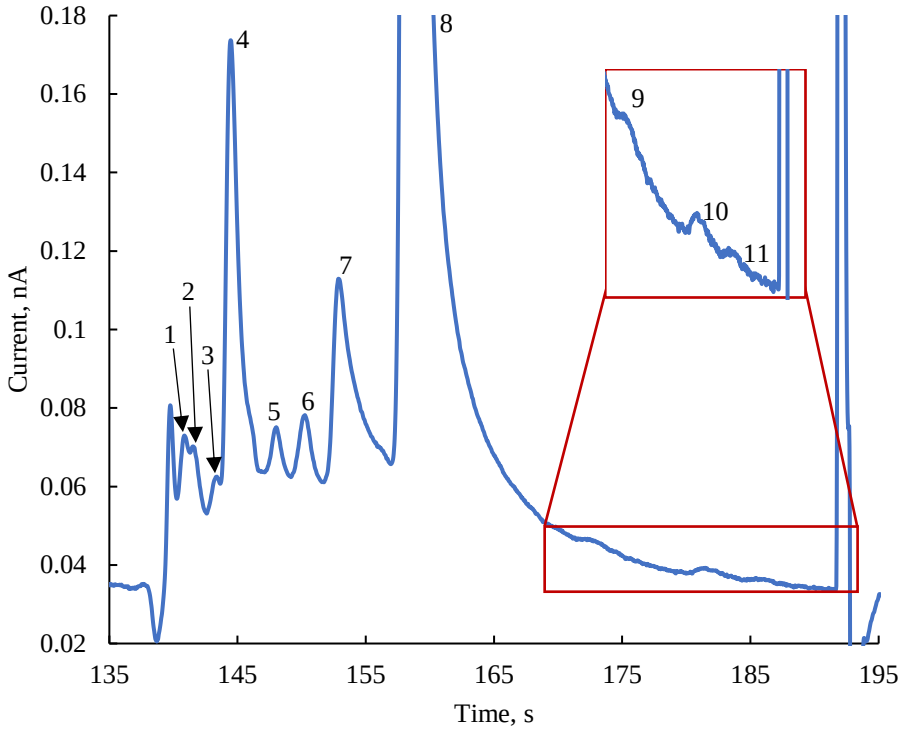

Figure 3.11. Electropherogram of rat brain homogenate sample diluted with water 1:1 by volume. Signal for peaks 1-8 is above the limits of detection. BGE: 30 mM phosphate at pH 7.4, 5 mM boric acid, 20 mM SDS, and 10% v/v DMSO. 5 cm separation channel, 220 V/cm. Detection using a 35 μm PPF working electrode at 0.8 V vs Ag/AgCl.

Identification of the detected compounds was performed by calculating their experimental mobilities using their migration times and migration time of the EOF marker (negative peak due

to the absence of BGE components in the sample matrix) and comparing them to those of the analyte standards (Table 3.2). The decision to use mobilities instead of migration times was made due to the run-to-run variations of EOF, and evident from the changes of the neutral marker migration time. Peaks matching the mobilities of the monoamine neurotransmitters were observed. NEPI and DA were quantified at high nanomolar – low micromolar concentrations, which agreed with values available in literature[30,31], although it is clear that there is some heterogeneity in the normal tissue concentrations determined during similar studies performed by different authors.

The peak identified as EPI could not be reliably integrated due to the unstable baseline and partial comigration with a neighboring peak, and the signal correlating with 5-HT was too low for both reliable identification and quantification. A large AA peak (8 in Figure 3.11) was also present and apparently masked the peaks of the negatively charged dopamine metabolites HVA and DOPAC. In future experiments, quantification of these compounds in homogenate samples can be carried out following enzymatic degradation of AA using L-ascorbate oxidase. Moreover, to improve the reliability of quantification of the compounds of interest, an internal standard can be added to the homogenate sample during dilution, thus allowing for control of injection repeatability.

Table 3.2. Electrophoretic mobilities, peak identities, and concentrations calculated for the peaks present in the rat brain homogenate sample. Experimental mobilities were calculated using peak migration times and migration time of the EOF marker (negative peak due to the absence of BGE components in the sample matrix). N = 3 for the data obtained in the course of the current study.

Peak #	Experimental mobility, $10^{-4}\cdot cm^2/(V\cdot s)$	Peak identity	Concentration, nM	Found ng/g of brain tissue	Literature[30] ng/g of brain tissue	Literature[31] ng/g of brain tissue
1	-0.19 ± 0.09					
2	-0.329 ± 0.009	NEPI	900 ± 100	300 ± 40	270 ± 40	1775.32 ± 548.39
3	-0.521 ± 0.008	EPI	N/A	N/A		
4	-0.62 ± 0.02					
5	-0.95 ± 0.04					
6	-1.12 ± 0.04	DA	1800 ± 400	600 ± 20	4270 ± 80	650.52 ± 111.64
7	-1.31 ± 0.04					
8	-1.68 ± 0.04	AA	$> 1\cdot10^6$	> 400000		
9	-2.30 ± 0.08	5-HT*	N/A	N/A	450 ± 50	887.16 ± 362.67
10	-2.62 ± 0.07					
11	-2.76 ± 0.06					

*Peak 9 is only tentatively identified at 5-HT as it is not above LOD.

3.4. Conclusions

An electrophoretic separation method for four biogenic amine neurotransmitters, two metabolites of dopamine, and ascorbic acid was developed in order to resolve metabolite peaks from the EPI peak. The optimized BGE contained 30 mM phosphate at pH 7.4, 5 mM boric acid, 20 mM SDS, and 10% v/v DMSO, with the separation carried out using a 5 cm hybrid quartz glass-PDMS microchip and a PPF working electrode. Submicromolar limits of detection were achieved for all analytes of interest with a linearity range of 2 orders of magnitude. The method was successfully

evaluated for the analysis of rat brain homogenate samples; however it must be noted that if determination of the negatively charged metabolites of dopamine HVA and DOPAC is desired, the AA contained in the sample must be enzymatically degraded. Lastly, the method can be further improved by introducing an internal standard to accommodate for both run-to-run sample injection variation and the differences in injection between the standard solutions in 15 mM phosphate pH 7.4 and diluted homogenate samples.

3.5. References

(1) Hyman, S. E. Neurotransmitters. *Curr. Biol.* **2005**, *15* (5).

(2) Nonogaki, K.; Iguchi, A. Role of Central Neural Mechanisms in the Regulation of Hepatic Glucose Metabolism. *Life Sci.* **1997**, *60* (11), 797–807.

(3) Rommelfanger, K. S.; Weinshenker, D. Norepinephrine: The Redheaded Stepchild of Parkinson's Disease. *Biochem. Pharmacol.* **2007**, *74* (2), 177–190.

(4) Bloom, F. E.; Schulman, J. A.; Koob, G. F. Catecholamines and Behavior. **1989**, 27–88.

(5) Ittner, C.; Burek, M.; Störk, S.; Nagai, M.; Förster, C. Y. Increased Catecholamine Levels and Inflammatory Mediators Alter Barrier Properties of Brain Microvascular Endothelial Cells in Vitro. *Front. Cardiovasc. Med.* **2020**, *7*, 73.

(6) Grant, A. H.; Terminel, M. A.; Ramos, J.; Alatorre, L. F.; Castañeda, E. Electrical Stimulation Evokes Rotational Behavior In Tandem with Exocytotic-like Increases in Dopamine Measured by In Vivo Intracerebral Microdialysis. *J. Neurosci. Methods* **2020**, *346*, 108894.

(7) Rakovska, A.; Javitt, D.; Petkova-Kirova, P.; Balla, A.; Ang, R.; Kalfin, R. Neurochemical

Evidence That Cysteamine Modulates Amphetamine-Induced Dopaminergic Neuronal Activity in Striatum by Decreasing Dopamine Release: An in Vivo Microdialysis Study in Freely Moving Rats. *Brain Res. Bull.* **2019**, *153*, 39–46.

(8) Sanna, F.; Bratzu, J.; Piludu, M. A.; Corda, M. G.; Melis, M. R.; Giorgi, O.; Argiolas, A. Dopamine, Noradrenaline and Differences in Sexual Behavior between Roman High and Low Avoidance Male Rats: A Microdialysis Study in the Medial Prefrontal Cortex. *Front. Behav. Neurosci.* **2017**, *11*, 108.

(9) M. Gunawardhana, S.; A. Bulgakova, G.; M. Barybin, A.; R. Thomas, S.; M. Lunte, S. Progress toward the Development of a Microchip Electrophoresis Separation-Based Sensor with Electrochemical Detection for on-Line in Vivo Monitoring of Catecholamines. *Analyst* **2020**, *145* (5), 1768–1776.

(10) Suyama, J. A.; Sakloth, F.; Kolanos, R.; Glennon, R. A.; Lazenka, M. F.; Negus, S. S.; Banks, M. L. Abuse-Related Neurochemical Effects of Para-Substituted Methcathinone Analogs in Rats: Microdialysis Studies of Nucleus Accumbens Dopamine and Serotonin. *J. Pharmacol. Exp. Ther.* **2016**, *356* (1), 182–190.

(11) Portas, C. M.; Bjorvatn, B.; Ursin, R. Serotonin and the Sleep/Wake Cycle: Special Emphasis on Microdialysis Studies. *Prog. Neurobiol.* **2000**, *60* (1), 13–35.

(12) Castner, S. A.; Xiao, L.; Becker, J. B. Sex Differences in Striatal Dopamine: In Vivo Microdialysis and Behavioral Studies. *Brain Res.* **1993**, *610* (1), 127–134.

(13) Westerink, B. H. C. Brain Microdialysis and Its Application for the Study of Animal Behaviour. *Behav. Brain Res.* **1995**, *70* (2), 103–124.

(14) Zestos, A. G.; Kennedy, R. T. Microdialysis Coupled with LC-MS/MS for In Vivo Neurochemical Monitoring. *AAPS J. 2017 195* **2017**, *19* (5), 1284–1293.

(15) Kennedy, R. T. Emerging Trends in in Vivo Neurochemical Monitoring by Microdialysis. *Curr. Opin. Chem. Biol.* **2013**, *17* (5), 860–867.

(16) Linthorst, A. C. E.; Reul, J. M. Stress and the Brain: Solving the Puzzle Using Microdialysis. *Pharmacol. Biochem. Behav.* **2008**, *90* (2), 163–173.

(17) Nandi, P.; Lunte, S. M. Recent Trends in Microdialysis Sampling Integrated with Conventional and Microanalytical Systems for Monitoring Biological Events: A Review. *Anal. Chim. Acta* **2009**, *651* (1), 1–14.

(18) Guihen, E.; O'Connor, W. T. Current Separation and Detection Methods in Microdialysis the Drive towards Sensitivity and Speed. *Electrophoresis* **2009**, *30* (12), 2062–2075.

(19) Guihen, E.; O'Connor, W. T. Capillary and Microchip Electrophoresis in Microdialysis: Recent Applications. *Electrophoresis* **2010**, *31* (1), 55–64.

(20) Nirogi, R.; Mudigonda, K.; Kandikere, V.; Ponnamaneni, R. Quantification of Acetylcholine, an Essential Neurotransmitter, in Brain Microdialysis Samples by Liquid Chromatography Mass Spectrometry. *Biomed. Chromatogr.* **2010**, *24* (1), 39–48.

(21) Schultz, K. N.; Kennedy, R. T. Time-Resolved Microdialysis for In Vivo Neurochemical Measurements and Other Applications. *Annual Rev. Anal. Chem.* **2008**, *1* (1), 627–661.

(22) Saylor, R. A.; Lunte, S. M. A Review of Microdialysis Coupled to Microchip Electrophoresis for Monitoring Biological Events. *J. Chromatogr. A* **2015**, *1382*, 48–64. https://doi.org/10.1016/J.CHROMA.2014.12.086.

(23) E. Scott, D.; D. Willis, S.; Seth Gabbert; David Johnson; Erik Naylor; M. Janle, E.; E. Krichevsky, J.; E. Lunte, C.; M. Lunte, S. Development of an On-Animal Separation-Based Sensor for Monitoring Drug Metabolism in Freely Roaming Sheep. *Analyst* **2015**.

(24) Schilly, K. M.; Gunawardhana, S. M.; Wijesinghe, M. B.; Lunte, S. M. Biological Applications of Microchip Electrophoresis with Amperometric Detection: In Vivo Monitoring and Cell Analysis. *Anal. Bioanal. Chem. 2020 41224* **2020**, *412* (24), 6101–6119.

(25) Gunawardhana, S. M.; Bulgakova, G. A.; Barybin, A. M.; Thomas, S. R.; Lunte, S. M. Progress toward the Development of a Microchip Electrophoresis Separation-Based Sensor with Electrochemical Detection for on-Line: In Vivo Monitoring of Catecholamines. *Analyst* **2020**, *145* (5), 1768–1776.

(26) Saylor, R. A.; Reid, E. A.; Lunte, S. M. Microchip Electrophoresis with Electrochemical Detection for the Determination of Analytes in the Dopamine Metabolic Pathway. *Electrophoresis* **2015**, *36* (16), 1912–1919.

(27) Miele, M.; Fillenz, M. In Vivo Determination of Extracellular Brain Ascorbate. *J. Neurosci. Methods* **1996**, *70* (1), 15–19.

(28) Routledge, C.; Marsden, C. A. Adrenaline in the CNS: In Vivo Evidence for a Functional Pathway Innervating the Hypothalamus. *Neuropharmacology* **1987**, *26* (7), 823–830.

(29) Al-Sherbini, E. S. A. M.; Abdel-Kader, M. H.; Hamzah, R. Y. Effect of Binary Solvents on the Critical Micelles Concentration by Using 1-Methyl-4-[4′-Aminostyryl]Pyridinium Iodide. *Colloids Surfaces A Physicochem. Eng. Asp.* **2001**, *194* (1–3), 133–142.

(30) Yoshitake, T.; Kehr, J.; Yoshitake, S.; Fujino, K.; Nohta, H.; Yamaguchi, M. Determination of Serotonin, Noradrenaline, Dopamine and Their Metabolites in Rat Brain Extracts and Microdialysis Samples by Column Liquid Chromatography with Fluorescence Detection Following Derivatization with Benzylamine and 1,2-Diphenylethylenediamine. *J. Chromatogr. B* **2004**, *807* (2), 177–183.

(31) Su, F.; Wang, F.; Zhu, R.; Li, H. Determination of 5-Hydroxytryptamine, Norepinephrine, Dopamine and Their Metabolites in Rat Brain Tissue by LC-ESI-MS-MS. *Chromatographia* **2009**, *69* (3–4), 207–213.

4. Coupling *in vivo* microdialysis sampling with microchip electrophoresis: compatibility of the separation with Ca^{2+}-containing perfusates

4.1. Introduction

On-line analysis of biological samples is a very attractive approach to studies that aim at drawing connections between behavior or disease states and the presence of specific compounds in tissues. Improved temporal resolution and elimination of errors and sample loss during sample handling are two major advantages to this mode of analyte quantification. At the same time, direct coupling of sampling method to detection raises two critical questions: availability of instrumentation and compatibility of the sample and the analysis method.

Microdialysis (**MD**) is a commonly utilized sampling technique that produces macromolecule-free solutions with small molecule composition representative of the probe environment (e.g. extracellular space). Studies utilizing MD sampling from the brain typically utilize perfusates that contain metal ions in the concentrations matching those in the extracellular fluid to ensure zero net flux of these ions across the probe membrane preventing their depletion in the tissues due to their diffusion into dialysate. Therefore, during cerebral MD either artificial cerebrospinal fluid (**aCSF**), artificial extracellular fluid, or Ringer's solution[1–3] are used for perfusion and make up the MD sample matrix.

Microchip electrophoresis (**ME**) is a microfluidic separation technique that when paired with an appropriate detection method makes it possible to monitor multiple compounds in small volumes of sample. It is an analytical method well-suited for paring with MD, and several instrumental approaches are available for coupling continuous flow of MD sample with the ME separation channel[4]. While some studies have been able to use aCSF as perfusate when coupling MD with ME[5,6], in general use of samples with high salt content is not favored, as it results in sample destacking due to the lower ionic strength of the background electrolyte (**BGE**) used for the separation. To prevent degradation of the separation due to sample destacking, some brain MD-

ME experiments have utilized perfusates similar in composition to that of the separation BGE[7,8]. At the same time, omission of Ca^{2+} from perfusates has been shown to significantly lower the recovery of monoamine neurotransmitters from the brain in both awake[9–11] and anesthetized[12] rats with microdialysis sampling. This means that simply using BGE buffers as perfusates instead of aCSF during MD sampling will inevitably have a negative effect on the results of any MD-ME experiment.

Chapter 3 of this thesis describes the development of a ME separation with electrochemical detection (**ME-EC**) for monitoring of four monoamine neurotransmitters dopamine (**DA**), epinephrine (**EPI**), norepinephrine (**NEPI**), and serotonin (**5-HT**), two DA metabolites homovanillic acid (**HVA**) and 3,4-dihydroxyphenylacetic acid (**DOPAC**) and endogenous antioxidant ascorbic acid (**AA**). The BGE utilized in those studies was 30 mM sodium phosphate pH 7.4. However, the use of this BGE as a microdialysis perfusate did not allow us to add $CaCl_2$ at the physiological concentration of 1.2 mM due to the formation of the highly insoluble calcium phosphate. Furthermore, when 2.4 mM solution of $CaCl_2$ either in water or in HEPES buffer pH 7.4 was injected into the ME-EC system using the previously developed BGE, a precipitate formed in the sample channel at the sample and buffer channel intersection where the BGE flow and the sample flow came in contact (Figure 4.1).

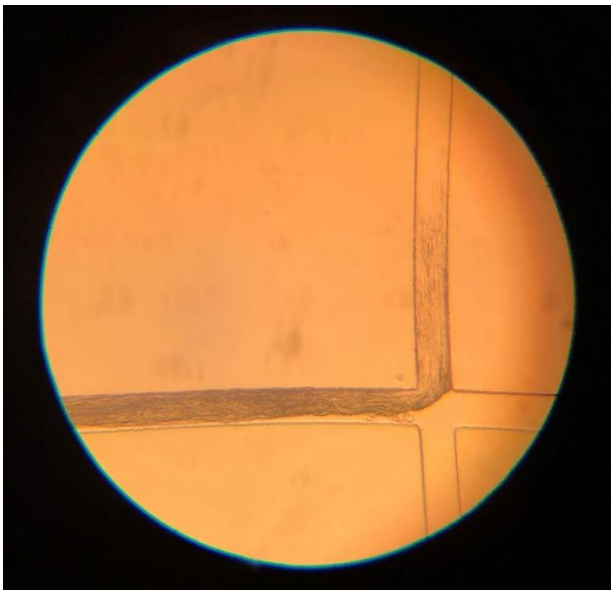

Figure 4.1. Formation of precipitate in the sample channels of a ME-EC device in the presence of 2.4 mM Ca^{2+} in the sample matrix and BGE consisting of 30 mM phosphate at pH 7.4, 5 mM boric acid, 20 mM SDS, and 10% v/v DMSO. 5 cm separation channel, 220 V/cm, detection at 0.8 V vs Ag/AgCl.

The goal of the present study was to develop a new ME-EC method for the analytes of interest (DA, EPI, NEPI, 5-HT, HAV, DOPAC, and AA) that would not employ phosphate buffer and would be compatible with MD perfusates containing calcium ions, ensuring optimal recovery of the neurotransmitters of interest from the tissues.

4.2. Materials and methods

4.2.1. *Chemicals and reagents*

Dopamine hydrochloride, (±)-norepinephrine bitartrate salt, sodium phosphate monobasic, sodium phosphate dibasic, boric acid, 4-(2-hydroxyethyl)-1-piperazineethanesulfonic acid (**HEPES**), magnesium chloride, and calcium chloride were obtained from Sigma-Aldrich (St. Louis, MO, USA). 3,4-Dihydroxyphenylacetic acid, L-(+)-ascorbic acid, serotonin hydrochloride,

and homovanillic acid were purchased from Alfa Aesar (Ward Hill, MA, USA). L-(-)-epinephrine was supplied by Acros Organics (Geel, Belgium), sodium dodecyl sulfate (**SDS**) – by Thermo Scientific (Waltham, MA, USA), and 2-(N-morpholino)ethanesulfonic acid (**MES**) monohydrate, ethylenediamine tetraacetic acid, disodium salt dihydrate (**EDTA**), hydrochloric acid, sodium hydroxide, sodium chloride, potassium chloride, isopropyl alcohol (**IPA**), acetonitrile (**ACN**), and dimethyl sulfoxide (**DMSO**) were purchased from Fisher Scientific (Fairlawn, NJ, USA). All chemicals were used as received. Solutions were prepared using 18.2 MΩ water (Millipore, Kansas City, MO, USA).

Device fabrication was carried out using the following reagents and materials: AZ 1518 positive photoresist and AZ 300 MIF developer (AZ Electronic Materials, Sommerville, NJ, USA); SU-8 10 photoresist and SU-8 developer (Micro-Chem, Newton, MA, USA), polydimethylsiloxane resin and curing agent (Sylgard 184 silicon elastomer base and curing agent, Dow Corning Corp., Midland, MI, USA), quartz glass plates (5 in × 5 in × 0.085 in, Glass Fab, Rochester, NY, USA), copper wire (22 gage, Westlake Hardware, Lawrence, KS, USA), and colloidal silver liquid (Ted Pella, Inc., Redding, CA, USA). 0.5 mm diameter platinum wires (Goodfellow, Huntingdon, England) and Ag/AgCl reference electrodes (Bioanalytical Systems, West Lafayette, IN, USA) were also used in the experiments.

4.2.2. *PPF electrode fabrication*

The 35 μm-wide PPF electrodes were fabricated on quartz plates according to a previously published procedure[8]. In short, a bare quartz plate cut to 4 in × 2.5 in × 0.085 in was spin coated (Brewer Science Cee 200CBX Programmable Spin Coater) with AZ 1518 positive photoresist and prebaked at 100°C for 3 minutes. The coated plate was then allowed to cool to room temperature and exposed to a UV flood source at 20 mW/cm^2 for 10 s through a photomask. Following the

exposure, the plate was baked at 100°C for 10 min and developed using AZ 300 MIF developer. After complete removal of the exposed photoresist, the plate was rinsed with reverse osmosis water, dried with N_2 flow, and postbaked at 100°C for 10 min. The quartz plate containing an electrode photofilm feature was then placed into a tube furnace and pyrolyzed at 925°C for 1 hour in N_2 atmosphere. This resulted in formation of a PPF carbon electrode that was 35 μm wide and approximately 500 nm tall. A copper lead was then attached to the plate with thin (~1 mm) bands of lab tape and hot glue and connected to the PPF electrode using colloidal silver liquid.

4.2.3. *"Simple t" hybrid PDMS/glass chip fabrication*

Microchips with three walls of PDMS and one wall of quartz glass were fabricated using a previously published procedure using soft lithography techniques[13]. Silicon masters with raised features (see chip geometry and dimensions in Figure 4.2*a*) were produced using SU-8 negative photoresist. Chips were cast from 10:1 elastomer:curing agent mixture and cured at 70 °C for at least 3 hours. A 4 mm biopsy punch was used to create buffer, buffer waste, sample, and sample waste wells. The chip was then aligned on a PPF electrode plate using pseudo in-channel alignment (Figure 4.2*c*).

4.2.4. *"Double t" hybrid PDMS/glass chip fabrication*

Microchips from PDMS were fabricated using a previously published procedure via soft lithography[13]. Silicon masters with raised features for a 5 cm "double t" on-line chip (see geometry and dimensions in Figure 4.2*b*) were produced using SU-8 negative photoresist. Chips were cast from 10:1 elastomer:curing agent mixture and cured at 70 °C for at least 3 hours. A 4 mm biopsy punch was used to create buffer, buffer waste, sample solution, and sample waste wells. The on-line sample inlet was punched in the chip with a 20-gauge needle with a flat sharp edge. The chip

was then aligned on the PPF electrode using pseudo in-channel alignment (Figure 4.2*c*), the top half of it was then irreversibly bonded to the quartz plate using a hand-held corona discharger wand (Model BD 20: Electro-Technic Products, Inc., Chicago, IL, USA) and a blow dryer as described in reference 14. Following bonding of PDMS to quartz, a 10–15 mm stainless steel pin was inserted into the sample inlet and fixed in place with epoxy glue. PEEK tubing carrying the sample from the MD probe or syringe pump (CMA/102 microdialysis pump, CMA Microdialysis, Kista, Sweden) to the microchip was then connected to this pin with a silicon tubing connector.

4.2.5. *Off-line microchip separation conditions*

Prior to analysis, all microchips were conditioned with IPA for 1 minute, 0.1 M NaOH for 3 minutes, and BGE for 3 minutes using pressure. Platinum leads were then placed in the sample and buffer wells for the application of buffer and sample potentials. Platinum grounds were placed in the sample waste and buffer waste reservoirs. Two Spellman CZE 1000R (Hauppauge, NY, USA) high voltage power supplies were used to apply the buffer (+1900 V) and sample (+1600 V) potentials. Sample injection was carried out by floating the buffer potential for 1.5 s while keeping the sample potential on. Detection of analytes was carried out at 0.8 V vs. Ag/AgCl with a Pt counter electrode using a BAS 4C-LC Epsilon electrochemical detector (Bioanalytical Systems, West Lafayette, IN, USA) and in-house written LabView software (National Instruments, Austin, TX, USA). Data analysis was carried out using Origin 2020 (OriginLab Corporation, Northampton, MA, USA) and Microsoft Excel (Redmond, WA, USA).

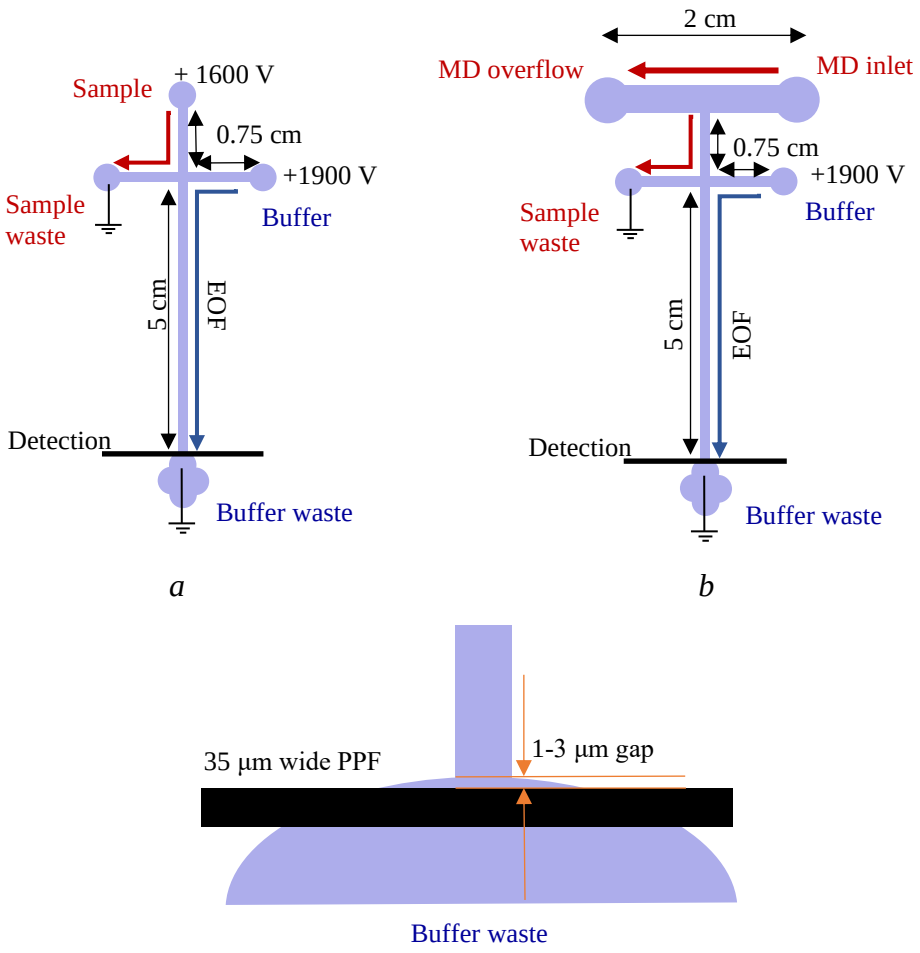

Figure 4.2. (*a*) Geometry and dimensions of a 5 cm "simple t" ME device. All channels 40 µm wide and 15 µm tall. (*b*) Geometry and dimensions of a 5 cm "double t" ME device for on-line analysis. All channels are 40 µm wide except the top MD sample channel which is 600 µm wide. All channels 15 µm tall. (*c*) Pseudo in-channel alignment of the working electrode of a ME-EC device.

4.2.6. *On-line microchip separation conditions*

Prior to analysis, microchips were conditioned with IPA for 1 min and BGE for 3 min. MD sample channel was filled with blank perfusion solution during chip conditioning with BGE. A platinum lead was placed in the buffer well and used to apply the separation potential of +1900 V via Spellman CZE 1000R high voltage power supply (Hauppauge, NY, USA). The sample waste and buffer waste reservoirs were grounded with two more Pt leads. Sample flow into the microchip was maintained at 1 μL/min for all experiments using a CMA/102 microdialysis pump (Bioanalytical Systems, West Lafayette, IN, USA). Sample injection was carried out by floating the separation potential for 1 s thus allowing the syringe pump to push a sample plug into the separation channel. Detection of analytes was carried out at 0.8 V vs. Ag/AgCl with a Pt counter electrode using BAS 4C-LC Epsilon potentiostat (Bioanalytical Systems, West Lafayette, IN, USA) and in-house written LabView software (National Instruments, Austin, TX, USA). Data analysis was carried out using Origin 2020 (OriginLab Corporation, Northampton, MA, USA) and Microsoft Excel (Redmond, WA, USA).

4.3. Results and discussion

Optimization of the BGE composition was carried out using the analyte standard mixture containing DA, EPI, NEPI, 5-HT, DOPAC, HVA, and AA at 100 μM each in 15 mM sodium phosphate buffer pH 7.4.

4.3.1. *Effect of EDTA on compatibility of BGE and calcium-containing samples*

To prevent precipitate formation at the interface of BGE and calcium-containing sample flows in the ME devices, the first step was to eliminate phosphate from the BGE. To maintain the pH of the solution we originally selected 15 mM HEPES pH 7.4 – a buffer that is commonly used in

aCSF formulations and is even known to prevent edema in brain slices[14]. During the first tests of the new phosphate-free BGE, other components were kept at the same concentrations as in the separation described in Chapter 3 (15 mM SDS + 5 mM boric acid + 10% DMSO). However, when samples containing 2.4 mM $CaCl_2$ (double of CSF concentration to evaluate the possibility of using elevated calcium concentrations in perfusate for *in vivo* DA release stimulation) were used, precipitate formation was still observed, although it was slower than that in the presence of phosphate. We attributed this to the interaction between SDS and Ca^{2+} – a process that is known to inhibit functions of surfactants in "hard water"[15]. In order to prevent the reaction between SDS, the presence of which in the BGE is critical for analyte separation, and Ca^{2+}, which is a perfusate component critical for optimal analyte recovery during MD sampling, EDTA was evaluated as additive to the BGE as a well-known chelator of divalent metal ions[16].

Figure 4.3. Effect of EDTA concentration on formation of precipitate in solutions containing Ca^{2+} and SDS. All contain 2.4 mM $CaCl_2$ + (15 mM HEPES pH 7.4 + 15 mM SDS + 5 mM boric acid + 10% DMSO) + X mM EDTA.

Mixtures containing 2.4 mM $CaCl_2$ and phosphate-free BGE components (15 mM HEPES pH 7.4, 15 mM SDS, 5 mM boric acid, and 10% DMSO) were prepared with EDTA concentrations in the range from 0 to 4 mM (Figure 4.3). Starting from 1 mM EDTA, no precipitation of calcium and surfactant was observed in a test tube, however during operation of a ME-EC device it was

necessary to use 3 mM of this additive to reproducibly prevent clogging of the channels. For all the following BGE optimization steps described below, 3 mM of EDTA was maintained as part of the composition.

4.3.2. *Buffer selection*

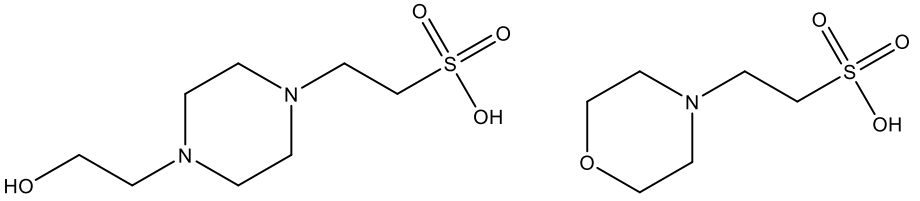

a *b*

Figure 4.4. Structures of the organic buffers used in the study (*a*) HEPES, (*b*) MES.

The first attempt at the optimization of the separation of four neurotransmitters (DA, EPI, NEPI, 5-HT), two dopamine metabolites (HVA, DOPAC), and the endogenous interferent (AA) with a phosphate-free BGE used HEPES buffer (Figure 4.4*a*) for the reasons noted in the previous subsection. However, following variation of BGE component concentrations (HEPES, SDS, boric acid, DMSO), the best separation resulted in 4 partially resolved peaks: (1) NEPI, (2) a mixed peak of EPI, DOPAC, HVA, and AA, (3) DA, and (4) 5-HT (Figure 4.5).

Further investigation of optimal BGE composition involved testing of several alternate buffering systems including tris(hydroxymethyl)aminomethane (**Tris**), Tris + boric acid + EDTA, and 2-(N-morpholino)-ethanesulfonic acid (**MES**) (Figure 4.4*b*). The latter provided the best results, and a detailed description of the separation optimization steps is presented in the following section.

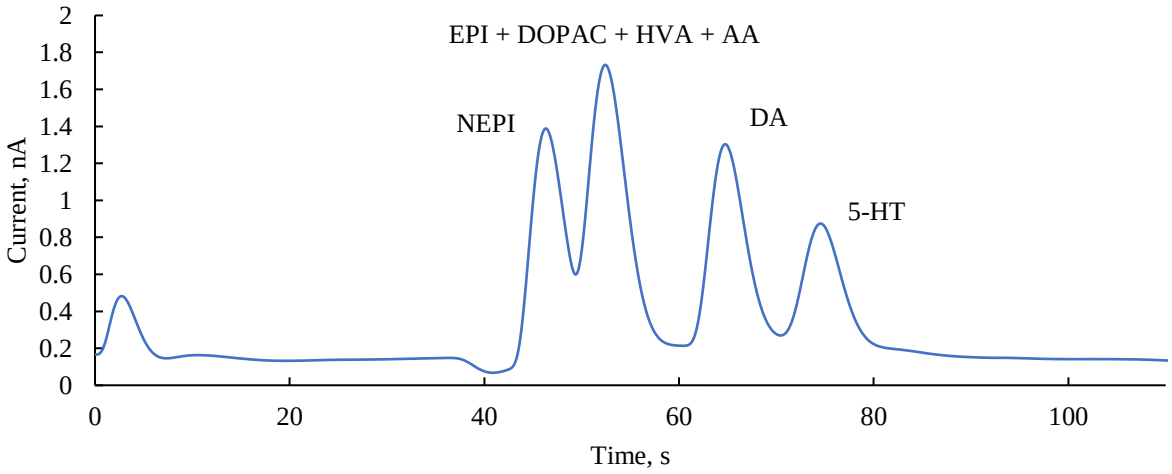

Figure 4.5. Best separation obtained with HEPES as buffering agent in the BGE. BGE: 60 mM HEPES pH 7.4, 15 mM SDS, 3 mM EDTA. 7 cm separation channel, 330 V/cm, detection at 0.8 V vs Ag/AgCl.

4.3.3. *Optimization of phosphate-free separation with MES buffer*

Optimization of the separation conditions was carried out on an "simple t" microchip with a 100 µM sample mixture prepared in 15 mM phosphate pH 7.4. Details regarding the optimization of the microdialysis perfusate composition to include calcium and other ions can be found in Chapter 5.

4.3.3.1. Concentration of the surfactant

In a ME separation on a hybrid glass/PDMS device the surfactant, in this case SDS, has two primary functions: creation of a charged surface on the PDMS channel walls thanks to the hydrophobic interactions of the carbon chain tails with the polymer material, and participation in the separation via electrostatic and hydrophobic interactions of the analytes with the free surfactant and/or its aggregates (micelles). The concentration of SDS was varied from 0 to 20 mM with the remaining components kept constant at 20 mM MES pH 7.4 and 3 mM EDTA (Figure 4.6).

With seven compounds present in the sample mixture, the number of peaks observed in the electropherograms varied from three without SDS to four at 2mM and 15 mM SDS and five at 5, 10, and 20 mM SDS. The negatively charged analytes HVA, DOPAC, and AA appeared to migrate together as a mixed peak (indicated with an asterisk in Figure 4.6) that started separating from the peak of DA at 5 mM SDS and was fully resolved from this neurotransmitter at 10 mM, above the critical micelle concentration (**CMC**) of SDS. At 15 mM the mixed peak comigrated completely with EPI and migrated between NEPI and EPI at the highest surfactant concentration of 20 mM.

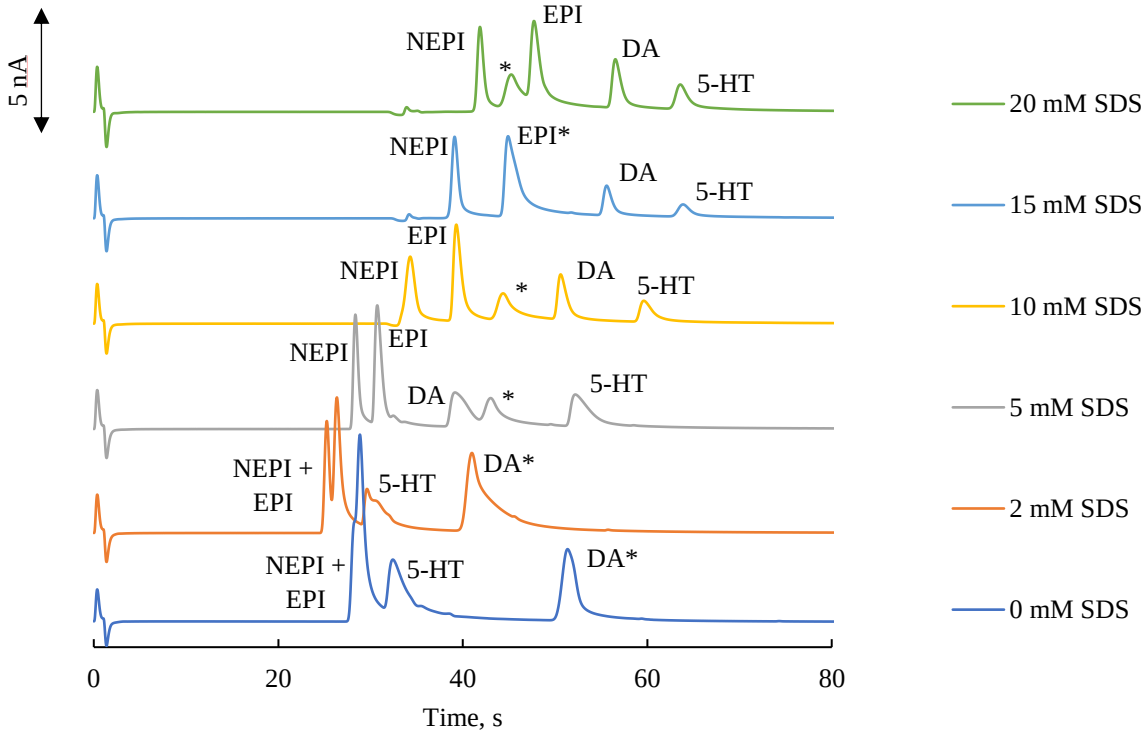

Figure 4.6. Electropherograms of standard separation obtained with BGEs containing 20 mM MES at pH 7.4, 3 mM EDTA, and various concentrations of SDS. 5 cm separation channel, 220 V/cm, detection at 0.8 V vs Ag/AgCl.

Interestingly, serotonin was also highly affected by the different SDS concentrations as it initially migrated immediately after NEPI and EPI but starting at 5 mM SDS became the last peak in the

electropherogram and remained in this position during the rest of the SDS content increase. This points at a strong interaction between the negatively charged surfactant and 5-HT, which results in high negative mobility of serotonin ions in the direction opposed to the EOF observed in the system and away from the detection zone.

As a result of the studies on BGE surfactant content variation, 10 mM of SDS was selected for the next separation optimization steps as it resulted in maximum resolution of the neurotransmitters from the endogenous interferences AA, DOPAC, and HVA. Due to this concentration being above the CMC of the surfactant, the separation mechanism under these conditions can be classified as micellar electrokinetic chromatography (**MEKC**).

4.3.3.2. MES buffer concentration

The goal of changing the concentration of the buffer used in the background electrolyte is generally to alter the electrical double layer at the silica surface and therefore the electroosmotic flow. The higher the ionic strength of the BGE, the slower the EOF. A slower EOF allows for more time between injection and detection during which the differences in analyte mobilities can affect their resolution. Increase of the ionic strength also results in a lower CMC of the surfactants and larger aggregation numbers (31% increase when switching from 0.01 NaCl to 0.10 NaCl), increasing the size of the micelles[17]. Organic buffers such as MES are less conductive than phosphate and can therefore be used in higher concentrations in ME experiments before unsustainably high separation currents are observed. The MES concentration was varied from 20 to 40 mM, while SDS and EDTA remained at 10 mM and 3 mM respectively (Figure 4.7).

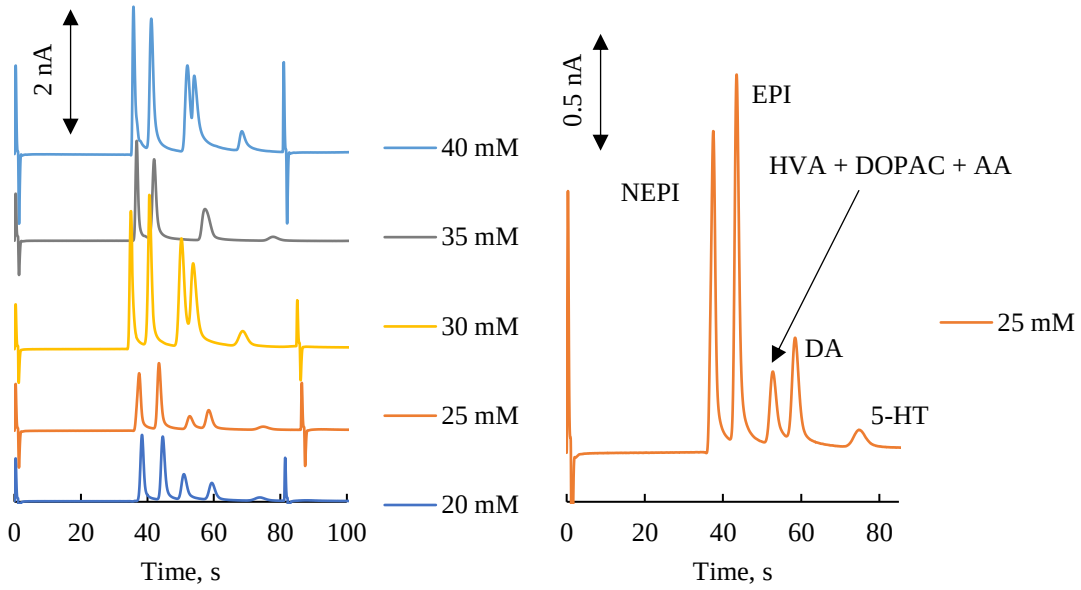

a *b*

Figure 4.7. (*a*) Electropherograms of standard separations obtained with BGEs containing various concentrations of MES at pH 7.4, 3 mM EDTA, and 10 mM SDS. (*b*) Separation observed with the BGE chosen for further optimization: 25 mM MES at pH 7.4, 3 mM EDTA, and 10 mM SDS. 5 cm separation channel, 220 V/cm, detection at 0.8 V vs Ag/AgCl.

Since the concentration of SDS used in the experiment is already above CMC and no change of separation mechanism should be occurring, one would not expect changes in migration order with increased buffer concentrations. However, an increase of the MES concentration resulted in a partial comigration of DA with the peak of the negatively charged metabolites and AA at 30 mM and complete comigration at 35 mM. A further increase to 40 mM MES resulted in partial resolution again, but at such high concentrations of electrolytes in the system the separation suffered from poor run-to-run reproducibility. The change in the migration of the negatively charged analytes could be a sign of an interaction between the BGE buffering system and the negatively charged analytes of interest. It appears that, unlike phosphate, MES complexed with

these compounds and therefore its concentration had an additional effect on the separation. We found no prior literature evidence of such interaction and speculate that it occurs through the protonated tertiary amine of the buffer. Overall, 25 mM MES resulted in the best separation of analytes in terms of peak resolution and migration time reproducibility.

4.3.3.3. Addition of boric acid

Complexation of borate with *cis*-diols can be used to improve resolution of catecholamines and related compounds. In the case of the MES-based separation developed in the course of this investigation, boric acid was added to the BGE in order to resolve HVA (which has a methyl ether group instead of one of the hydroxyls on the aromatic ring) from DOPAC and AA, both of which can complex with borate[18,19]. As can be seen from Figure 4.8, addition of 10–20 mM boric acid to the BGE resulted in partial comigration of one of the negatively charged species with DA at 10 and 15 mM, and while at 20 mM DA peak is fully resolved from the endogenous interferences, the mixed metabolite and AA only shows slight shouldering indicating that multiple compounds are responsible for peak migration.

While the addition of borate did not result in improvement of analyte resolution, it was decided to maintain 20 mM boric acid concentration during the next step – optimization of the organic solvent additive. This decision was based on the expectation that the presence of organic solvents in the BGE would interrupt SDS micelle formation, either changing the properties of the micelles (size, composition) present in the BGE or disrupting them completely and changing the separation mechanism from MEKC to capillary zone electrophoresis (**CZE**), therefore the possibility of complexation between *cis*-diols and borate could play a role in analyte resolution.

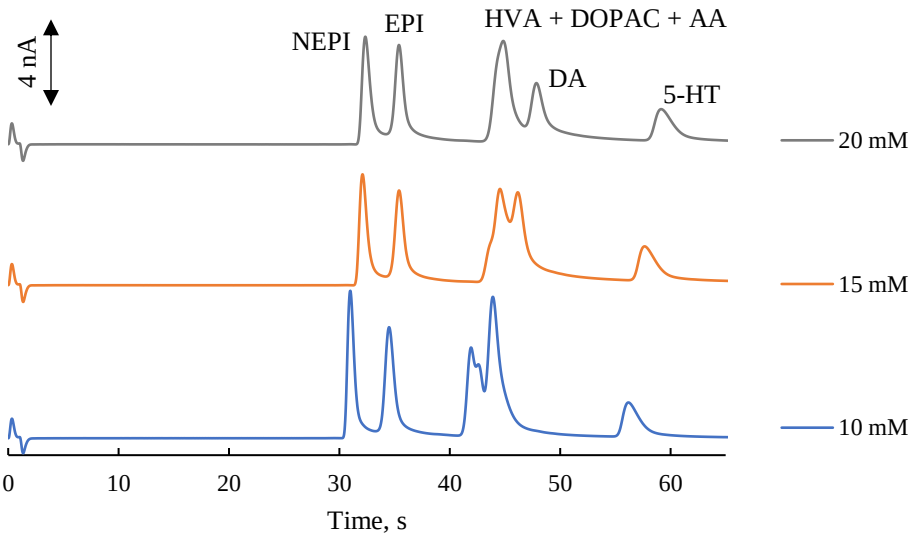

Figure 4.8. Electropherograms of standard mixture separations using BGE containing various concentrations of boric acid (in legend), 25 mM MES at pH 7.4, 3 mM EDTA, and 10 mM SDS. 5 cm separation channel, 220 V/cm, detection at 0.8 V vs Ag/AgCl.

4.3.3.4. Evaluation of organic solvent addition

Two organic solvents – DMSO and ACN – were evaluated for the improvement of analyte separation (Figure 4.9). In both cases a similar effect was observed – the peaks corresponding to the negatively charged analytes HVA, DOPAC, and AA began migrating between the DA peak and 5-HT peak. As was discussed in the previous chapter for the phosphate-based BGE, the addition of organic solvents alters (or even disrupts) SDS micelle formation[21] and can change the separation mode from MEKC back to CZE, leading to a change in analyte migration order and the role of SDS in the separation being limited to maintaining the negative charge of the channel walls to ensure stable EOF. In the case of DMSO, peaks of HVA, DOPAC, and AA shifted closer to the 5-HT peak, with HVA migrating first in the group and mostly resolved from AA and DOPAC, and the latter two comigrating almost completely. With BGE containing ACN, these peaks migrate

closer to DA, and it is HVA which is partially comigrating with AA, while DOPAC is nearly completely resolved from the peak of AA.

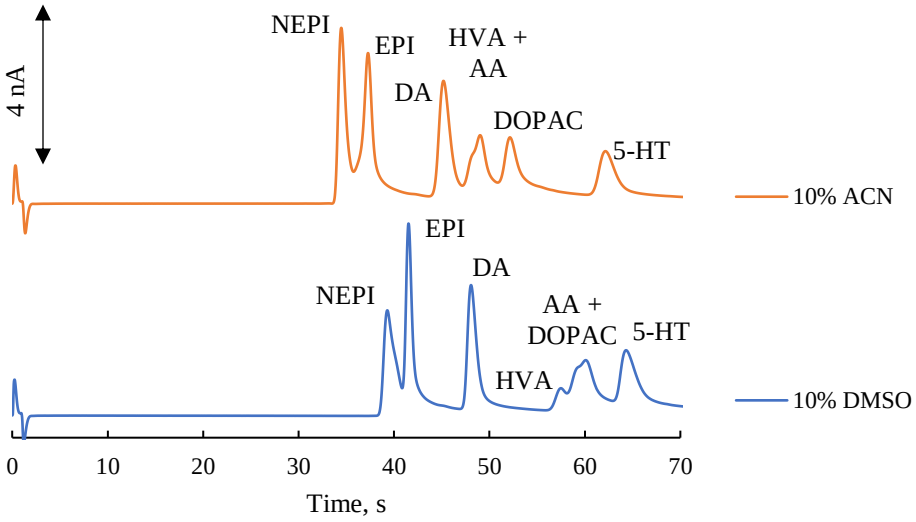

Figure 4.9. Electropherograms of standard mixture separations using BGE containing 25 mM MES at pH 7.4, 3 mM EDTA, 20 mM boric acid, 10 mM SDS, and 10% v/v additions of DMSO and ACN. 5 cm separation channel, 220 V/cm, detection at 0.8 V vs Ag/AgCl.

As a result of all optimization steps described above, the BGE consisting of 25 mM MES at pH 7.4, 3 mM EDTA, 20 mM boric acid, 10 mM SDS, and 10% v/v ACN was selected as the one providing the best resolution of the analytes of interest. Figure 4.10 shows the separations of analytes obtained with a phosphate-based BGE developed in Chapter 3 (*a*) and with the new phosphate-free BGE compatible with calcium-containing sample matrices (*b*). Overall, the separations are very similar to each other (migration order and times), although phosphate made it possible to achieve better resolution of the negatively charged peaks. The relative peak heights in the two buffers are also different, suggesting that changes in BGE composition affect EC detection efficiency for each analyte.

While baseline resolution of all analytes from each other was not achieved in the new phosphate-free BGE, our current investigative efforts are mainly focused on the neurotransmitters themselves and not their metabolites, so complete resolution of HVA, DOPAC, and AA from the signals of NEPI, EPI, DA, and 5-HT makes the developed separation suitable for further studies. It should also be noted that migration of AA after the catecholamine neurotransmitters is highly beneficial as this endogenous antioxidant is present in brain tissues and microdialysis samples in high concentrations.

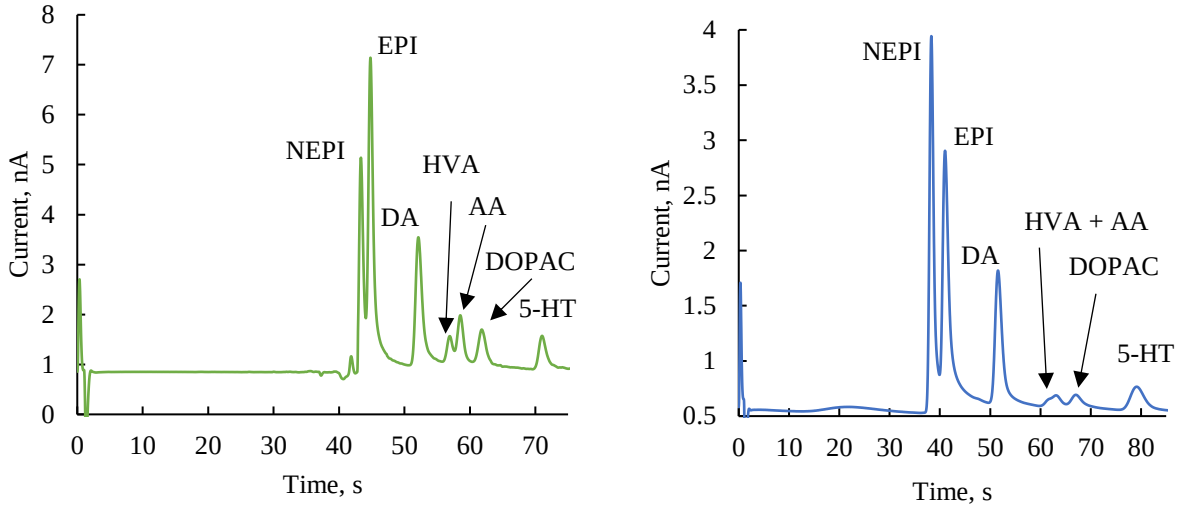

a *b*

Figure 4.10. Comparison of the optimized separations in BGEs with and without phosphate: (*a*) 30 mM phosphate at pH 7.4, 5 mM boric acid, 20 mM SDS, and 10% v/v DMSO and (*b*) 25 mM MES at pH 7.4, 3 mM EDTA, 20 mM boric acid, 10 mM SDS, and 10% v/v ACN. 5 cm separation channel, 220 V/cm, detection at 0.8 V vs Ag/AgCl.

4.3.4. *Analytical figures of merit for on-line ME-EC*

As end goal of this study is to develop an ME-EC method for future integration with MD sampling for on-line *in vivo* analysis, the following experiment was carried out using an on-line "double t"

microchip. Calibration curves for the on-line ME-EC system were carried out for the neurotransmitters NEPI, EPI, DA, and 5-HT in a sample matrix containing physiological CSF concentrations of Ca^{2+} (1.2 mM), K^{+} (2.7 mM), Mg^{2+} (0.9 mM) and 20% of the physiological Na^{+} concentration (30 mM). As HVA and DOPAC migrate very closely to AA in the developed separation, high concentrations of AA present in microdialysis samples would mask the metabolite peaks. Therefore, it was decided to exclude these negatively charged compounds from calibration curves. The correlation coefficients (R^2) for the neurotransmitters were all greater than 0.98 (Figure 4.11). The limits of detection (LODs) were estimated as 10 µM for 5-HT, 3 µM for DA and NEPI, and 1.5 µM for EPI (S/N = 3). A considerable portion of the noise present in the system originated from use of a syringe pump for sample introduction. This was determined to be the primary source of noise contributing to LODs being higher than those observed for the separation with phosphate-based BGE described in Chapter 3. An upgrade of the microdialysis pump should help mitigate this issue. Additionally, decoupling of the detection electrodes from the separation electric field[21] should be investigated for the purposes of further improving method LODs.

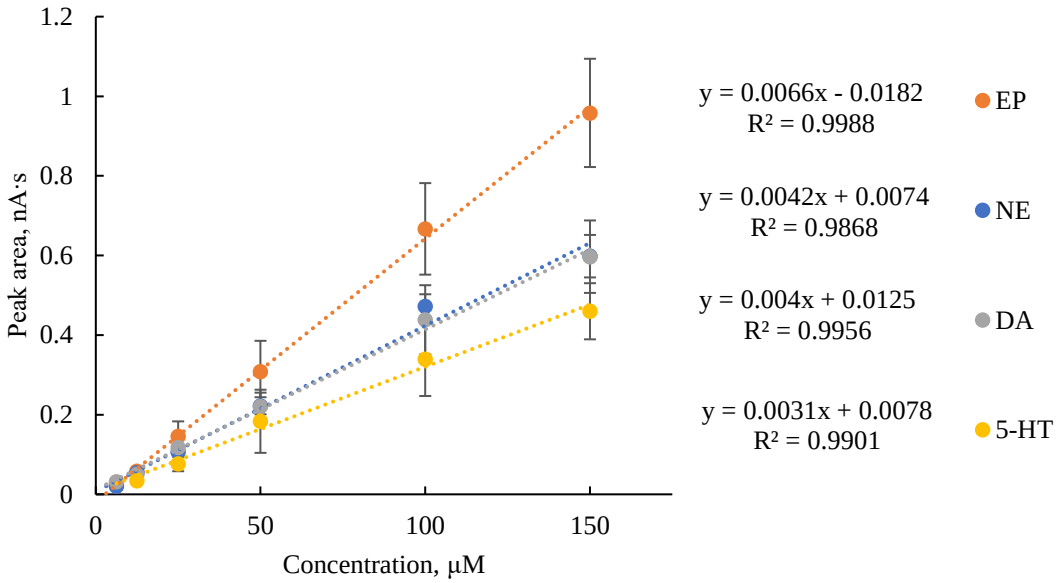

Figure 4.11. Calibration curves for the neurotransmitters of interest. All R^2 values above 0.99.

4.4. Conclusions

The ionic composition of the perfusate has a very strong effect on analyte recovery during microdialysis sampling. A ME-EC separation of four monoamine neurotransmitters DA, EPI, NEPI, and 5-HT, two DA metabolites HVA and DOPAC, and AA was developed with a BGE that does not use phosphate buffer to maintain pH 7.4. The new BGE also contains EDTA in order to ensure its compatibility with the presence of calcium ions in the sample matrix. While the developed on-line MD-ME-EC method and instrumentation allow for micromolar limits of detection for the neurotransmitters of interest, it should serve as a good starting point for further improvement of sensitivity of their quantification during on-line analysis.

4.5. References

(1) Chefer, V. I.; Thompson, A. C.; Zapata, A.; Shippenberg, T. S. Overview of Brain Microdialysis. *Curr. Protoc. Neurosci.* **2009**, *47* (1), 7.1.1-7.1.28.

(2) Westerink, B. H. C. Brain Microdialysis and Its Application for the Study of Animal Behaviour. *Behav. Brain Res.* **1995**, *70* (2), 103–124.

(3) Anderzhanova, E.; Wotjak, C. T. Brain Microdialysis and Its Applications in Experimental Neurochemistry. *Cell Tissue Res.* **2013**, *354* (1), 27–39.

(4) Karlinsey, J. M. Sample Introduction Techniques for Microchip Electrophoresis: A Review. *Anal. Chim. Acta* **2012**, *725*, 1–13.

(5) Nandi, P.; Desai, D. P.; Lunte, S. M. Development of a PDMS-Based Microchip Electrophoresis Device for Continuous Online in Vivo Monitoring of Microdialysis Samples. *Electrophoresis* **2010**, *31* (8), 1414–1422.

(6) Sandlin, Z. D.; Shou, M.; Shackman, J. G.; Kennedy, R. T. Microfluidic Electrophoresis Chip Coupled to Microdialysis for in Vivo Monitoring of Amino Acid Neurotransmitters. *Anal. Chem.* **2005**, *77* (23), 7702–7708.

(7) Johnson, A. S.; Selimovic, A.; Martin, R. S. Integration of Microchip Electrophoresis with Electrochemical Detection Using an Epoxy-Based Molding Method to Embed Multiple Electrode Materials. *Electrophoresis* **2011**, *32* (22), 3121–3128.

(8) M. Gunawardhana, S.; A. Bulgakova, G.; M. Barybin, A.; R. Thomas, S.; M. Lunte, S. Progress toward the Development of a Microchip Electrophoresis Separation-Based Sensor with Electrochemical Detection for on-Line in Vivo Monitoring of Catecholamines. *Analyst* **2020**, *145* (5), 1768–1776.

(9) Osborne, P. G.; O'Connor, W. T.; Ungerstedt, U. Effect of Varying the Ionic Concentration of a Microdialysis Perfusate on Basal Striatal Dopamine Levels in Awake Rats. *J. Neurochem.* **1991**, *56* (2), 452–456.

(10) Westerink, B. H. C.; Hofsteede, H. M.; Damsma, G.; de Vries, J. B. The Significance of Extracellular Calcium for the Release of Dopamine, Acetylcholine and Amino Acids in Conscious Rats, Evaluated by Brain Microdialysis. *Naunyn-Schmiedeberg's Arch. Pharmacol. 1988 3374* **1988**, *337* (4), 373–378.

(11) Imperato, A.; Di Chiara, G. Trans-Striatal Dialysis Coupled to Reverse Phase High Performance Liquid Chromatography with Electrochemical Detection: A New Method for the Study of the in Vivo Release of Endogenous Dopamine and Metabolites. *J. Neurosci.* **1984**, *4* (4), 966–977.

(12) Moghaddam, B.; Bunney, B. S. Ionic Composition of Microdialysis Perfusing Solution

Alters the Pharmacological Responsiveness and Basal Outflow of Striatal Dopamine. *J. Neurochem.* **1989**, *53* (2), 652–654.

(13) Saylor, R. A.; Reid, E. A.; Lunte, S. M. Microchip Electrophoresis with Electrochemical Detection for the Determination of Analytes in the Dopamine Metabolic Pathway. *Electrophoresis* **2015**, *36* (16), 1912–1919.

(14) MacGregor, D. G.; Chesler, M.; Rice, M. E. HEPES Prevents Edema in Rat Brain Slices. *Neurosci. Lett.* **2001**, *303* (3), 141–144.

(15) Rodriguez, C. H.; Lowery, L. H.; Scamehorn, J. F.; Harwell, J. H. Kinetics of Precipitation of Surfactants. I. Anionic Surfactants with Calcium and with Cationic Surfactants. *J. Surfactants Deterg.* **2001**, *4* (1), 1–14.

(16) Sawyer, D. T.; Paulsen, P. J. Properties and Infrared Spectra of Ethylenediaminetetraacetic Acid Complexes. I. Alkaline Earth Chelates1. *J. Am. Chem. Soc.* **1958**, *80* (7), 1597–1600.

(17) Ikeda, S.; Ozeki, S.; Hayashi, S. Size and Shape of Charged Micelles of Ionic Surfactants in Aqueous Salt Solutions. *Biophys. Chem.* **1980**, *11* (3–4), 417–423.

(18) Zhu, R.; Kok, W. T. Determination of Catecholamines and Related Compounds by Capillary Electrophoresis with Postcolumn Terbium Complexation and Sensitized Luminescence Detection. *Anal. Chem.* **1997**, *69* (19), 4010–4016.

(19) Köse, D. A.; Zümreoglu-Karan, B. Complexation of Boric Acid with Vitamin C. *New J. Chem.* **2009**, *33* (9), 1874–1881.

(20) Al-Sherbini, E. S. A. M.; Abdel-Kader, M. H.; Hamzah, R. Y. Effect of Binary Solvents on the Critical Micelles Concentration by Using 1-Methyl-4-[4′-Aminostyryl]Pyridinium

Iodide. *Colloids Surfaces A Physicochem. Eng. Asp.* **2001**, *194* (1–3), 133–142.

(21) Lacher, N. A.; Lunte, S. M.; Martin, R. S. Development of a Microfabricated Palladium Decoupler/Electrochemical Detector for Microchip Capillary Electrophoresis Using a Hybrid Glass/Poly(Dimethylsiloxane) Device. *Anal. Chem.* **2004**, *76* (9), 2482–2491.

5. Coupling *in vivo* microdialysis sampling with microchip electrophoresis: optimization of perfusate composition

5.1. Introduction

Microdialysis (**MD**) is a technique that is well-suited and consequently widely used for neurophysiological studies[1–3]. As the aim of utilizing MD is to carry out sampling in tissues of a living subject, biocompatibility of the perfusates is critical to the success of any such experiment[4]. The diffusion of analytes occurs from the extracellular space of the brain tissue into the dialysate, which makes artificial cerebrospinal fluid (**aCSF**) and artificial extracellular fluid (**aECF**) the best options for mimicking the natural environment surrounding the probe[2]. Ringer's solution is also occasionally used for cerebral MD experiments[1]. Since matching the perfusate concentrations of all small molecule compounds present in the extracellular space of the brain is not feasible, the focus is mainly kept on the metal ions – Na^+, K^+, Ca^{2+}, Mg^{2+}.

A variety of studies have evaluated the effects of perfusate composition on the recovery of analytes from the extracellular space. For example, a study by McNay, *et al.*[5] determined that a small decrease of Mg^{2+} (from 1.0 mM to 0.85 mM) in perfusate used for brain MD resulted in a 2-fold decrease of glucose present in dialysate and a decrease of K^+ (from 3.0 mM to 2.7 mM) in perfusate caused a 2-fold increase of the glucose concentration in the collected sample. Following a direct determination of the metal ion concentrations in the extracellular space of the rat hippocampus using microdialysis sampling with water as perfusate and really low flow rates (100 nL/min), a perfusate matching the extracellular fluid composition was used to quantify glucose content in the tissues, resulting in a value significantly different from the initial control measurement (1.26 ± 0.04 mM vs 1.06 ± 0.08 mM).[5]

Similarly, in a study by Osborne, *et al.*[6], the amount of neurotransmitter dopamine (**DA**) and its metabolites 3,4-dihydroxyphenylacetic acid (**DOPAC**) and homovanillic acid (**HVA**) recovered *in vivo* was evaluated in relationship to the concentration of several key metal ions present in

perfusates. The data presented in Table 5.1 shows that the amount of DA, DOPAC, and HVA recovered during MD sampling from rat striatum is dependent on the concentrations of calcium, potassium, and magnesium. Dopamine recovery was the most dependent on the changes of perfusate composition, with the strongest effect – 92% decrease of DA peak area – being observed when Ca^{2+} was absent from the sampling solution. Similarly, a reduction in K^{+} concentration resulted in a 27% decrease of signal, while the addition of Mg^{2+} caused a 20% drop in the recovery of the neurotransmitter.[6]

Table 5.1. Perfusates used in an *in vivo* microdialysis study with relative dopamine, DOPAC, and HVA signals in the resulting dialysates. Adapted from Osborne, *et al.*[6]

Na^{+} (mM)	K^{+} (mM)	Ca^{2+} (mM)	Mg^{2+} (mM)	Relative DA in dialysate	Relative DOPAC in dialysate	Relative HVA in dialysate
148	4.0	2.4	0	1	1	1
148	4.0	**0**	0	0.08	0.6	0.63
148	4.0	2.4	**1.7**	0.8	0.84	1
148	**3.0**	2.4	0	0.73	0.86	0.85

Another perfusate parameter that must be considered when designing MD studies is its osmolarity[7–9]. Investigations performed *in vivo* have shown that hypotonic perfusates change the recovery of exogenous analytes (administered either via peripheral injection[7] or from perfusate[8]) both immediately after the switch from isotonic perfusate to hypotonic and after prolonged perfusion of hypotonic solution. The short-term effect consisted in reduced analyte recovery and was attributed to dilution of the extracellular fluid due to osmosis of water from the probe into the tissue, followed by swelling of cells and decrease of extracellular volume fraction[8]. The long-term effect (post 48 and 72 h of hypotonic perfusion) consisted in increased recovery for a peripherally administered hydrophilic drug atenolol and was thought to be caused by the disruption of the blood-brain barrier caused by influx of water from the perfusate into the tissues[7].

This literature evidence highlights the need to maintain physiological concentrations of the metal ions in perfusates used for *in vivo* MD experiments. To this end, our group has developed a microchip electrophoresis with electrochemical detection (**ME-EC**) method that utilizes a BGE compatible with aCSF-like sample matrices. The buffer in this BGE was changed from phosphate, which readily precipitates in the presence of Ca^{2+} and Mg^{2+}, to 2-(N-morpholino)ethanesulfonic acid (**MES**). 3 mM EDTA was also added to prevent precipitation of these metal ions with sodium dodecyl sulfate. SDS was used to create a negatively charged surface on the polydimethylsiloxane (**PDMS**) walls of the microchip as well as to form micelles for a MEKC based separation of analytes. More details are available in Chapter 4.

However, the presence of Ca^{2+} and Mg^{2+} in the sample matrix is not the only hurdle standing in the way of utilizing conventional aCSF for MD-ME-EC studies. Electrophoretic separations are notoriously poorly compatible with high ionic strength sample matrices. Sample de-stacking (broadening of analyte zones) is observed when the BGE is a weaker solution than the sample. At the same time, the salt content of the BGE should be kept low in order to minimize current, and therefore Joule heating, generated during high separation voltage application. This is even more important to keep in mind in the case of microchips, which unlike conventional capillary electrophoresis instruments, are in general not equipped with cooling systems. Furthermore, more dilute BGEs are desirable as they lead to higher electroosmotic flows, making the separations faster and more efficient. Therefore, increasing the ionic strength of the background electrolyte is not a strategy that is useful to pursue. Thus, it important to develop a perfusate for which the ionic strength is low enough to minimize sample de-stacking, while retaining analyte recoveries at levels sufficiently high for their successful monitoring.

5.2. Materials and methods

5.2.1. *Chemicals and reagents*

Dopamine hydrochloride, (±)-norepinephrine bitartrate salt (**NE**), 3-nitro-L-tyrosine (**3-NT**), boric acid, and calcium chloride, anhydrous sodium phosphate monobasic were obtained from Sigma-Aldrich (St. Louis, MO, USA). 3,4-dihydroxyphenylacetic acid, L-(+)-ascorbic acid (**AA**), serotonin hydrochloride (**5-HT**), and homovanillic acid, 5-hydroxyindoleacetic acid (**5-HIAA**) were purchased from Alfa Aesar (Ward Hill, MA, USA). L-(-)-epinephrine (**EPI**) and 1-octanesulfonic acid were supplied by Acros Organics (Geel, Belgium), sodium dodecyl sulfate by Thermo Scientific (Waltham, MA, USA), and 2-(N-morpholino)ethanesulfonic acid monohydrate, ethylenediamine tetraacetic acid, disodium salt dihydrate, hydrochloric acid, orthophosphoric acid, sodium hydroxide, sodium chloride, potassium chloride, glacial acetic acid, isopropyl alcohol (**IPA**), LC-MS grade methyl alcohol (**MeOH**), and acetonitrile (**ACN**) were purchased from Fisher Scientific (Fairlawn, NJ, USA). All chemicals were used as received. Solutions were prepared using 18.2 MΩ water (Millipore, Kansas City, MO, USA) and filtered with syringe filters or a vacuum filter.

Device fabrication was carried out using the following reagents and materials: AZ 1518 positive photoresist and AZ 300 MIF developer (AZ Electronic Materials, Sommerville, NJ, USA); SU-8 10 and SU-8 developer (Micro-Chem, Newton, MA, USA), PDMS resin and curing agent (Sylgard 184 silicon elastomer base and curing agent, Dow Corning Corp., Midland, MI, USA), quartz plates (5 in × 5 in × 0.085 in, Glass Fab, Rochester, NY, USA), copper wire (22 gage, Westlake Hardware, Lawrence, KS, USA), epoxy (Gorilla Glue, Cincinnati, OH, USA), and colloidal silver liquid (Ted Pella, Inc., Redding, CA, USA). 0.5 mm OD platinum wires (Goodfellow, Huntingdon,

England) and Ag/AgCl reference electrodes (Bioanalytical Systems, West Lafayette, IN, USA) were also used in the experiments.

5.2.2. *Pyrolyzed photoresist film (**PPF**) electrode fabrication*

The 35 μm-wide PPF electrodes were fabricated on quartz plates according to a previously published procedure[10]. In short, a bare quartz plate cut to 4 in × 2.5 in × 0.085 in was spin coated (Brewer Science Cee 200CBX Programmable Spin Coater) with AZ 1518 positive photoresist and prebaked at 100°C for 3 minutes. The coated plate was then allowed to cool to room temperature and exposed to a UV flood source at 20 mW/cm2 for 10 s through a photomask. Following the exposure, the plate was baked at 100°C for 10 min and developed using AZ 300 MIF developer. After complete removal of the exposed photoresist, the plate was rinsed with reverse osmosis water, dried with N_2 flow, and post baked at 100°C for 10 min. The quartz plate containing an electrode photofilm feature was then placed into a tube furnace and pyrolyzed at 925°C for 1 hour in N_2 atmosphere. This resulted in formation of a PPF carbon electrode that was 35 μm wide and approximately 500 nm high. A copper lead was then attached to the plate with thin (~1 mm) bands of lab tape and hot glue and connected to the PPF electrode using colloidal silver.

5.2.3. *Double T hybrid PDMS/glass chip fabrication*

Microchips from PDMS were fabricated using previously published procedure via soft lithography[10]. Silicon masters with 15 μm high raised features for a 5 cm double T on-line chip (see geometry and dimensions in Figure 5.1) were produced using SU-8 negative photoresist. Chips were cast from 10:1 elastomer:curing agent mixture and cured at 70 °C for at least 3 hours. A 4 mm biopsy punch was used to create buffer, buffer waste, sample solution, and sample waste wells. An on-line sample inlet was punched in the chip with a 20-gauge needle with a flat sharp

edge. The chip was then aligned on the PPF electrode using pseudo in-channel alignment (see Materials and Methods in Chapter 4), the top half of it was then irreversibly bonded to the quartz plate using a hand-held corona discharger wand (Model BD 20: Electro-Technic Products, Inc., Chicago, IL, USA) and a blow dryer as described previously[10]. Following the bonding of the PDMS layer to the quartz substrate, a 10–15 mm stainless steel pin was inserted into the sample inlet and fixed in place with epoxy glue. Tubing carrying the sample from the MD probe or syringe pump (CMA/102 microdialysis pump, CMA Microdialysis, Kista, Sweden) to the microchip was then connected to this pin with a silicon tubing connector.

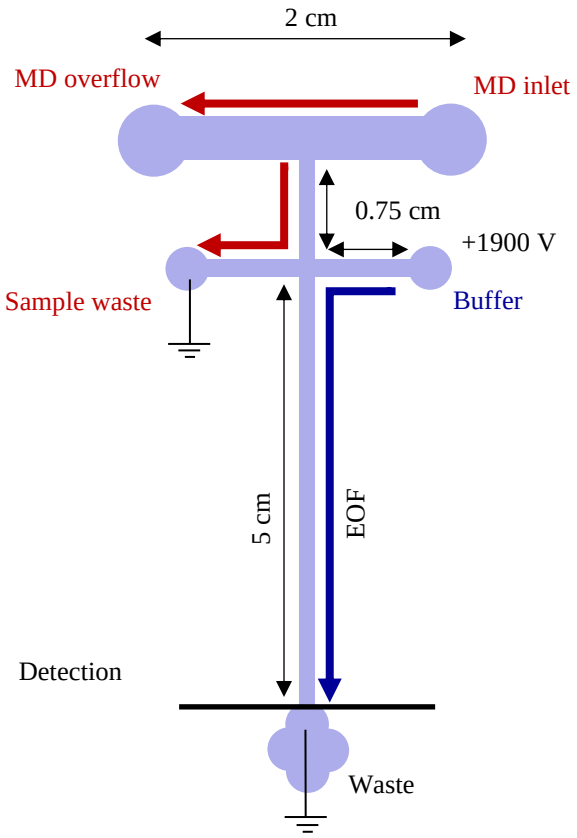

Figure 5.1. Geometry and dimensions of a 5-cm double T microchip for on-line analysis. All channels 40 μm wide except the top MD channel which is 600 μm wide.

5.2.4. *On-line ME-EC*

Prior to analysis, microchips were conditioned with IPA for 1 min and BGE for 3 min. The MD sample channel was filled with blank perfusion solution during chip conditioning with BGE. A platinum lead was placed in the buffer well and used to apply the separation potential of +1900 V via Spellman CZE 1000R high voltage power supply (Hauppauge, NY, USA). The sample waste and buffer waste reservoirs were grounded with two more Pt leads. Sample flow into the microchip was maintained at 1 μL/min for all experiments. Sample injection was carried out by floating the separation potential for 1 s thus allowing the syringe pump to push a sample plug into the separation channel. Detection of analytes was accomplished at 0.8 V vs. Ag/AgCl with a Pt counter electrode using BAS 4C-LC Epsilon potentiostat (Bioanalytical Systems, West Lafayette, IN, USA) and in-house written LabView software (National Instruments, Austin, TX, USA).

5.2.5. *Capillary electrophoresis with UV absorbance (**CE-UV**) and capacitively coupled contactless conductivity (**CE-C^{4}D**) detection*

CE analysis was carried out with Agilent 7100 CE-UV system (Santa Clara, CA, USA) coupled with a C^{4}D detector (eDAQ, Colorado Springs, CO). Fused silica capillary with 50 μm ID (Polymicro Technologies, Phoenix, AZ, USA) had a full length of 69.25 cm and effective length of 55.0 for the C^{4}D detector and 60.75 cm for the UV detector. The detection modes were utilized simultaneously for all runs. Prior to the first run the capillary was conditioned with water, 0.1 M NaOH, and water for 5 min each, followed by BGE for 10 min; conditioning between runs consisted in a 3 min rinse with water, 3 min with 0.1 M NaOH, 3 min with water, and 5 min with BGE. The initial longer conditioning step was repeated prior to switching to a new set of inlet and outlet BGE vials. Sample injection was carried out hydrodynamically with 69 mbar applied for

5 s. Analysis was carried out using +30 kV separation voltage and 5.0 M acetic acid as BGE in accordance with a procedure developed by Ferreira Santos *et al.*[11]

5.2.6. *Liquid chromatography with electrochemical detection (**LC-EC**)*

LC-EC analysis was carried out via a system consisting of an LC-20AD pump (Shimadzu Scientific Instruments, Columbia, MD, USA), Rheodyne MXP7900 stainless steel sample injector with a ZORBAX Rapid Resolution StableBond C18 column (1.0 mm × 50 mm, 3.5 μm, Agilent Technologies, Santa Clara, CA, USA), an electrochemical detection cell, and BAS 4C-LC Epsilon potentiostat (Bioanalytical Systems, West Lafayette, IN, USA). 3 mm glassy carbon working electrode and Ag/AgCl reference electrode were purchased from Bioanalytical Systems. A potential of 0.750 V vs Ag/AgCl was applied for the amperometric detection. Flow rate in the system was set at 0.1 mL/min, with mobile phase as follows: 140 mM NaH_2PO_4, 0.75 mM 1-octanesulfonic acid, and 10 mM EDTA disodium salt with pH adjusted to 3.5 with 85% orthophosphoric acid, and 9% methanol adapted from the procedure described by Crick *et al.*[12] Data collection and analysis were performed using Chrom & Spec software version 1.5 (Ampersand International Inc., Beachwood, OH, USA).

5.2.7. *In vivo microdialysis experiments*

Male Wistar rats (Charles River, Wilmington, MA, USA) were used to collect animal MD samples. All procedures were carried out in accordance with an Animal Use Statement approved by the Institutional Animal Care and Use Committee at the University of Kansas and meet the standards set by the Association for Assessment and Accreditation of Laboratory Animal Care.

5.2.7.1. Microdialysis probe implantation

Rats were anesthetized by isoflurane inhalation followed by i.p. injection of 100 mg/kg ketamine and 10 mg/kg xylazine diluted in saline. Anesthesia was maintained throughout probe implantation surgery and MD sampling by constant flow of isoflurane (0.5–2%) supplied via nose cone. Surgery was performed using a stereotaxic instrument with the probe guide cannula placed into the striatum at the following coordinates from bregma: A/P +0.7, M/L −2.7 and V/D −3.4. The cannula was fixed to the skull with metal screw anchors and dental cement. Once the CMA 12 Elite brain microdialysis probe with 4 mm PAES 20 kDA MWCO membrane (CMA Microdialysis, Kista, Sweden) was placed into the cannula, it was constantly perfused with aCSF (148 mM NaCl, 2.7 mM KCl, 1.2 mM $CaCl_2$, 0.9 mM $MgCl_2$, pH adjusted to 7.4 with $NaHCO_4$) at a flow rate of 1 μL/min using a CMA/102 microdialysis pump. The animal was allowed to recover for at least 1 h following surgery before MD samples were collected for off-line analysis.

5.2.7.2. Variation of NaCl content in perfusate

The first cohort of *in vivo* experiments was dedicated to investigating the effects of varying NaCl content in perfusate on the ionic and analyte composition of the resulting microdialysis samples. To switch between perfusates, a UniSwitch liquid switch syringe selector was placed between the syringe pump and the inlet of the microdialysis probe. Once the perfusate was switched from one composition to another, 10 min of dialysate flow was diverted to waste in order to clear out the previous perfusate from all tubing. Thirty microliter MD sample fractions were collected for each perfusate and used for LC-EC (18 μL) and CE-C^4D (10 μL) analysis. The samples were either analyzed immediately or stored frozen at –20 °C or –80 °C until analysis.

5.2.7.3. Time-dependence study

The second cohort of *in vivo* experiments investigated the changes in sodium ion and monoamine neurotransmitter metabolite recoveries as a function of time following a perfusate switch from aCSF to a low-NaCl aCSF mimic. In addition to the salt content studies, perfusion of aCSF containing 3-NT was carried out several times in each experiment in order to control for changes of probe performance. Switching between perfusates was accomplished using a UniSwitch with 10 min of dialysate diverted to waste following each switch. Microdialysis sample fraction collection was carried out manually according to the sequence shown in Table 5.2. The samples were then either analyzed immediately or stored frozen at –20 °C or –80 °C until analysis.

Table 5.2. Procedure for the study of the changes of sodium ion and monoamine neurotransmitter metabolite recoveries over time following perfusate switch from aCSF to a 20% NaCl aCSF solution.

Time from surgery, min	Action	Perfusate	# fractions collected	Sample use
0−59	Post-surgery recovery	aCSF	1	waste
60	Switch to perfusate with IS	aCSF, 50 μM 3-NT		NA
60−69	Exchange of solution in tubing	aCSF, 50 μM 3-NT	1	waste
70−99	Collection for IS delivery study	aCSF, 50 μM 3-NT	1	CE-UV
100	Switch to low NaCl perfusate	20% NaCl aCSF		NA
100−109	Exchange of solution in tubing	20% NaCl aCSF	1	waste
110−209	Collection for Na^+ recovery study	20% NaCl aCSF	10	CE-C^4D
210	Switch to perfusate with IS	aCSF, 50 μM 3-NT		NA
210−229	Exchange of solution in tubing	aCSF, 50 μM 3-NT	1	waste
230−259	Collection for IS delivery study	aCSF, 50 μM 3-NT	1	CE-UV
260	Switch to aCSF for recovery	aCSF		NA
260−319	Recovery	aCSF	1	waste
320	Switch to perfusate with IS	aCSF, 50 μM 3-NT		NA
320−329	Exchange of solution in tubing	aCSF, 50 μM 3-NT	1	waste
330−359	Collection for IS delivery study	aCSF, 50 μM 3-NT	1	CE-UV
360	Switch to low NaCl perfusate	20% NaCl aCSF		NA
360−369	Exchange of solution in tubing	20% NaCl aCSF	1	waste
370−459	Collection for metabolite recovery study	20% NaCl aCSF	3	LC-EC

5.3. Results and discussion

5.3.1. *Effect of perfusate NaCl content on analyte resolution during on-line MD-ME-EC while sampling from aCSF solution*

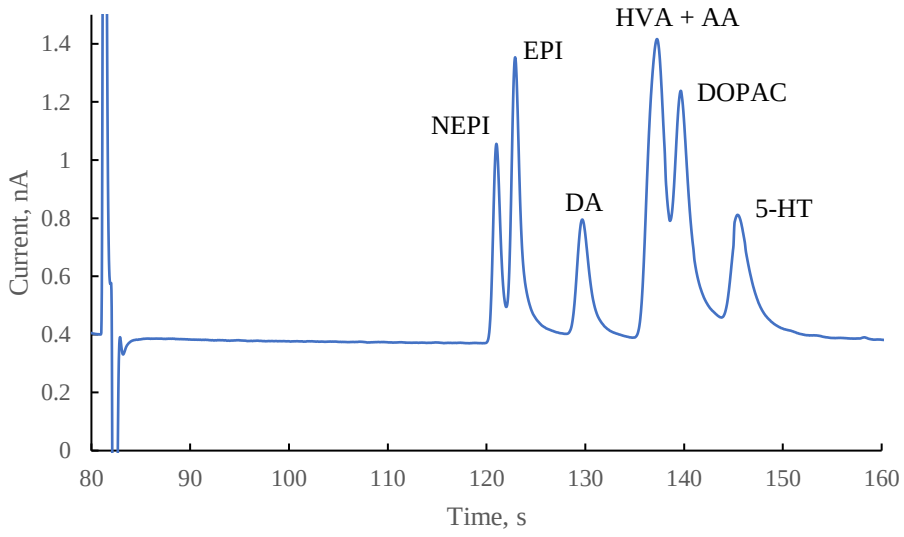

Figure 5.2. ME-EC separation of the 100 μM standard mixture in aCSF containing 20% of physiological NaCl injected directly into a double t microchip for on-line analysis. BGE: 25 mM MES at pH 7.4, 3 mM EDTA, 20 mM boric acid, 10 mM SDS, and 10% v/v ACN. 5 cm separation channel, 220 V/cm, detection at 0.8 V vs Ag/AgCl.

The literature data strongly indicates that optimal *in vivo* recovery of the analytes of interest can only be achieved if the concentrations of metal ions, most importantly Ca^{2+} and K^{+}, in perfusate are maintained at physiological concentrations[6]. At the same time, ME separations require relatively low ionic strength of all solutions (both BGE and sample) in order to minimize currents generated in the microchannels as a result of application of high separation voltage and prevent peak destacking. Therefore, it was necessary to determine the amount of salt which could be safely used in the perfusate for MD-ME-EC analysis, while keeping the composition as close as possible to aCSF (148 mM NaCl, 2.7 mM KCl, 1.2 mM $CaCl_2$, 0.9 mM $MgCl_2$), which is the gold standard

for studies using MD sampling from the brain. As NaCl makes up most of the ionic strength of aCSF, and its concentration is about two orders of magnitude higher than those of the other metals, this was the perfusate component that was varied in the following experiments.

Two stock solutions were prepared and utilized to prepare all perfusates used in these experiments:

(*A*) aCSF containing 100% of the physiological concentration of NaCl and physiological concentrations of potassium, calcium, and magnesium (148 mM NaCl, 2.7 mM KCl, 1.2 mM $CaCl_2$, 0.9 mM $MgCl_2$), and

(*B*) aCSF containing 0% of the physiological concentration of NaCl and physiological concentrations of potassium, calcium, and magnesium (2.7 mM KCl, 1.2 mM $CaCl_2$, 0.9 mM $MgCl_2$).

Both solutions were adjusted to the physiological pH value of 7.4 with 0.2 M $NaHCO_4$. Perfusates with varying NaCl contents were obtained by mixing solutions *A* and *B* at specific ratios (e.g. for 10% NaCl aCSF the solutions were mixed *A*:*B* = 1:9).

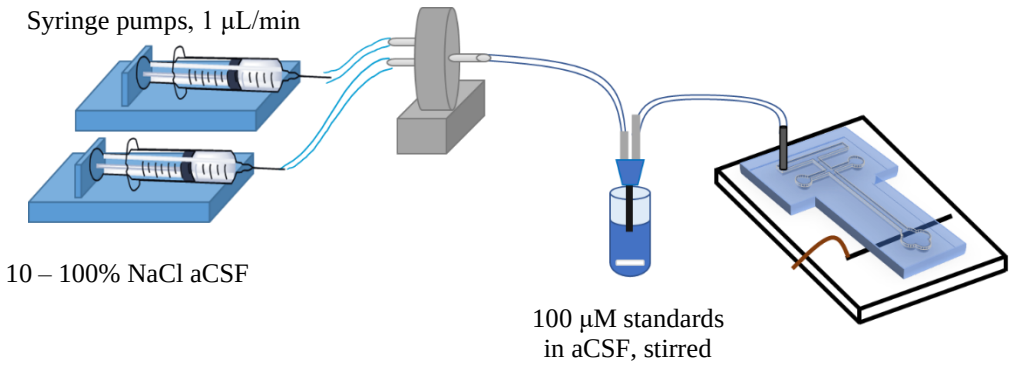

Figure 5.3. Experimental setup for *in vitro* MD-ME-EC studies.

It was observed that the monoamine neurotransmitters NEPI, EPI, DA, and 5-HT were resolved from each other and the comigrating negatively charged AA and dopamine metabolites HVA and

DOPAC when they were present in a solution of 20% NaCl aCSF that was directly introduced into the double t microchip via a syringe pump at 1 µL/min (Figure 5.2). The experimental setup was then modified to add the MD sampling component to the sample delivery (Figure 5.3). A microdialysis probe was placed in a 100 µM solution of analytes in *A* (100% NaCl aCSF), and sample collection was carried out at 1 µL/min using perfusates with NaCl content varying from 10 to 100% of the physiological concentration. The outlet of the MD probe was connected to the ME-EC device for on-line analysis.

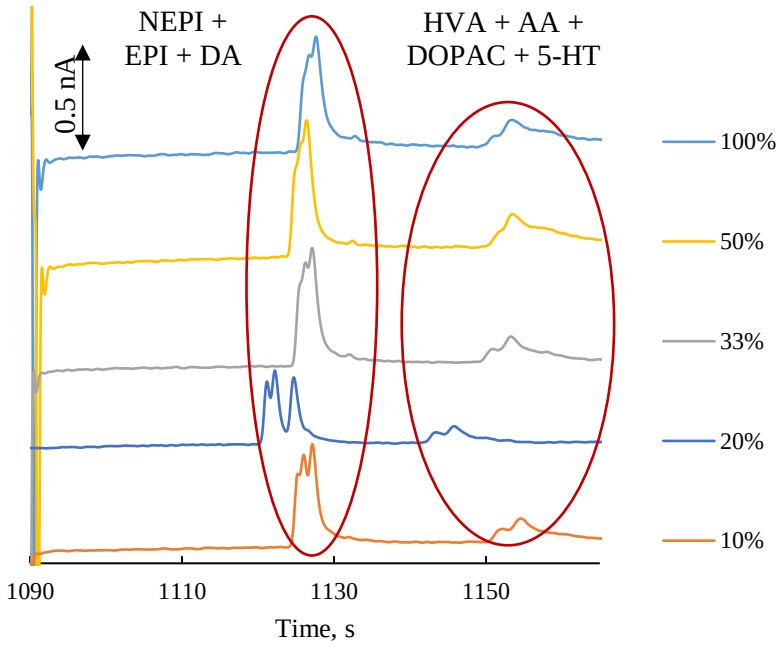

Figure 5.4. Electropherograms obtained during *in vitro* MD-ME-EC experiment where sampling of monoamine neurotransmitters, dopamine metabolites, and ascorbic acid was performed from a solution of analytes in aCSF with perfusates containing various NaCl concentrations relative to the physiological CSF value of 148 mM (in legend). For separation conditions see Figure 5.2.

Electropherograms obtained with this experimental setup illustrate dramatic degradation of analyte separation resulting in migration of all 7 analytes as 2 groups of overlapping peaks – NEPI, EPI,

and DA and HVA, AA, DOPAC, and 5-HT (Figure 5.4). This outcome was observed for all perfusates, suggesting that even at the lowest initial concentration of NaCl in the perfusate, the uptake of salt from the aCSF-based sample was great enough to significantly impact chip performance. When the solution of the sample in the vial was switched to 20% NaCl aCSF and the same NaCl concentration was used in the perfusate, analyte resolution was retained in comparison with the direct injection of analyte solution into the microchip without MD sampling (Figure 5.5). This shows that it is indeed the diffusion of NaCl from the sample matrix into the dialysate that is responsible for the degradation of resolution in the MD-ME-EC experiments using 100% aCSF in sample matrix.

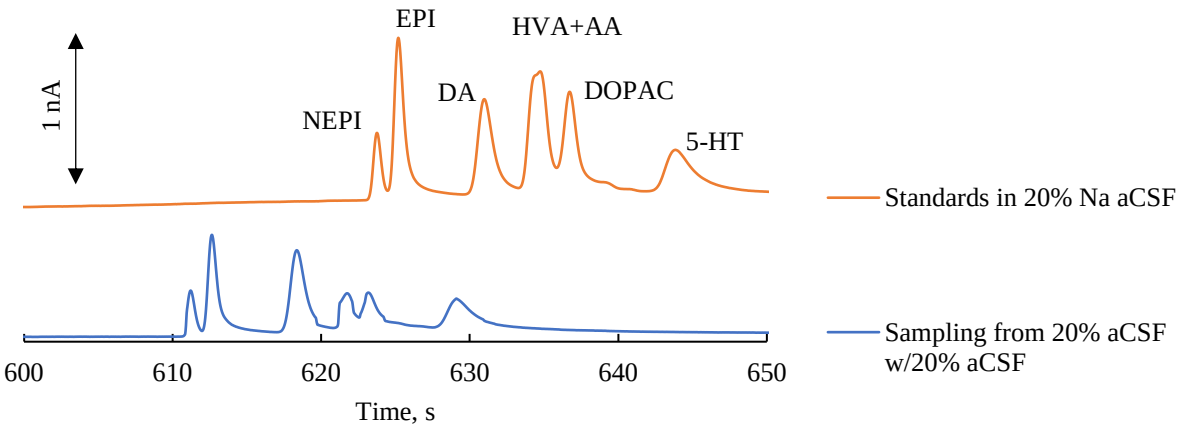

Figure 5.5. Electropherograms obtained during *in vitro* MD-ME-EC experiment where sampling of monoamine neurotransmitters, dopamine metabolites, and ascorbic acid was performed from a solution of analytes in 20% NaCl aCSF with the same solution used as perfusate.

5.3.2. *Effect of perfusate NaCl content on the amount of Na^+ in dialysate during MD sampling from aCSF solution*

As the diffusion of NaCl from the aCSF-based sample solution into dialysate negatively affected the ME-EC separation, the following study was carried out to quantify how the recovery of Na^+ ions under these conditions depends on the perfusate NaCl content. Off-line MD sample collection (Figure 5.6) and CE-C^4D were utilized for metal ion quantification. Both the perfusates and the collected MD samples were diluted twenty-fold with DI water prior to analysis to ensure resolution of Ca^{2+} and Mg^{2+} peaks (which were maintained at the same concentration for all solutions) from Na^+ and maintain linearity of the signal vs concentration dependence. It was observed in these studies that the Na^+ response for the dialysates independently of the NaCl present in perfusate were virtually identical to each other and matched that of 100% aCSF (Figure 5.7).

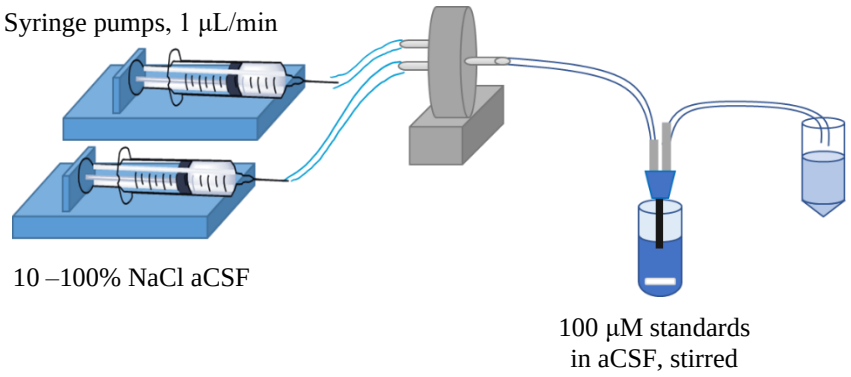

Figure 5.6. Experimental setup for off-line studies of Na^+ recovery from aCSF-based solutions via microdialysis sampling.

This indicates a 100% recovery of Na^+ under the conditions of the *in vitro* experiment, leading to the conclusion that further optimization of the perfusate NaCl content cannot be carried out *in vitro* with sampling from solutions. It also means that future *in vitro* MD experiments should not be

performed with analytes dissolved in aCSF, as the final salt content of the MD samples reaching the microchip will be too high to allow satisfactory chip performance.

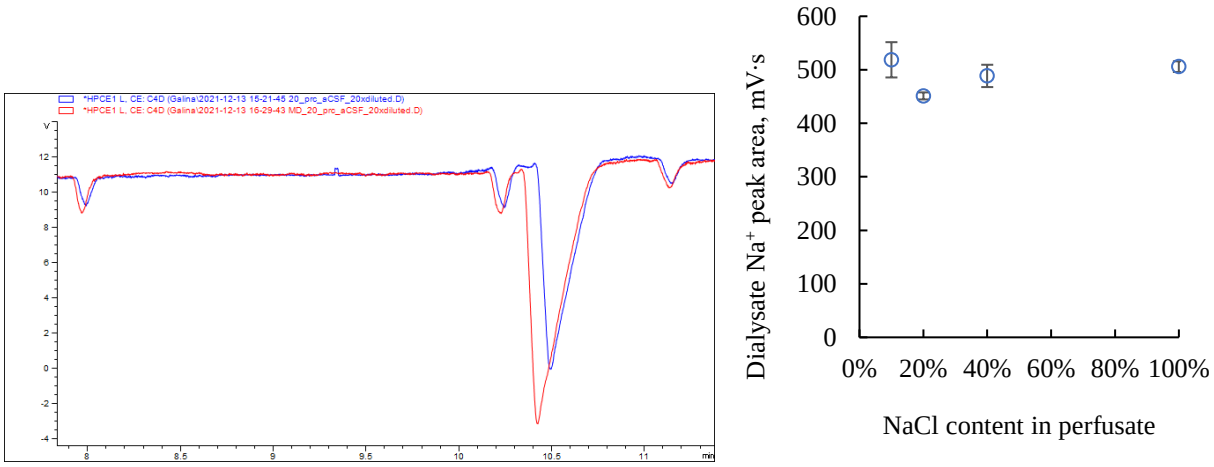

a *b*

Figure 5.7. (*a*) CE-C^{4}D signals for 20% NaCl aCSF perfusate (blue) and a microdialysate obtained using this perfusate when sampling from a vial of 100% NaCl aCSF solution (red). (*b*) Na^+ peak areas detected for microdialysates obtained using perfusates with various NaCl concentrations during sampling from 100% NaCl aCSF.

In addition to the evaluation of Na^+ recovery with perfusates containing different NaCl concentrations, the same experimental setup was used to determine whether the changes in perfusate ionic strength affected the transport of an internal standard 3-NT across the probe membrane, changing its delivery from perfusate into the sampling environment. Off-line MD sample collection was repeated using perfusates containing 50 µM 3-NT. Undiluted dialysates were analyzed via CE-UV using the same separation conditions that were used for metal ion analysis. It was determined that changing the concentration of NaCl had no significant effect on the delivery of the internal standard from the perfusate (Figure 5.8), suggesting that any changes of analyte recoveries in further studies must be caused by specific physiological effects.

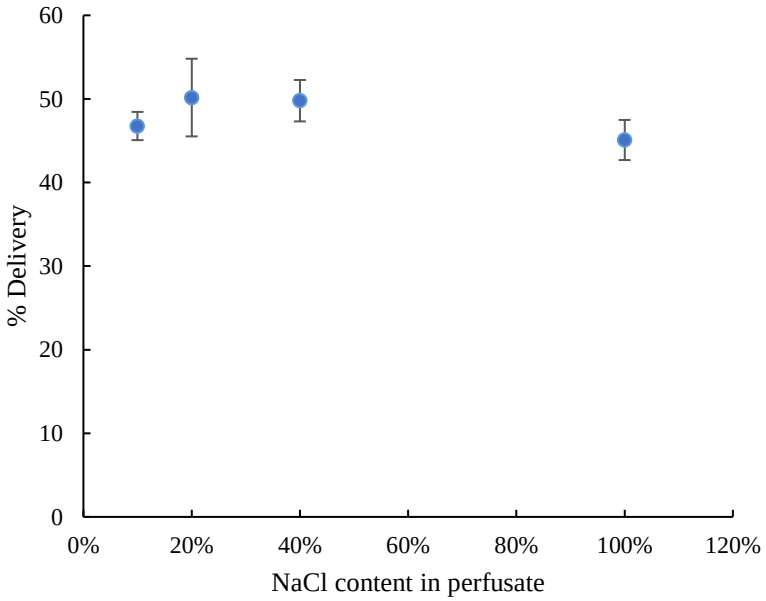

Figure 5.8. Delivery of the internal standard 3-NT during *in vitro* microdialysis using perfusates with varying NaCl concentrations.

5.3.3. *Variation of NaCl content in perfusate during in vivo microdialysis*

5.3.3.1. Dependence of the Na^+ content in dialysate on perfusate NaCl content

The Na^+ content of rat brain microdialysis samples obtained *in vivo* using perfusates containing 10–40% of the physiological sodium concentration was determined using CE-C^4D. Figure 5.9 shows that the Na^+ content increases with the maximum increase (~50%) of the initial perfusate concentration observed with 10% NaCl aCSF, making the NaCl content in the MD sample ~15%. An ~30% increase was observed for 20% NaCl aCSF, leading to the final content of ~26%. However, in the case of the perfusate containing 40% of physiological NaCl, no significant increase of Na^+ signal in the dialysate was observed. These conditions would simplify creation of calibration curves and make the overall performance of the system more predictable since the ionic strength of the perfusate and the dialysate would be the same. However, when a standard mixture containing 40% of physiological concentration of NaCl in the matrix was injected directly into the

double t ME-EC device, it resulted in nearly complete comigration of the NEPI and EPI peaks. These two analytes were resolved at 20% and 30% NaCl. Therefore, the 20% NaCl aCSF was chosen as a more optimal perfusate for future evaluation as it should enable resolution of the analyte peaks even after Na^+ is taken up from brain tissue during MD sampling.

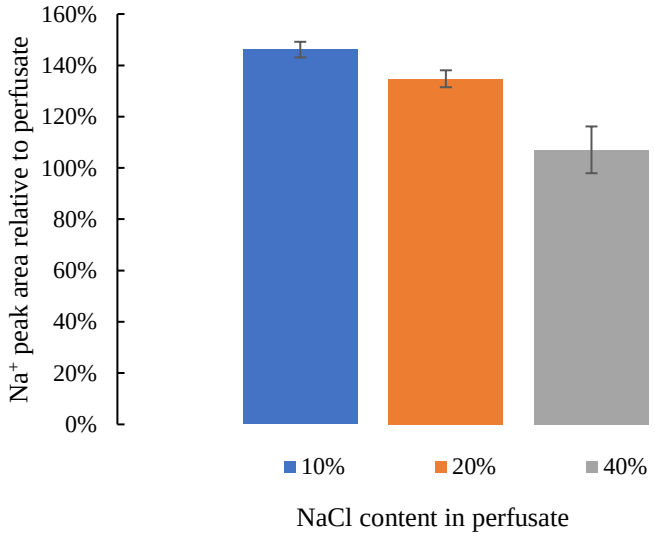

Figure 5.9. Dependence of the sodium signal increase in rat brain microdialysis samples relative to perfusate for sampling solutions containing 10–40% of physiological concentration of NaCl. N = 3, error bars – standard deviation.

5.3.3.2. Dependence of analyte recovery on perfusate NaCl content

The rat brain microdialysis samples collected with perfusates containing various NaCl concentrations were also analyzed via LC-EC to determine how changing this parameter affected the *in vivo* analyte recovery from tissues. Perfusates were switched in the following order:

100%, 40%, 20%, and 10% NaCl aCSF for animal 1, and

100%, 20%, 40%, and 10% NaCl aCSF for animals 2 and 3.

Only peaks of two DA metabolites DOPAC and HVA and of a 5-HT metabolite 5-HIAA could be quantified in the MD samples. The results of data analysis suggest that the duration of sample collection played a more important role than the amount of NaCl present in perfusate. More specifically, when the peak areas were averaged based on NaCl content in perfusate (Figure 5.10*a*), no significant difference was observed for 20% and 40% NaCl containing perfusates. However, when the averaging was carried out based on fraction number (Figure 5.10*b*), and therefore the amount of time that passed between sample collection and the initial probe implantation, a gradual decrease of signal from fraction to fraction was evident even though collection of fractions 2 and 3 was carried out with either 20% or 40% NaCl aCSF depending on the animal.

While the amount of NaCl in the perfusate still appears to have an effect on the amount of analyte transported into the MD sample across the probe membrane, as expected from literature[7–9], this experimental data suggests that in order to specifically focus on the influence of NaCl perfusate content (or any other parameter) on analyte recovery in the future experiments, more time should be allowed to pass between probe implantation and collection of dialysates for quantification of neurotransmitters and metabolites. Based on the results of the previous section, the same principle does not appear to apply to the studies of metal ion recovery from tissues, as in that case the amount of Na^+ recovered into dialysate depended on the concentration of NaCl in perfusate and not the order of perfusion.

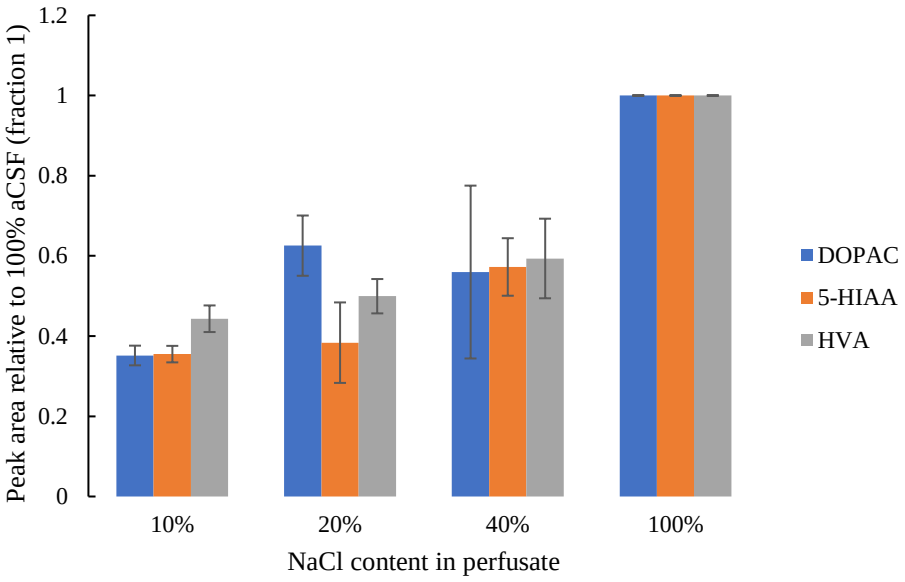

a

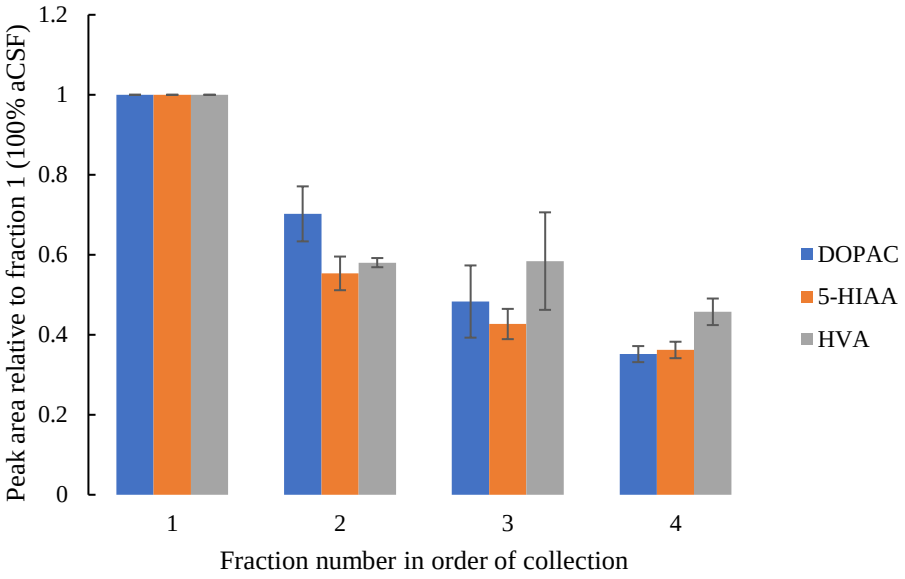

b

Figure 5.10. *In vivo* analyte recovery for DOPAC, 5-HIAA, and HVA with peaks averaged based on (*a*) NaCl content in perfusate or (*b*) fraction number in order of collection.

5.3.4. *Time dependence of the recovered Na^+ in brain microdialysate samples obtained using perfusate with 20% of physiological NaCl content*

5.3.4.1. Effect on Na^+ content in dialysate

Determination of the time dependence of the recovered Na^+ in *in vivo* microdialysis samples was carried out with the perfusate containing 20% of physiological NaCl concentration. Figure 5.11 shows that the sample collected in the first 10 minutes following the switch from 100% NaCl aCSF to 20% NaCl aCSF had the highest recovery of sodium ions from the tissues at ~60% of the initial perfusate concentration. However, all following fractions for the duration of the experiment showed half of this sodium recovery at ~30% of the perfusate concentration and were not significantly different from each other.

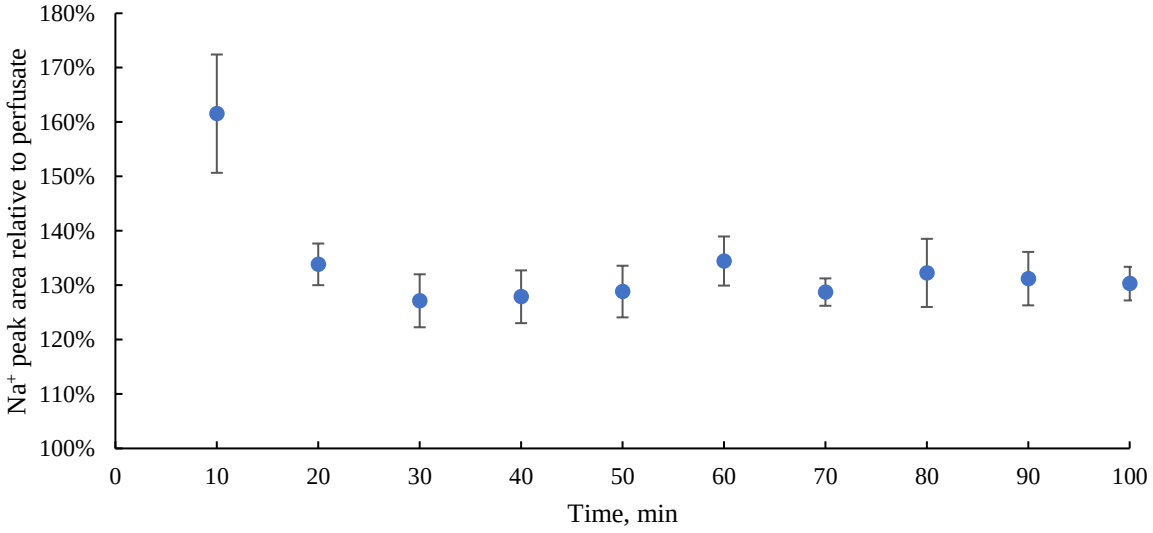

Figure 5.11. Time dependence of percent peak area of Na^+ C^4D signal in rat brain microdialysis samples relative to perfusate containing 20% physiological NaCl concentration. N = 3, error bars – standard deviation.

It was also determined using CE-UV that the delivery of the internal standard 3-NT from perfusate to the tissues was the same prior to, immediately following, and 120 min after the 100 min of 20% NaCl aCSF perfusion (Figure 5.12), indicating that probe permeability remained unchanged in these conditions. This allows us to make a conclusion that for a study spanning no more than 100 minutes the concentration of sodium ions in the dialysate can be considered constant following the first 10 minutes of equilibration. A longer study must be carried out to determine if this remains true for experiments that utilize low sodium content perfusates *in vivo* on timescales beyond 100 min.

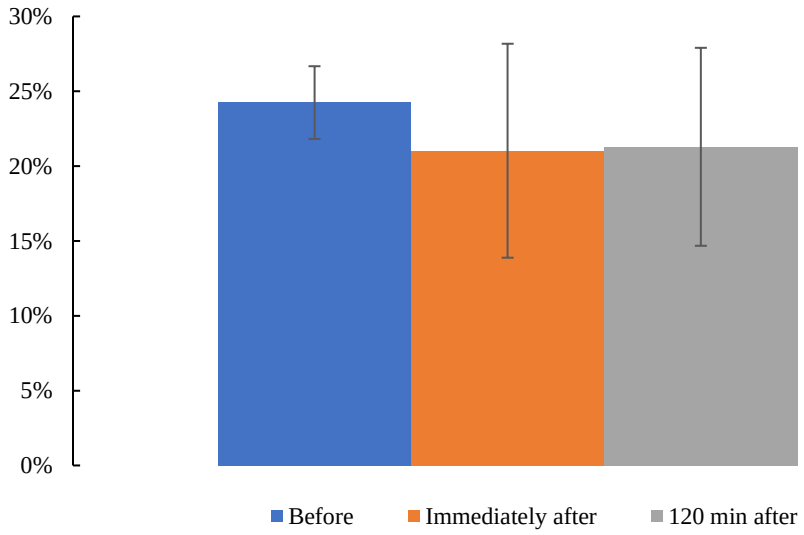

Figure 5.12. Percent delivery of internal standard from perfusate into tissues prior to, immediately following, and 120 min after the 100 min perfusion of 20% NaCl aCSF through the probe. N = 3, error bars – standard deviation.

5.3.4.2. Dependence of analyte recovery on the duration of perfusion of a low sodium containing solution

To complement the study of time-dependence of Na^+ recovery from tissues, LC-EC analysis of microdialysates collected with 20% NaCl aCSF over the span of 90 min was performed. Three 30-

min fractions were collected for this purpose, and the analyte peak areas were compared to the first fraction collected. Figure 5.13 presents the results of these measurements. It was determined that similar to the effect observed for Na^+, analyte peak areas decrease by at least 20% for the second fraction relative to the original observed signal and remain at this decreased level for the third fraction. Evidently, there is an equilibration step that occurs immediately following the switch from 100% NaCl aCSF to 20% NaCl aCSF perfusate, which is followed by stable levels of recovered analytes during the following hour. As was mentioned above, a longer study is necessary to determine whether any further changes to recoveries of both Na^+ and neurotransmitter metabolites occur beyond 90-100 minutes of tissue exposure to low-NaCl perfusates.

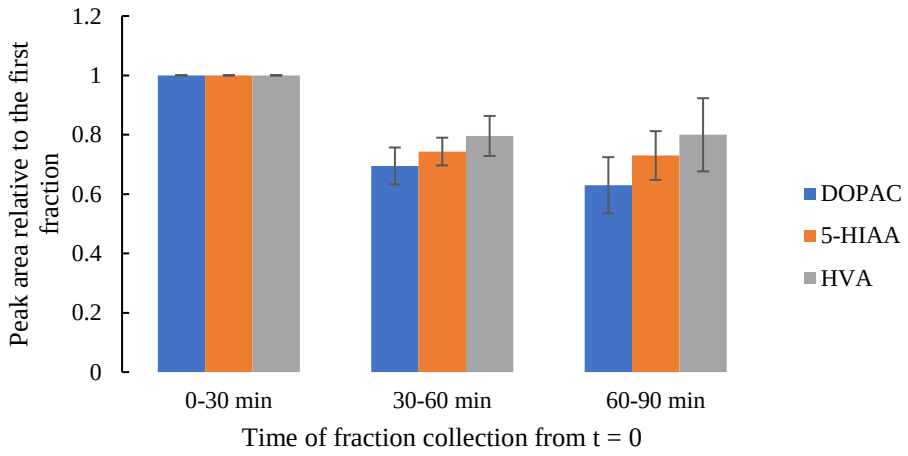

Figure 5.13. Time dependence of analyte peak areas relative to the first fraction collected following the switch from 100% NaCl aCSF to 20% NaCl aCSF. N = 3, error bars – standard deviation.

5.4. Conclusions

To determine the composition of perfusate suitable for *in vivo* MD-ME-EC monitoring of monoamine neurotransmitters, a range of aCSF-mimicking solutions with NaCl contents ranging from 10 to 40% of the physiological concentration were evaluated. While the initial experiments

utilized *in vitro* MD sampling from a vial containing sample solutions in aCSF, it was determined that under these conditions the recovery of Na^+ is at 100%, making the ionic strength of the dialysates reaching the ME-EC device too high to enable quality performance of the system. Two sets of *in vivo* experiments were carried out instead – one to evaluate the salt concentration in the brain dialysates obtained using perfusates with various NaCl contents, and another to elucidate the time-dependence of the dialysate sodium ion recovered analyte concentrations for 20% NaCl aCSF perfusate. It was determined that at the lower the NaCl concentrations of 10 and 20% the sodium content in the perfusate increased to 15 and 26% respectively, however for 40% NaCl there was no significant change in the response for Na^+. It was also shown that while lower NaCl content caused a reduction of analyte recoveries from the tissues by 40–65%, the time between probe implantation and off-line sample collection had a stronger effect on recovery, indicating that longer post-surgery rest times are necessary for future studies. Finally, it was established that following the initial equilibration after the switch from 100% NaCl aCSF perfusion to 20%, both the Na^+ and analyte recoveries remained at the same level until at least 90 – 100 min after the switch, indicating that no corrections for salt content or analyte recovery variation need to be made for experiments conducted on these timescales.

5.5. References

(1) Chefer, V. I.; Thompson, A. C.; Zapata, A.; Shippenberg, T. S. Overview of Brain Microdialysis. *Curr. Protoc. Neurosci.* **2009**, *47* (1), 7.1.1–7.1.28.

(2) Anderzhanova, E.; Wotjak, C. T. Brain Microdialysis and Its Applications in Experimental Neurochemistry. *Cell Tissue Res.* **2013**, *354* (1), 27–39.

(3) Westerink, B. H. C. Analysis of Biogenic Amines in Microdialysates of the Brain. *J.*

Chromatogr. B Biomed. Sci. Appl. **2000**, *747* (1–2), 21–32.

(4) Kho, C. M.; Enche Ab Rahim, S. K.; Ahmad, Z. A.; Abdullah, N. S. A Review on Microdialysis Calibration Methods: The Theory and Current Related Efforts. *Mol. Neurobiol. 2016 545* **2016**, *54* (5), 3506–3527.

(5) McNay, E. C.; Sherwin, R. S. From Artificial Cerebro-Spinal Fluid (ACSF) to Artificial Extracellular Fluid (AECF): Microdialysis Perfusate Composition Effects on in Vivo Brain ECF Glucose Measurements. *J. Neurosci. Methods* **2004**, *132* (1), 35–43.

(6) Osborne, P. G.; O'Connor, W. T.; Ungerstedt, U. Effect of Varying the Ionic Concentration of a Microdialysis Perfusate on Basal Striatal Dopamine Levels in Awake Rats. *J. Neurochem.* **1991**, *56* (2), 452–456.

(7) de Lange, E. C. M.; Danhof, M.; de Boer, A. G.; Breimer, D. D. Critical Factors of Intracerebral Microdialysis as a Technique to Determined the Pharmacokinetics of Drugs in Rat Brain. *Brain Res.* **1994**, *666* (1), 1–8.

(8) Borg, N.; Ståhle, L. Recovery as a Function of the Osmolality of the Perfusion Medium in Microdialysis Experiments. *Anal. Chim. Acta* **1999**, *379* (3), 319–325.

(9) de Lange, E. C. M. Recovery and Calibration Techniques: Toward Quantitative Microdialysis. In *Microdialysis in Drug Development*; Springer, New York, NY, 2013; pp 13–33.

(10) Gunawardhana, S. M.; Bulgakova, G. A.; Barybin, A. M.; Thomas, S. R.; Lunte, S. M. Progress toward the Development of a Microchip Electrophoresis Separation-Based Sensor with Electrochemical Detection for on-Line: In Vivo Monitoring of Catecholamines.

Analyst **2020**, *145* (5), 1768–1776.

(11) Ferreira Santos, M. S.; Noell, A. C.; Mora, M. F. Methods for Onboard Monitoring of Silver Biocide during Future Human Space Exploration Missions. *Anal. Methods* **2020**, *12* (25), 3205–3209.

(12) Crick, E. W.; Osorio, I.; Frei, M.; Mayer, A. P.; Lunte, C. E. Correlation of 3-Mercaptopropionic Acid Induced Seizures and Changes in Striatal Neurotransmitters Monitored by Microdialysis. *Eur. J. Pharm. Sci.* **2014**, *57* (1), 25–33.

6. ME-EC detection of ascorbate recovered during microdialysis sampling with perfusates containing glutamate

6.1. Introduction

Ascorbic acid (**AA**), also known as vitamin C, has many functions in the brain ranging from antioxidant activity and prevention of cellular damage during acute insults, to participation in the synthesis of norepinephrine as an enzyme co-factor and neuromodulation of dopamine and glutamate (**Glu**) neurotransmission. AA is not produced endogenously by humans and is absorbed into bloodstream from dietary sources. It is then distributed to all cell types with the highest concentrations found in brain, spinal cord, and adrenal glands. Transport into the nervous system begins at the choroid plexus, where it enters the cerebral spinal fluid (**CSF**), diffuses into the extracellular fluid (**ECF**) of the brain and is taken up into the cells. In the pathway blood → CSF/ECF → brain cells, the concentration of AA increases 10–20 times during each transition, with the healthy serum concentrations of ~50 μM, 200–500 μM in CSF and ECF, 10 mM in neurons, and 1 mM in glia.[1,2]

The extracellular concentration of ascorbate in the brain is primarily regulated homeostatically through uptake into and release from cells. Experiments with cell cultures and tissue slices show that removal of ascorbate from the surrounding media results in the depletion of the cells' internal stores of AA, suggesting that ascorbate has very important extracellular functions. At the same time, dynamic changes of extracellular AA in the brain have been observed in both a circadian manner (in rats ascorbate levels are 20–60% higher at night, when they are the most active, than during the day) and during pharmaceutical intervention through amphetamine administration[2]. These variations of extracellular ascorbate have been associated with the activation of Glu pathways and are supported by *in vivo* experiments including direct injection of Glu into the brain[3], Glu uptake inhibitors (but not antagonists), and lesioning of cortical Glu inputs[2]. Some researchers attribute these effects to the so-called glutamate-ascorbate heteroexchange[4,5], a process during

which glutamate transporters (most likely EAAT2 and EAAT3) facilitate the release of AA from the cells during uptake of Glu[2]. Others, based on *in vitro* studies in astrocyte[6] and neuroblastoma[7] cell cultures have concluded that the heteroexchange process is unlikely and that organic anion channels are responsible for the release of AA into the extracellular space in the presence of elevated Glu concentrations. Therefore, the question of the exact mechanism of the dynamic changes of ascorbate in the extracellular space of the brain due to activation of glutamatergic pathways remains open.

Multiple studies using microdialysis (**MD**) sampling aiming to elucidate the relationship between Glu, AA, and other neuroactive compounds have been carried out over the last three decades[4,8–12]. However, we were able to identify only two such studies that utilized retrodialysis of Glu from perfusate in order to illicit changes in AA concentration during sampling from the cortex[4] and spinal cord[11]. In these experiments, quantification of the analytes of interest in the perfusates was carried out off-line using several different analytical methods that required long sample collection times and use of a large number of animals to obtain statistically relevant data. In this study, we take the first steps to utilizing MD sampling coupled to microchip electrophoresis with electrochemical detection (**MD-ME-EC**) for the on-line monitoring of ascorbic acid in rat striatum during perfusion of Glu-containing perfusates. If successful, this approach can be used in future studies to monitor multiple compounds (*e.g.* ascorbate and monoamine neurotransmitters) simultaneously with high temporal resolution and without additional sample handling.

6.2. Materials and methods

6.2.1. *Chemicals and reagents*

Dopamine hydrochloride (**DA**), D-glutamic acid, boric acid, sodium phosphate monobasic and dibasic were obtained from Sigma-Aldrich (St. Louis, MO, USA). 3,4-Dihydroxyphenylacetic

acid, L-(+)-ascorbic acid, and L-glutamate sodium salt were purchased from Alfa Aesar (Ward Hill, MA, USA). Sodium dodecyl sulfate was supplied by Thermo Scientific (Waltham, MA, USA), hydrochloric acid, sodium hydroxide, and isopropyl alcohol (**IPA**) were purchased from Fisher Scientific (Fairlawn, NJ, USA). All chemicals were used as received. Solutions were prepared using 18.2 MΩ water (Millipore, Kansas City, MO, USA) and filtered with 0.2 μm pore nylon syringe filters.

Device fabrication was carried out using the following reagents and materials: AZ 1518 positive photoresist and AZ 300 MIF developer (AZ Electronic Materials, Sommerville, NJ, USA); SU-8 10 and SU-8 developer (Micro-Chem, Newton, MA, USA), PDMS resin and curing agent (Sylgard 184 silicon elastomer base and curing agent, Dow Corning Corp., Midland, MI, USA), quartz plates (5 in × 5 in × 0.085 in, Glass Fab, Rochester, NY, USA), copper wire (22 gage, Westlake Hardware, Lawrence, KS, USA), epoxy (Gorilla Glue, Cincinnati, OH, USA), and colloidal silver liquid (Ted Pella, Inc., Redding, CA, USA). 0.5 mm OD platinum wires (Goodfellow, Huntingdon, England) and Ag/AgCl reference electrodes (Bioanalytical Systems, West Lafayette, IN, USA) were also used in the experiments.

6.2.2. *Pyrolyzed photoresist film (**PPF**) electrode fabrication*

The 35 μm-wide PPF electrodes were fabricated on quartz plates according to a previously published procedure[13]. In short, a bare quartz plate cut to 4 in × 2.5 in × 0.085 in was spin coated (Brewer Science Cee 200CBX Programmable Spin Coater) with AZ 1518 positive photoresist and prebaked at 100°C for 3 minutes. The coated plate was then allowed to cool to room temperature and exposed to a UV flood source at 20 mW/cm2 for 10 s through a photomask. Following the exposure, the plate was baked at 100°C for 10 min and developed using AZ 300 MIF developer. After complete removal of the exposed photoresist, the plate was rinsed with reverse osmosis

water, dried with N_2 flow, and postbaked at 100°C for 10 min. The quartz plate containing an electrode photofilm feature was then placed into a tube furnace and pyrolyzed at 925°C for 1 hour under N_2. This resulted in formation of a PPF carbon electrode that was 35 μm wide and approximately 500 nm high. A copper lead was then attached to the plate with thin (~1 mm) bands of lab tape and hot glue and connected to the PPF electrode using colloidal silver liquid.

6.2.3. *"Double t" hybrid PDMS/glass chip fabrication*

Microchips from PDMS were fabricated using previously published procedure via soft lithography[13]. Silicon masters with 15 μm high raised features for a 5 cm double t on-line chip (see geometry and dimensions in Figure 6.1) were produced using SU-8 negative photoresist. Chips were cast from a 10:1 elastomer:curing agent mixture and cured at 70 °C for at least 3 hours. A 4 mm biopsy punch was used to create buffer, buffer waste, sample solution, and sample waste wells. The on-line sample inlet was punched in the chip with a 20-gauge needle with a flat sharp edge. The chip was then aligned on the PPF electrode using pseudo in-channel alignment (see Materials and Methods in Chapter 4), the top half of it was then irreversibly bonded to the quartz plate using a hand-held corona discharger wand (Model BD 20: Electro-Technic Products, Inc., Chicago, IL, USA) and a blow dryer as described in reference 13. Following bonding of PDMS to quartz, a 10-15 mm stainless steel pin was inserted into the sample inlet and fixed in place with epoxy glue. Tubing carrying the sample from the MD probe or syringe pump (CMA/102 microdialysis pump, CMA Microdialysis, Kista, Sweden) to the microchip was then connected to this pin with a silicon tubing connector.

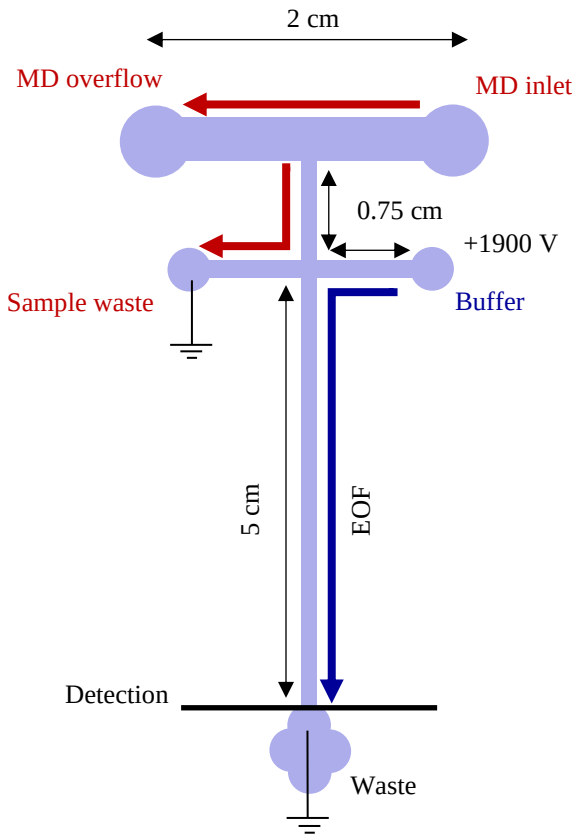

Figure 6.1. Geometry and dimensions of a 5-cm double T microchip for on-line analysis. All channels 40 µm wide except the top MD channel which is 600 µm wide.

6.2.4. *On-line ME-EC*

Prior to analysis, microchips were conditioned with IPA for 1 min and BGE for 3 min. The MD sample channel was filled with blank perfusion solution during chip conditioning with BGE. A platinum lead was placed in the buffer well and used to apply the separation potential of +1900 V via Spellman CZE 1000R high voltage power supply (Hauppauge, NY, USA). The sample waste and buffer waste reservoirs were grounded with two more Pt leads. Sample flow into the microchip was maintained at 1 µL/min for all experiments. Sample injection was carried out by floating the separation potential for 1 s thus allowing the syringe pump to push a sample plug into the separation channel. Detection of analytes was carried out at 0.8 V vs. Ag/AgCl with a Pt counter

electrode using BAS 4C-LC Epsilon potentiostat (Bioanalytical Systems, West Lafayette, IN, USA) and in-house written LabView software (National Instruments, Austin, TX, USA).

6.2.5. *In vivo microdialysis experiments*

Male Sprague Dawley rats (Charles River, Wilmington, MA, USA) were used for *in vivo* MD-ME-EC experiments. All procedures were carried out in accordance with an Animal Use Statement approved by the Institutional Animal Care and Use Committee at the University of Kansas and meet the standards set by the Association for Assessment and Accreditation of Laboratory Animal Care.

6.2.5.1. Microdialysis probe implantation

Rats were anesthetized by isoflurane inhalation followed by i.p. injection of 100 mg/kg ketamine and 10 mg/kg xylazine diluted in saline. Anesthesia was maintained throughout probe implantation surgery and MD sampling by a constant flow of isoflurane (0.5–2%) supplied via nose cone. Surgery was performed using a stereotaxic instrument with the probe guide cannula placed into the striatum at the following coordinates from bregma: A/P +0.7, M/L −2.7 and V/D −3.4. The cannula was fixed to the skull with metal screw ankers and dental cement. Once the CMA 12 Elite brain microdialysis probe with 4 mm polyarylethersulfone (**PAES**) (Figure 6.2) 20 kDA MWCO membrane (CMA Microdialysis, Kista, Sweden) was placed into the cannula, it was constantly perfused with 15 mM sodium phosphate pH 7.4 at 1 μL/min using a CMA/102 microdialysis pump. The animal was allowed to recover for at least 2.5 h following surgery before the MD-ME-EC experiments.

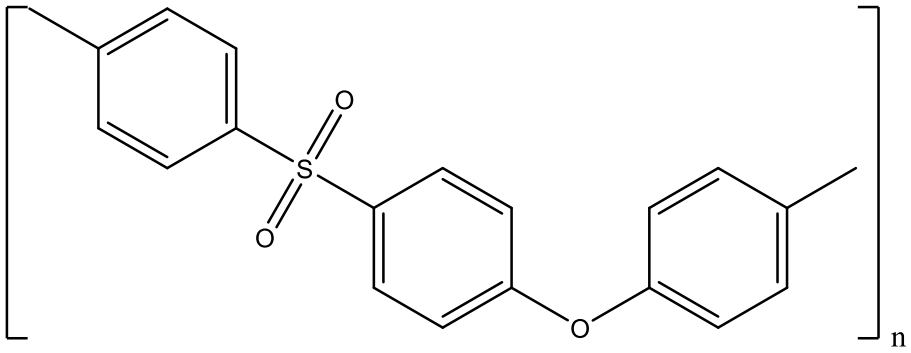

Figure 6.2 Polyarylethersulfone polymer.

6.2.5.2. Stimulation of ascorbate release with glutamate-containing perfusates

Following 2.5 h of post-surgery recovery time, the outlet tubing of the MD probe implanted in the striatum of the anesthetized rat was connected to the MD sample inlet of the "double t" ME-EC device. Thirty baseline electropherograms were collected using 15 mM sodium phosphate pH 7.4 as perfusate (blank perfusate), followed by a 30 min stimulation with glutamate-containing perfusate prepared in 15 mM sodium phosphate pH 7.4. Perfusate was switched back to blank perfusate for 30–45 min of recovery time, which was again followed by perfusion of the stimulation perfusate for at least 30 min, followed by another recovery with blank perfusate.

6.3. Results and discussion

6.3.1. *Perfusion of 1 mM L-Glu in 15 mM sodium phosphate pH 7.4*

The central premise of the experiments conducted in the course of this investigation was that delivery of exogenous glutamate (or more specifically, L-Glu) to the brain via retrodialysis from MD perfusate should elicit the release of AA into the extracellular space reflected by an increase of its concentration in the MD sample. During a preliminary *in vivo* experiment (not shown) it was discovered that using 10 μM L-Glu (about 10 times higher than the healthy extracellular concentration[14]) in the perfusate was not enough to trigger the physiological response. It was

therefore decided to increase the concentration of L-Glu in perfusate to 1 mM (1000 times the physiological concentration).

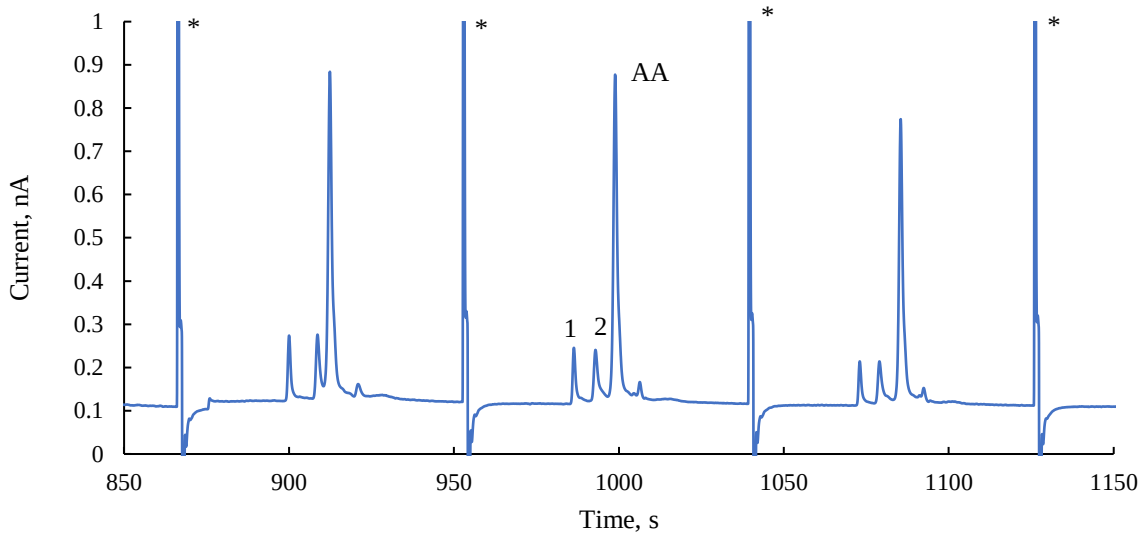

Figure 6.3. Example of baseline electropherograms observed during perfusion of 15 mM phosphate pH 7.4. Asterisks indicate signals corresponding to sample injection, identities of peaks 1 and 2 are unknown. BGE: 15 mM sodium phosphate pH 8.5, 2 mM SDS, 10 mM boric acid. 5 cm separation channel, 220 V/cm, detection at 0.8 V vs Ag/AgCl.

An example of three consecutive baseline electropherograms observed for MD samples collected with blank perfusate is shown in Figure 6.3. Three peaks above LOD were consistently present in these runs – two corresponding to the unknown compounds 1 and 2 and an intense peak of AA. Following the switch to the L-Glu containing perfusate, an unexpected effect was observed: instead of a gradual increase of the AA signal stimulated by the presence of elevated glutamate concentrations in the extracellular space, the ascorbate peak height dropped very rapidly (over the course of 1–2 sample runs) to 10–30% of its baseline value (Figure 6.4). This decrease of signal was significant enough to allow detection of compounds that comigrated with the large peak of AA in the baseline runs (Figure 6.5), although we were not able to identify these compounds.

Signals corresponding to the unknown compounds 1 and 2 remained unaltered by the changes of perfusate. While the signal of AA slowly increased over the course L-Glu perfusion, its return to baseline levels was observed only following the return to sampling with glutamate-free perfusate (15 mM phosphate pH 7.4) (Figure 6.6). This experiment was reproduced for n = 3 with similar results to confirm the reliability of these unexpected observations.

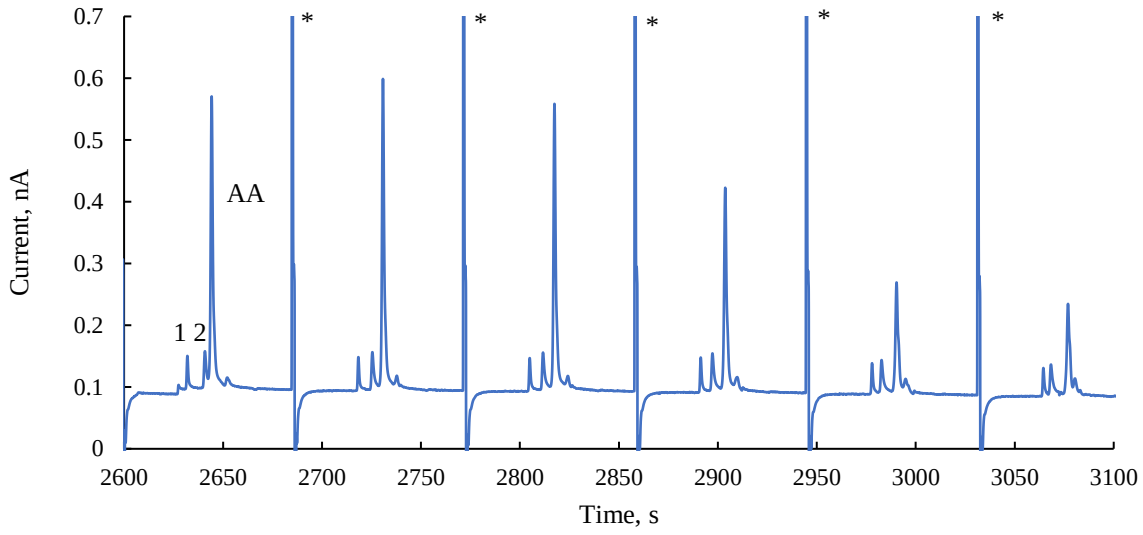

Figure 6.4. Example of ascorbic acid signal change during the switch to perfusion of 1 mM solution of L-Glu in 15 mM sodium phosphate pH 7.4. Asterisks indicate signals corresponding to sample injection. BGE: 15 mM sodium phosphate pH 8.5, 2 mM SDS, 10 mM boric acid. 5 cm separation channel, 220 V/cm, detection at 0.8 V vs Ag/AgCl.

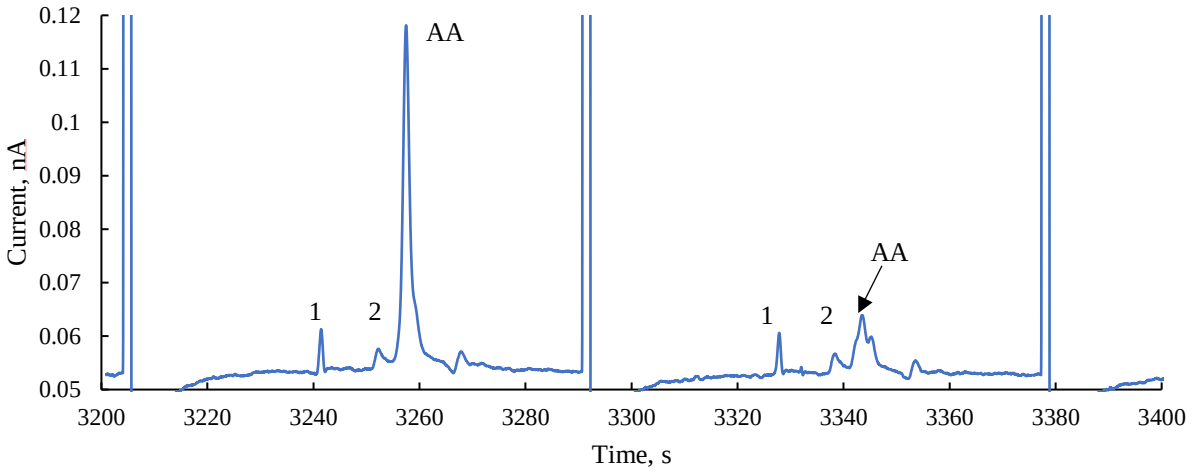

Figure 6.5. Ascorbate signal drop caused by perfusion of 1 mM solution of L-Glu in 15 mM sodium phosphate pH 7.4 allowed the detection of other analytes that were comigrating with its peak. BGE: 15 mM sodium phosphate pH 8.5, 2 mM SDS, 10 mM boric acid. 5 cm separation channel, 220 V/cm, detection at 0.8 V vs Ag/AgCl.

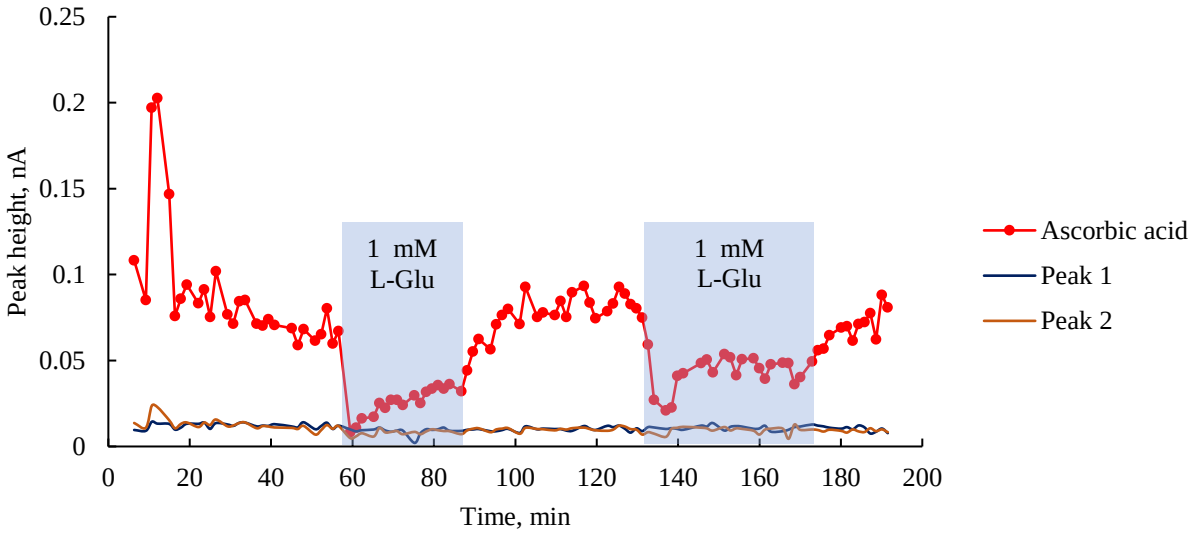

Figure 6.6. Peak heights of the unknown analytes and ascorbic acid in the course of one of the *in vivo* on-line MD-ME-EC experiments involving perfusion of 1 mM L-Glu solution. Blue boxes indicate the stimulation time windows.

6.3.2. *Use of D-Glu to elucidate the nature of the ascorbate signal change*

The first set of animal experiments produced an effect opposite of the increase of AA signal expected from literature. To gain insight into the cause of this disagreement, another set of n = 3 experiments was carried out where MD perfusate contained 1 mM of the "unnatural" chiral isomer of glutamate – D-Glu. Substitution of the stimulating agent for its chiral isomer meant that its interactions with the probe membrane and detection system were not altered, however the effects on the L-Glu transporters and receptors were eliminated. This idea was supported by a study carried out in rat synaptosomes, where the release of AA was observed in the presence of L-Glu but not D-Glu[15]. Therefore, if the same AA signal change was observed during perfusion of D-Glu as in the presence of the L-isomer, the effect was not physiological in nature, and further investigations should be carried out *in vitro*.

As can be seen from the electropherogram shown in Figure 6.7, a rapid drop of AA signal followed by graduate recovery was still observed even with the D-isomer of glutamate. The initial change of the ascorbate peak height was also around 60–90%, the same as for L-Glu. This led to the conclusion that an effect not involving glutamate receptors and transporters is responsible for the observed signal change.

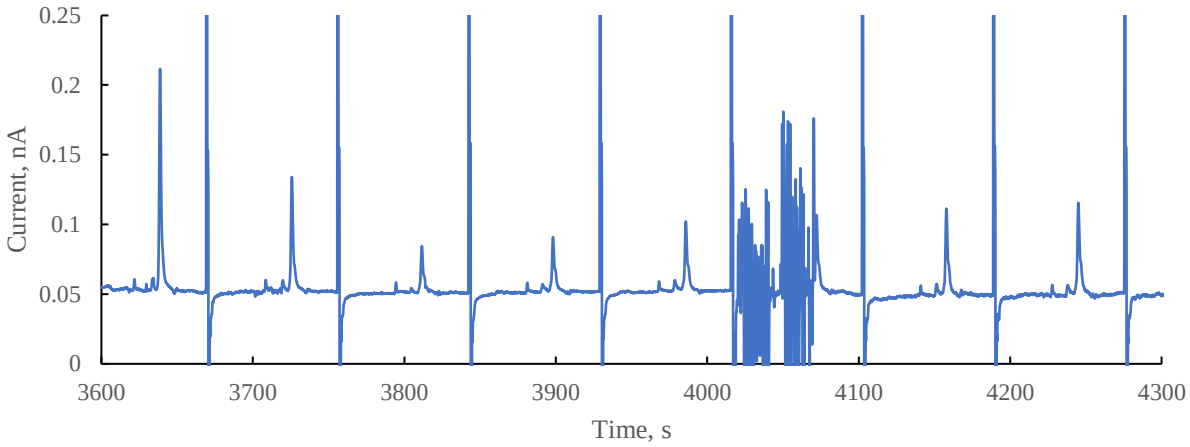

Figure 6.7. Ascorbate signal drop and graduate recover during perfusion of 1 mM solution of D-Glu in 15 mM sodium phosphate pH 7.4. BGE: 15 mM sodium phosphate pH 8.5, 2 mM SDS, 10 mM boric acid. 5 cm separation channel, 220 V/cm, detection at 0.8 V vs Ag/AgCl.

6.3.3. *In vitro investigation of the effect of Glu on ascorbate signal*

The first line of investigation was to experimentally determine whether the presence of Glu in the sample matrix negatively affected the detection of ascorbate during on-line ME-EC. Two standard mixtures of 100 μM dopamine and 100 μM ascorbate were prepared either in 15 mM sodium phosphate pH 7.4 or in 1 mM Glu and 15 mM sodium phosphate pH 7.4. Figure 6.8 shows the electropherograms obtained when the two standard solutions were directly introduced into the device from a syringe (without microdialysis sampling). As can be seen, the opposite effect was observed and the signals of DA and AA increased in the presence of Glu in the sample. While the nature of signal enhancement due to the addition of Glu to the sample matrix warrants its own detailed investigation, it is beyond the scope of this study and will not be further addressed here.

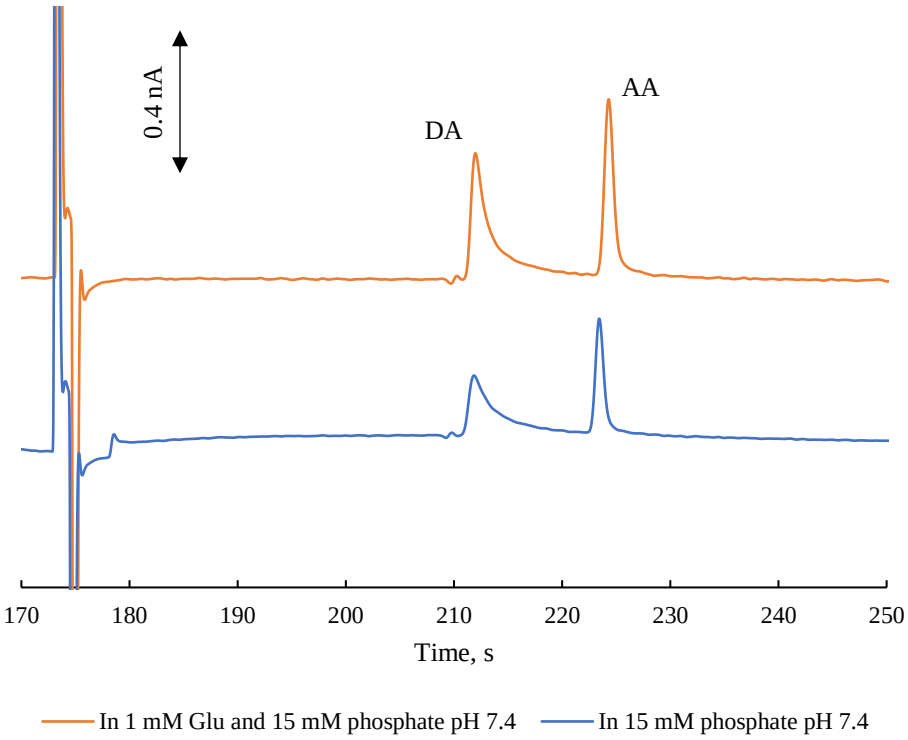

Figure 6.8. Comparison of the DA and AA peaks obtained by direct injection of standard solutions (without MD sampling) with and without the addition of 1 mM Glu into the sample matrix. BGE: 15 mM sodium phosphate pH 8.5, 2 mM SDS, 10 mM boric acid. 5 cm separation channel, 220 V/cm, detection at 0.8 V vs Ag/AgCl.

Next, an *in vitro* study of the effect of Glu concentration in perfusate on the signal of DA and AA was executed using MD-ME-EC. DA was added to the standard mixture in order to see if a positively charged analyte would be affected in the same manner as ascorbate. The experimental setup used is shown in Figure 6.9. The solution of 100 µM DA and 100 µM AA was prepared in artificial CSF (**aCSF**) at pH 7.4 to mimic the extracellular space environment, placed in a glass vial, and stirred to prevent the depletion of analytes from the solution in immediate contact with the probe membrane. MD sampling was performed with 15 mM phosphate pH 7.4 as perfusate for consistency with the *in vivo* experiments.

Concentration of Glu in the perfusate was varied from 50 µM to 1 mM. Figure 6.10 shows the variation of the analyte peak heights in the course of the experiment. The peak height for DA remained at the same magnitude throughout, independent of the perfusate used for sampling. On the other hand, the peak height of AA was affected by the concentration of Glu in the perfusate. While the lowest glutamate concentration of 50 µM did not appear to change the signal of ascorbate, an increase to 100 µM Glu in perfusate caused a 60% decrease of AA peak height. Perfusion of 0.5 mM and 1 mM Glu solutions resulted in a complete loss of AA signal. Following "stimulations" the ascorbate signal recovered fully when only phosphate (without Glu) was used as the perfusate. Based on this experimental data we conclude that glutamate affected the recovery of ascorbate across the PAES membrane of the MD probe in a concentration-dependent manner. This interaction was fully reversible, as shown by the recovery of the AA signal once Glu had been removed from perfusate.

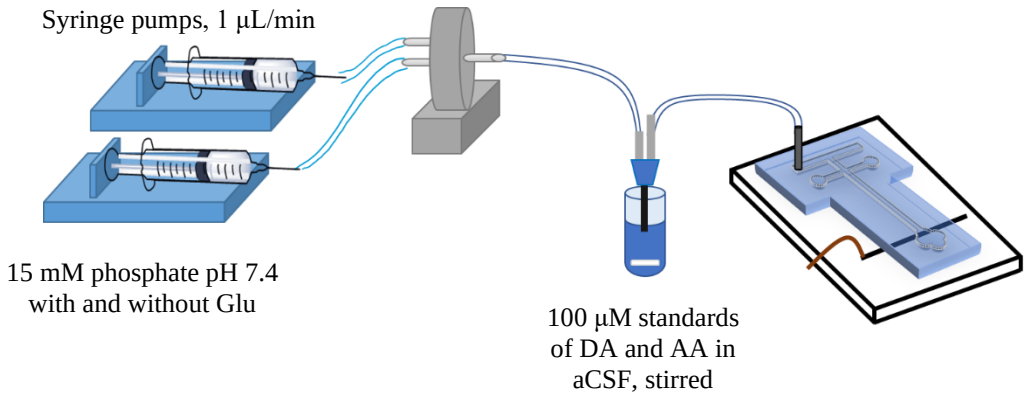

Figure 6.9. Experimental setup for *in vitro* MD-ME-EC studies.

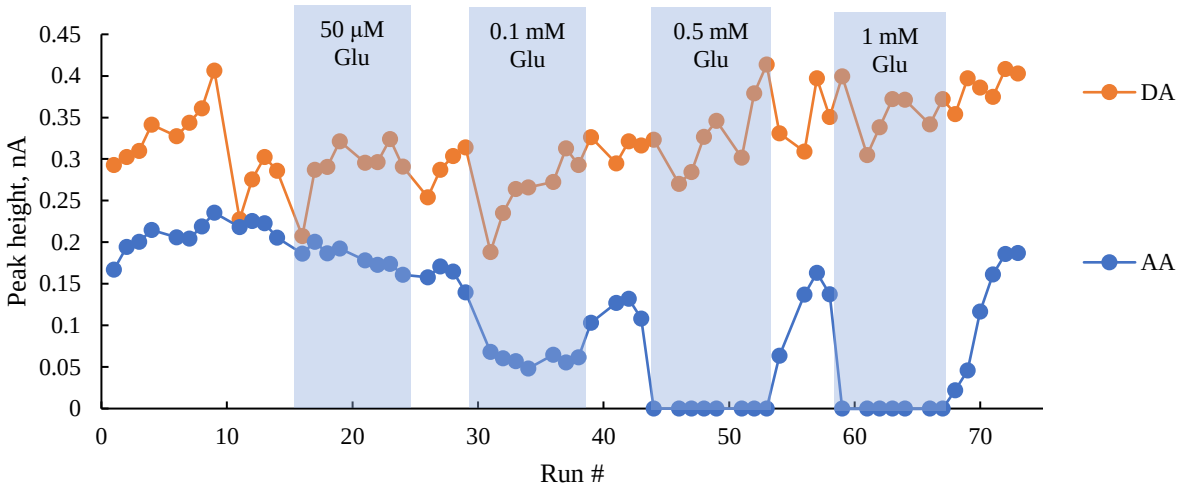

Figure 6.10. Effect of Glu concentration in perfusate on the signals of DA and AA during MD sampling from a vial containing solution of analyte standards in aCSF.

It should be noted that during *in vitro* experiments no recovery of the ascorbate signal was observed while Glu was present in perfusate. However, during the *in vivo* studies the AA peak gradually increased following the initial drop of signal after the switch to glutamate-containing perfusate. This could be an indication that the expected release of ascorbate actually does occur in our animal studies but is obscured by the overall degradation of ascorbate transport across the probe membrane caused by the presence of glutamate.

The experiment was repeated with the addition of a negatively charged dopamine metabolite 3,4-dihydroxyphenylacetic acid (**DOPAC**) to the standard mixture in the vial (also at 100 µM) in an attempt to determine whether the effect of Glu on the recovery of analytes depends on their charge. However, no changes of DOPAC signal were observed *in vitro* (Figure 6.11), pointing to a more complex mechanism of the AA signal change.

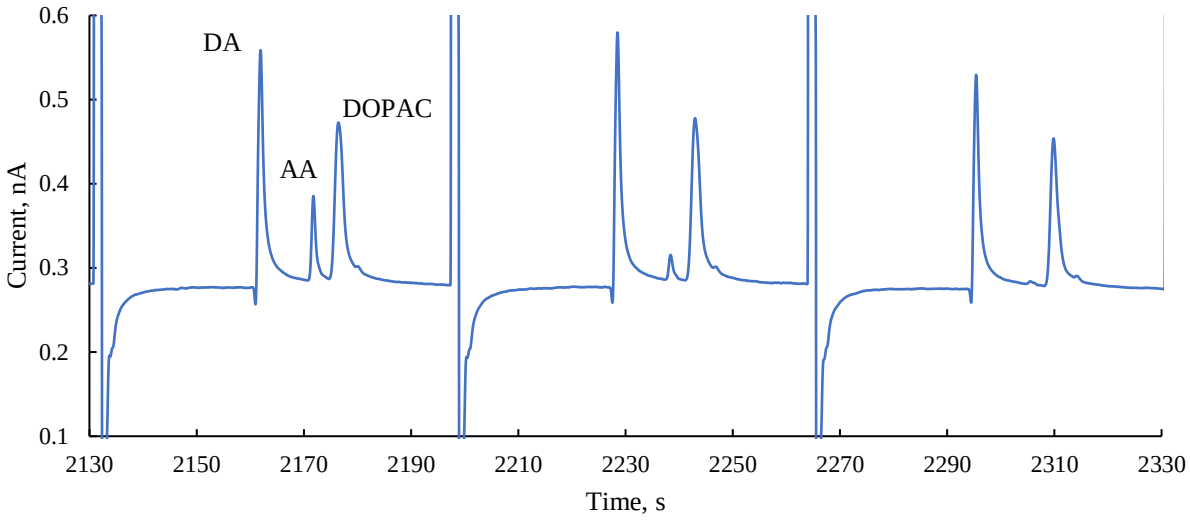

Figure 6.11. Neither DA nor DOPAC were affected by the presence of 1 mM Glu in perfusate the same way as AA. BGE: 15 mM sodium phosphate pH 8.5, 2 mM SDS, 10 mM boric acid. 5 cm separation channel, 220 V/cm, detection at 0.8 V vs Ag/AgCl.

6.3.4. *Artifactual nature of the presented observations*

In the course of experiments described in the previous sections we were able to collect a significant amount of evidence confirming a relationship between the observed ascorbate signal during on-line MD-ME-EC experiments and the presence of glutamate in perfusate. The collected data is not sufficient to draw definitive conclusions about the nature of the underlying interactions, and other experiments, for example those utilizing other perfusate additives similar to Glu (e.g. glutamine, aspartate, arginine) could shed more light on the nature of the observed phenomenon.

Unfortunately, having collected the presented data in the late 2019 – early 2020, we have since been unable to reproduce these results. When the *in vivo* and *in vitro* experiments were repeated in 2021–2022, perfusion of the MD probe with 15 mM phosphate pH 7.4 containing 1 mM L-Glu did not result in a decrease of the AA signal, which remained stable independently of the perfusate used. The only critical difference between the past experiments and our recent attempts to replicate

them which we have been able to identify are the microdialysis probes used. While the manufacturer and supplier of the CMA 12 concentric probes have not been changed, it is possible that alterations to the manufacturing process have taken place between 2019 (when probes used in the experiments above were purchased) and 2021. It is also possible that the specific batch of probes used in the original experiments was produces with a membrane artefact of unknown nature, which is absent in the devices produces today.

6.4. Conclusions

A series of *in vivo* on-line MD-ME-EC experiments exhibiting degradation of the ascorbate signal in the presence of both L- and D-Glu in perfusate was performed. While the AA content in dialysate was expected increase following retrodialysis of glutamate into the brain tissues, a rapid drop followed by slow recovery of ascorbate peak height was seen. A similar effect was observed *in vitro* and was shown to be concentration dependent, however the signal did not recover as long as Glu was present in the perfusate. The *in vitro* reduction of AA detector response was shown to be concentration-dependent, and signals of both positively charged dopamine and its negatively charged metabolite DOPAC did not experience the same degradation as ascorbate, suggesting that the effect did not simply depend on the analyte charge.

While we unfortunately have not been able to continue this investigation due to the inability to replicate past results with a new batch of microdialysis probes, this study is not the first to show a change of analyte recovery based on the changes of perfusate composition for this group of compounds. In a study by Lai *et al.* the *in vivo* recovery of Glu during microdialysis sampling changed from 89% to 39% when the concentration of ascorbate in aCSF-based perfusate was increased from 0 to 400 μM[8], although the authors list glutamate-ascorbate heteroexchange as one of the possible reasons for this change.

Nonetheless, these experiments serve to highlight the importance of approaching new experimental protocols for *in vivo* microdialysis studies with great caution. Based on the observed artifacts, it is recommended that any new sampling conditions are first evaluated *in vitro* before being applied with animals to account for any non-physiological effects of the novel parameters.

6.5. References

(1) Grünewald, R. A. Ascorbic Acid in the Brain. *Brain Res. Rev.* **1993**, *18* (1), 123–133.

(2) Rice, M. E. Ascorbate Regulation and Its Neuroprotective Role in the Brain. *Trends Neurosci.* **2000**, *23* (5), 209–216.

(3) Cammack, J.; Ghasemzadeh, B.; Adams, R. N. The Pharmacological Profile of Glutamate-Evoked Ascorbic Acid Efflux Measured by in Vivo Electrochemistry. *Brain Res.* **1991**, *565* (1), 17–22.

(4) Alessandri, B.; Landolt, H.; Langemann, H.; Gregorin, J.; Hall, J.; Gratzl, O. Application of Glutamate in the Cortex of Rats: A Microdialysis Study. *Acta Neurochir. Suppl.* **1996**, *1996* (67), 6–12.

(5) Corti, A.; Casini, A. F.; Pompella, A. Cellular Pathways for Transport and Efflux of Ascorbate and Dehydroascorbate. *Arch. Biochem. Biophys.* **2010**, *500* (2), 107–115.

(6) Wilson, J. X.; Peters, C. E.; Sitar, S. M.; Daoust, P.; Gelb, A. W. Glutamate Stimulates Ascorbate Transport by Astrocytes. *Brain Res.* **2000**, *858* (1), 61–66.

(7) May, J. M.; Li, L.; Hayslett, K.; Qu, Z. C. Ascorbate Transport and Recycling by SH-SY5Y Neuroblastoma Cells: Response to Glutamate Toxicity. *Neurochem. Res.* **2006**, *31* (6), 785–794.

(8) Lai, Y. J.; Shen, E. Y.; Pan, W. H. T. Effects of Ascorbate in Microdialysis Perfusion Medium on the Extracellular Basal Concentration of Glutamate in Rat's Striatum. *Neurosci. Lett.* **2000**, *279* (3), 145–148.

(9) Morales, I.; Fuentes, A.; Ballaz, S.; Obeso, J. A.; Rodriguez, M. Striatal Interaction among Dopamine, Glutamate and Ascorbate. *Neuropharmacology* **2012**, *63* (8), 1308–1314.

(10) Yusa, T. Increased Extracellular Ascorbate Release Reflects Glutamate Re-Uptake during the Early Stage of Reperfusion after Forebrain Ischemia in Rats. *Brain Res.* **2001**, *897* (1–2), 104–113.

(11) Tsai, P. J.; Chen, W. Y.; Tzeng, S. F.; Liang, W. M.; Yang, C. S. Experimental Spinal Cord Injury Induced an Increase of Extracellular Ascorbic Acid Concentration in Anesthetized Rats: A Microdialysis Study. *Clin. Chim. Acta* **2005**, *362* (1–2), 94–100.

(12) Liu, K.; Lin, Y.; Xiang, L.; Yu, P.; Su, L.; Mao, L. Comparative Study of Change in Extracellular Ascorbic Acid in Different Brain Ischemia/Reperfusion Models with in Vivo Microdialysis Combined with on-Line Electrochemical Detection. *Neurochem. Int.* **2008**, *52* (6), 1247–1255.

(13) Gunawardhana, S. M.; Bulgakova, G. A.; Barybin, A. M.; Thomas, S. R.; Lunte, S. M. Progress toward the Development of a Microchip Electrophoresis Separation-Based Sensor with Electrochemical Detection for on-Line: In Vivo Monitoring of Catecholamines. *Analyst* **2020**, *145* (5), 1768–1776.

(14) Zhou, Y.; Danbolt, N. C. Glutamate as a Neurotransmitter in the Healthy Brain. *J. Neural Transm.* **2014**, *121* (8), 799–817.

(15) Grünewald, R. A.; Fillenz, M. Release of Ascorbate from a Synaptosomal Fraction of Rat Brain. *Neurochem. Int.* **1984**, *6* (4), 491–500.

7. Separation method for on-line tITP preconcentration and quantification of ATP, ADP, and AMP with capillary electrophoresis with UV absorption detection

7.1. Introduction

The brain is notorious for the high amounts of energy it requires for normal operation. Adenosine triphosphate (**ATP**) is the chief chemical source of energy in living cells and is produced in the brain mainly through phosphorylation of adenosine diphosphate (**ADP**) in mitochondria. While oxidative metabolism of ATP is involved in a wide range of cerebral processes from neurotransmitter, protein, and lipid synthesis to fast axonal transport and maintenance of structural integrity of the cells, most of the ATP produced in the brain is utilized to maintain Na^+, K^+, and Ca^{2+} ion gradients across neuronal membranes in order to enable generation, transmission, and processing of electrical impulses[1,2]. At the same time, research regarding the role of adenosine metabolites, including ATP, has been expanding in the last decades beyond their function as an energy source. Several ATP-sensitive receptors have been identified in neuronal, glial, and epithelial cells[3–6]. Closer investigations into their function has made it possible to identify ATP's involvement in synaptic neuromodulation via presynaptic regulation of neurotransmitter release, postsynaptic regulation of receptors and neuronal excitability, and control of synaptic plasticity[3].

While the use of ATP for energy purposes relies on intracellular stores of this adenosine metabolite[1], some of the more recently discovered "exotic" processes involving the compound require its presence in the extracellular space[3,7–9]. Additionally, a range of pathological conditions, such as cellular damage, hypoxia, and ischemia result in release of ATP into the extracellular space[10–12]. Thus, methods to quantitate ATP and its metabolites adenosine diphosphate (**ADP**) and adenosine monophosphate (**AMP**) in the extracellular space of the brain are in high demand by the investigators interested in gaining insight into the mechanics of such pathologies and developing therapeutic approaches to mitigating tissue damage.

A range of approaches to quantifying ATP and its metabolites have been developed over the years (enzyme and aptamer-based biosensors, luminescence-based assays, *in vivo* fluorescent probes,[13–16] etc.), but in general the simultaneous monitoring of ATP and its metabolites in the brain has been accomplished through analysis of microdialysis samples collected from brain using artificial cerebrospinal fluid (**aCSF**) as perfusate by high-performance liquid chromatography (**HPLC**) paired with fluorescence[11], UV absorbance[17], and electrochemical detection[18]. Capillary electrophoresis (**CE**) serves as an alternative to HPLC for ATP quantification, especially when coupled to mass-spectrometry (**MS**)[19,20], due to its low sample and solvent requirements, high separation efficiency, and relatively short analysis times. It should be noted, however, that MS detection of anionic species is considerably more challenging than the detection of cations. Furthermore, while UV detectors coupled to CE tend to yield higher limits of detection than MS, several approaches to improving CE-UV sensitivity using modified detection cells and on-line sample preconcentration have been developed and successfully utilized with high ionic strength samples such as aCSF-based microdialysates[21–25].

In his Ph. D. thesis[26], Lunte group alumnus Shamal M. Ungawel Durayalage discussed the development of a reverse polarity CE-UV separation method and an accompanying transient isotachophoresis (tITP) on-line preconcentration technique for ATP, ADP, and AMP in aCSF, which he developed in collaboration with Dr. Ebru Buyuktuncel (Figure 7.1). The described method utilized a background electrolyte (**BGE**) comprised of 100 mM Tris·HCl buffer pH 7.0, 0.05 mM tetradecyltrimethylammonium chloride (**TTAC**), and 15% ACN. To implement tITP preconcentration, sample injection was followed by an injection of 75 mM β-Ala which served as trailing electrolyte (**TE**). Chloride ions present in the Tris·HCl buffer functioned as the leading electrolyte (**LE**).

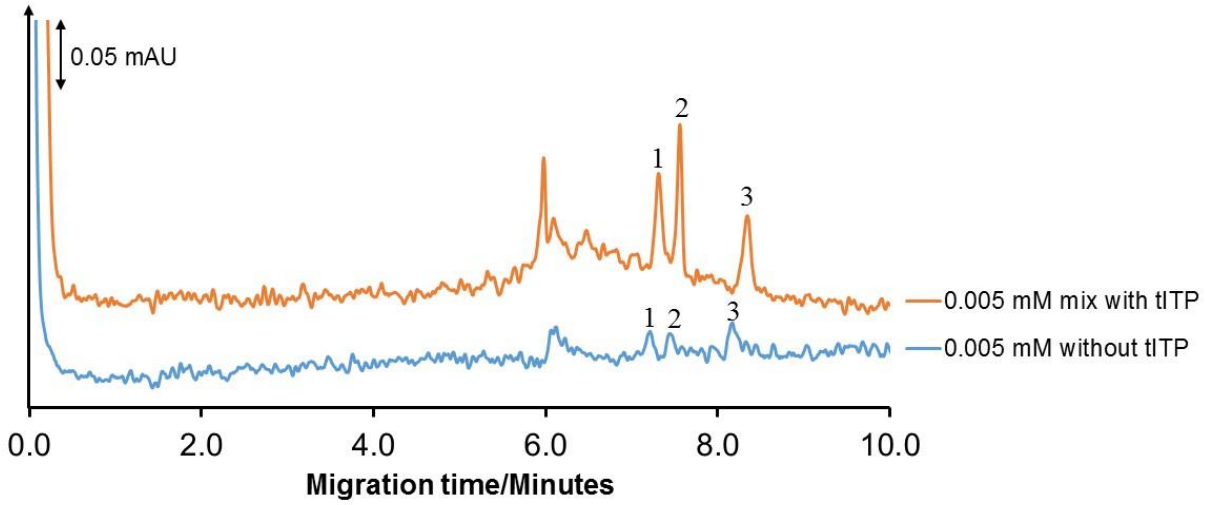

Figure 7.1. Signal enhancement for an ATP (1), ADP (2), and AMP (3) sample prepared in aCSF achieved through implementation of tITP with CE-UV separation. Reproduced from S. M. Ungawel Durayalage[26].

The tITP-CE-UV method resulted in a significant improvement of analyte signals in aCSF-based sample matrices and was used to monitor ATP, ADP, and AMP in microdialysis samples collected from rat striatum. However, further utilization of the method revealed two major shortcomings: it was prone to failure due to frequent clogging of the 25 μm i.d. capillary, and sample carryover was noted (Figure 7.2). The first issue could be resolved by switching to a larger i.d. capillary (50 μm). Although the applied separation voltage had to be decreased from -27.5 kV to -20 kV to maintain separation currents as an acceptable level (65 μA) using the larger i.d. capillary, it also increased the optical pathlength for UV detection, increasing the overall sensitivity of the method.

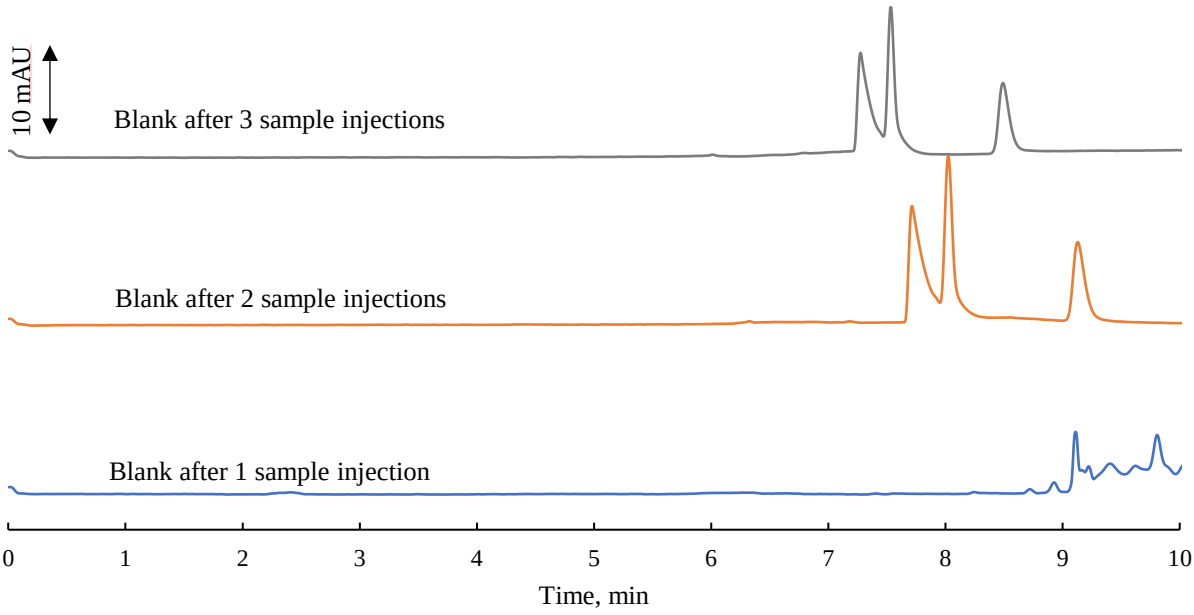

Figure 7.2. Sample carryover for tITP-CE-UV method developed by S. M. Ungawel Durayalage *et al.*[26]

Unfortunately, the problem of sample carryover could not be solved without changing the CE conditions. Analysis of the β-Ala solution used as trailing electrolyte (**TE**) for tITP revealed that analytes contaminated the TE vial after the very first tITP-CE run (Figure 7.3). No improvement was observed when the inlet capillary and electrode were rinsed in water between sample injection and TE injection, suggesting that part of the injected sample migrated out of the capillary during electrokinetic injection of the TE. This may have been caused by the electroosmotic flow (**EOF**) in the inlet section of the capillary being directed away from the detector, forcing some of the analyte ions out of the capillary. When β-Ala was injected hydrodynamically instead of electrokinetically, no sample carryover was observed, but the preconcentration of the analytes was less effective.

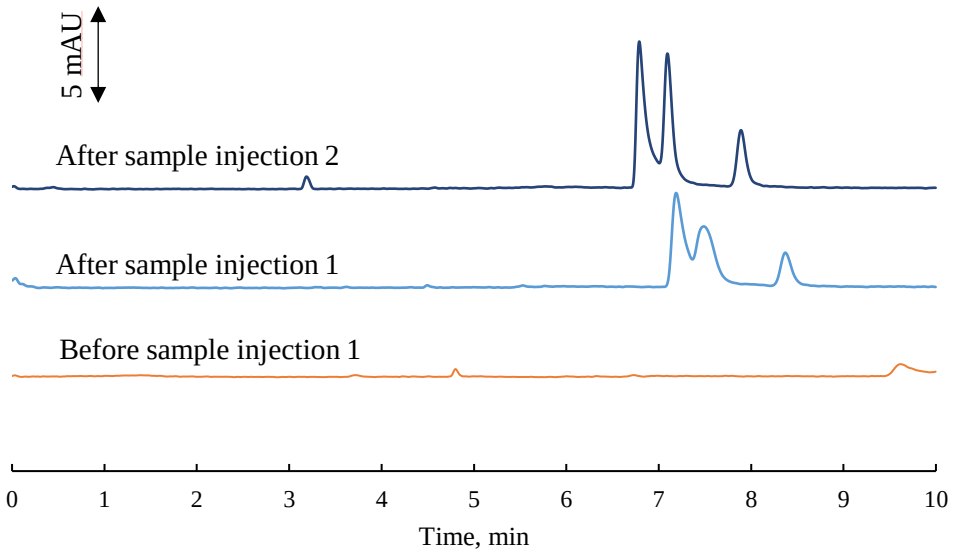

Figure 7.3. Electropherograms obtained for a β-Ala solution used for tITP with a 250 μM sample of ATP, ADP, and AMP prior to and following two injections of sample. Analyzed using the same tITP-CE-UV protocol as the adenosine metabolite sample mixture with a fresh β-Ala solution used for every analysis.

It was also revealed that day-to-day reproducibility of the separation method was suboptimal, likely due to the low concentration of surfactant (0.05 mM) that was used to create a positively charged surface of the capillary to enable the reversed polarity separation. Small variations in capillary conditioning (e.g., base solution freshness) prior to runs resulted in degradation of analyte resolutions. This in combination with the suggestion that sample carryover could be caused by EOF reversal at the inlet led us to the conclusion that in order to improve the performance of the method, a new set of separation conditions needed to be developed using a higher concentration of TTAC.

The investigation described below focuses on the development of a reproducible CE separation method for application with the tITP on-line preconcentration based on the approach described by S. M. Ungawel Durayalage for the analysis of aCSF-based solutions of ATP, ADP, and AMP.

7.2. Materials and methods

7.2.1. *Chemicals and reagents*

Adenosine-5'-triphosphate disodium salt and adenosine-5'-monophosphate disodium salt were purchased from Alfa Aesar (Ward Hill, MA, USA). Adenosine-5'-diphosphate disodium salt was obtained from Acros Organics (Geel, Belgium). Tris(hydroxymethyl)aminomethane·HCl (**Tris·HCl**), β-alanine (**β-Ala**), tetradecyltrimethylammonium chloride (**TTAC**), calcium chloride, anhydrous sodium phosphate monobasic and were obtained from Sigma-Aldrich (St. Louis, MO, USA). Sodium dodecyl sulfate (**SDS**) was provided by Thermo Scientific (Waltham, MA, USA), and hydrochloric acid, orthophosphoric acid, acetic acid, sodium hydroxide, sodium chloride, potassium chloride, methyl alcohol (**MeOH**), and acetonitrile (**ACN**) were purchased from Fisher Scientific (Fairlawn, NJ, USA). All chemicals were used as received. Solutions were prepared using 18.2 MΩ water (Millipore, Kansas City, MO, USA) and filtered with 0.2 μm nylon syringe filters.

7.2.2. *Capillary electrophoresis*

CE analysis was carried out with Agilent 7100 CE-UV system (Santa Clara, CA, USA) equipped with a diode array UV absorbance detector. A 50 μm ID fused silica capillary (Polymicro Technologies, Phoenix, AZ, USA) with a total length of 63.5 cm and effective length of 55.0 cm was used for these studis. Prior to first use, capillaries were conditioned with methanol for 10 min, water for 5 min, 0.1 M HCl for 30 min, water for 5 min, 0.1 M NaOH for 60 min, and water for 5

min. Prior to each analysis run, the capillary was conditioned with BGE for at least 5 min. Sample injection was carried out electrokinetically by applying –5 kV for 20 s unless specified otherwise. Separation voltages varied from –20 kV to –27.5 kV and are indicated for each separation in the text.

7.3. Results and discussion

7.3.1. *Effect of increased TTAC concentration in BGE on the separation of analytes*

To ensure a stable positively charged surface of the capillary, the lowest concentration of TTAC tested was 1 mM, while the highest was 15 mM (Figure 7.4). Increasing the concentration of the surfactant from the 0.05 mM used in the original version of the separation to 1 mM resulted in complete comigration of all three compounds, with their gradual resolution when an increasing amount of surfactant was used. The critical micelle concentration (**CMC**) of TTAC in water is ~5 mM and decreases with increasing ionic strength of solution (~1 mM in the presence of 0.1 M NaCl)[27], therefore it is fair to conclude that it is the presence of micelles that is responsible for the resolution of analytes at TTAC concentrations above 2 mM. This would make micellar electrokinetic chromatography (**MEKC**) the primary separation mechanism under these conditions. It is also noteworthy that the migration order at the highest surfactant concentrations reversed from ATP→ADP→AMP to AMP→ADP→ATP. This is likely due to strong electrostatic interactions between the positively charged micelles and the negatively charged analytes. Therefore, ATP, which has the strongest negative charge of all three compounds (–4), spends more time interacting with the positively charged micelles, the mobility of which is directed towards the cathode and away from the detector, while AMP with its negative charge of –2 reaches the detection window quicker.

The effect of ACN addition on the separation was evaluated using the BGE that provided the best analyte resolution – 100 mM Tris·HCl pH 7.0 and 15 mM TTAC. Concentrations between 5 and 7% of the organic solvent were added to the BGE, however the resolution between AMP and ADP was degraded in the presence of ACN. Therefore it was decided to proceed to the evaluation of the preconcentration method performance with a BGE containing no organic solvent additive.

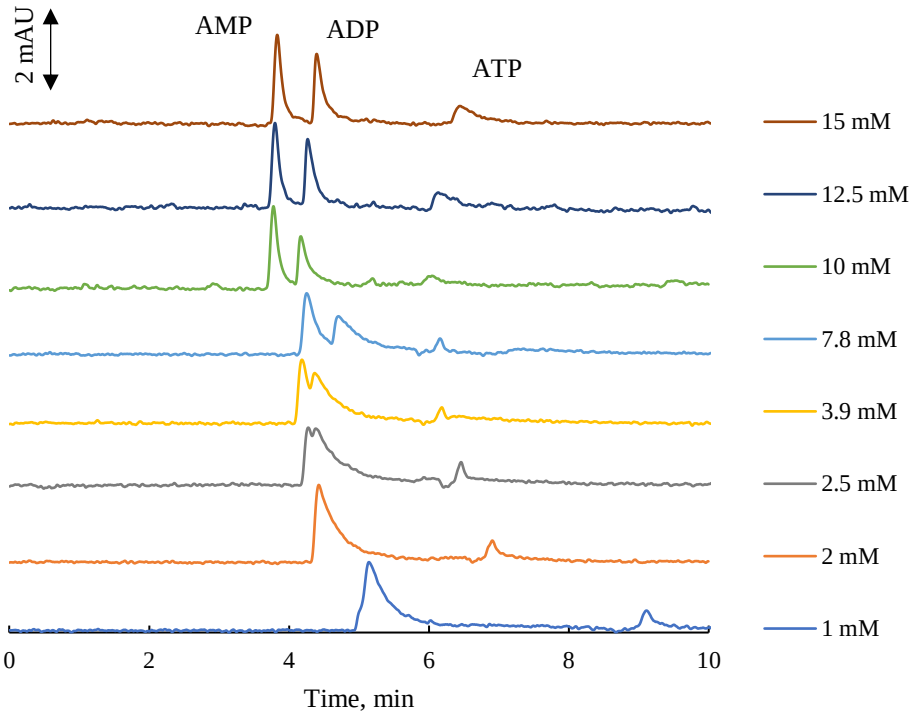

Figure 7.4. Electropherograms of ATP, ADP, and AMP separation in BGEs containing 100 mM Tris·HCl pH 7.0 and various concentrations of TTAC (in legend). 50 µm ID fused silica capillary, 55.0/63.5 cm long, –20.0 kV. Capillary temperature 25 °C Detection wavelength – 254 nm.

7.3.2. *Evaluation of preconcentration methods with MEKC separation*

7.3.2.1. tITP with chloride as leading electrolyte and β-Ala as trailing electrolyte

The on-line preconcentration procedure developed by Dr. Ungawel Durayalage and Dr. Buyuktuncel[26] was then tested with the new MEKC separation using 15 mM TTAC in the BGE. A 50 s electrokinetic injection (–5 kV) of 100 mM β-Ala followed the electrokinetic injection of sample (–5 kV for 20 s) in order to induce stacking of the sample zone. As can be seen in Figure 7.5, only the ADP peak experienced significant stacking, increasing its peak height >4 times. A small increase of the AMP signal was also observed, however the ATP peak remained unchanged. Variation of TE injection time did not lead to improvement of signal enhancement.

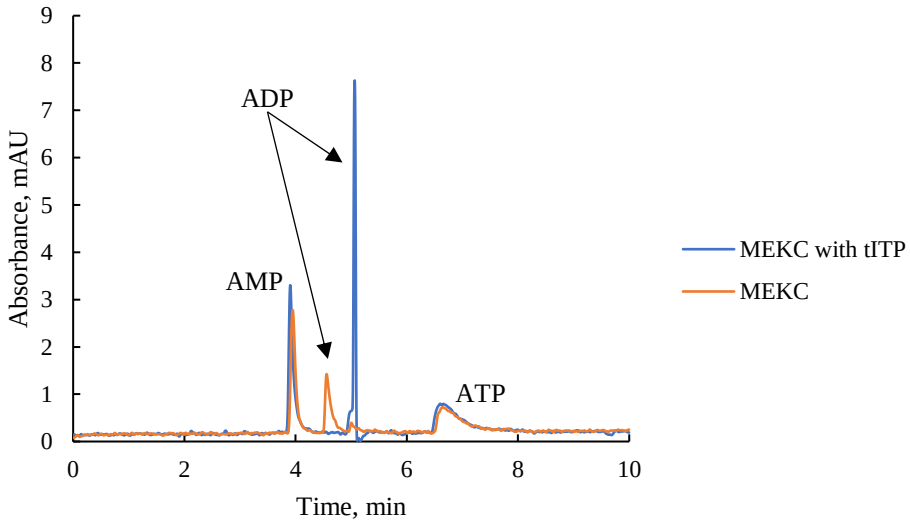

Figure 7.5. Electropherograms of ATP, ADP, and AMP MEKC separations with and without on-line preconcentration using tITP procedure developed by S. M. Ungawel Durayalage. BGE: 100 mM Tris·HCl pH 7.0, 15 mM TTAC. 50 µm ID fused silica capillary, 55.0/63.5 cm long, –20.0 kV. Capillary temperature 25 °C Detection wavelength – 254 nm.

7.3.2.2. pH-mediated stacking

Another method for on-line preconcentration of sample was tested with the developed MEKC separation – pH-mediated stacking. In this approach, a solution containing hydroxide ions was injected into the capillary following the sample injection. While migrating towards the detector under the influence of the negative polarity high voltage applied across the capillary, the OH^- encountered the positively charged TRIS species, which lead to a neutralization reaction between the protonated primary amine of TRIS and the hydroxide. As a result, neutral TRIS and water were produced in the capillary. Conversion of the two charged species into two neutral molecules resulted in a drop of conductivity in the neutralized portion of the solution filling the capillary, increasing the electric field strength, and resulting in stacking of the analyte anions at the boundary between the titrated zone and regular BGE.

Using the conditions described in a publication by S. Arnett and C. Lunte[24] for the preconcentration of several phenolic acids, a negatively charged peptide glutathione disulfide, an anti-inflammatory drug naproxen, and the nucleoside 8-hydroxy-2'-deozyguanosine, analysis was carried out as follows: sample mixture was injected for 60 s at –5 kV, followed by 0.1 M NaOH solution injected also for 60 s at –5 kV, followed by separation at –27.5 kV (Figure 7.6). Such long injection times resulted in a notable degradation of peak shapes, especially for ATP. However, similarly to the implementation of tITP described in the previous section, stacking was observed only for AMP and ADP peaks, with no signal enhancement for ATP. Variation of both sample and base injection times from 30 s to 120 s did not provide improvement of preconcentration efficiency.

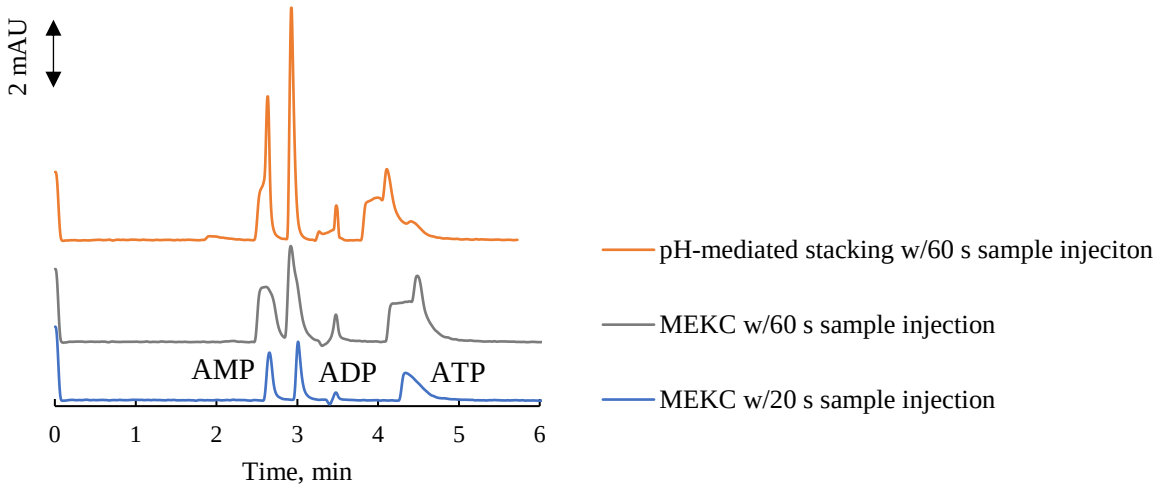

Figure 7.6. Results of pH-mediated stacking of the ATP, ADP, and AMP mixture in aCSF via injection of 0.1 M NaOH. BGE: 100 mM Tris·HCl pH 7.4, 15 mM TTAC. 50 µm ID fused silica capillary, 55.0/63.5 cm long, –27.5 kV. Capillary temperature 25 °C Detection wavelength – 254 nm.

7.3.2.3. Conclusion from preconcentration method application

Implementation of two sample stacking techniques – tITP and pH-mediated stacking – provided mixed results. While some degree of signal enhancement was observed for both AMP and ADP in these conditions, neither method appeared to affect the peak corresponding to ATP. To determine the cause of this lack of ATP signal response to the tested preconcentration approaches, a more detailed examination of the analyte migration order was undertaken. The presence of a system peak between ADP and ATP can be seen in all electropherograms in Figure 7.6. This suggests that the interactions between the positively charged micelles and the strongly negatively charged ATP are powerful enough to reverse the mobility of this species and result in it reaching the detector after the electroosmotic flow. This phenomenon could be responsible for the inability of the stacking methods to influence the peak of ATP: if their mobility is directed away from the detector,

ATP ions do not get a chance to migrate into the lower conductivity stacking zone of the capillary created by the injection of TE or base and therefore they do not experience electric field amplification and remain overall unaffected by the preconcentration procedures.

7.3.3. *Influencing ATP migration*

To enable preconcentration of ATP ions, the direction of their mobility had to be reversed by weakening the interactions between ATP and TTAC micelles. This can be accomplished by either decreasing the overall negative charge of the species or by introducing a competing interaction into the system. Three strategies were evaluated for this purpose: use of lower pH (below 6.5) BGE to partially protonate ATP, chelation of Mg^{2+} by ATP in order to produce a complex with a lower negative charge (see Figure 7.7), and addition of a complexing agent sulfobutyl ether β-cyclodextrin (**SBE-β-CD**) into the BGE.

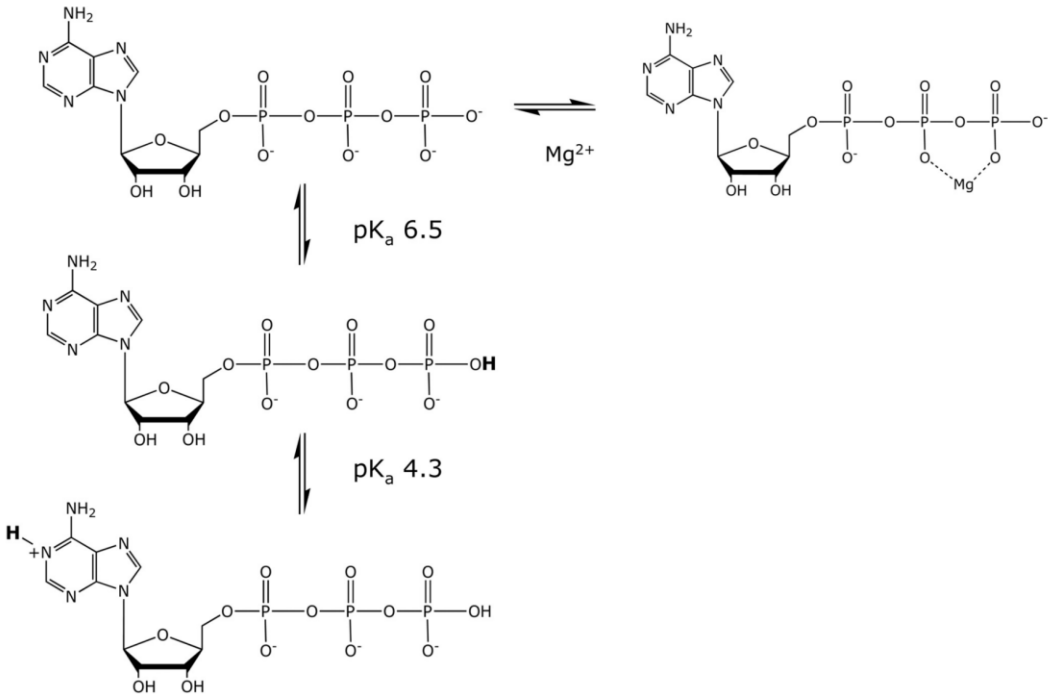

Figure 7.7. Acid-base and Mg^{2+} chelation equilibria of ATP. Reproduced from R. Stockbridge and R. Wolfenden[28].

7.3.3.1. Protonation of ATP in lower pH BGE

Two low pH buffers were tested as BGE for the separation – 15 mM phosphate pH 2.1 with 15 mM TTAC and 15 mM acetate pH 4.1 with 15 mM TTAC. In both cases it was presumed that protonation of the phosphate groups on all analytes would occur, lowering their negative charge and thus weakening their interactions with micelles. Unfortunately, in both cases the low pH was not sufficient to reverse the mobility of ATP. At the same time, low pH BGE results in slower EOF, and in both tested conditions where the overall mobility of ATP (which is a sum of its own mobility and the bulk EOF mobility) was negative, meaning that ATP ions never reached the detector in the course of the analysis. As can be seen from the example shown in Figure 7.8, the electropherogram following ATP sample injection obtained with the pH 2.1 BGE did not contain a sample peak. A similar result was seen at pH 4.1.

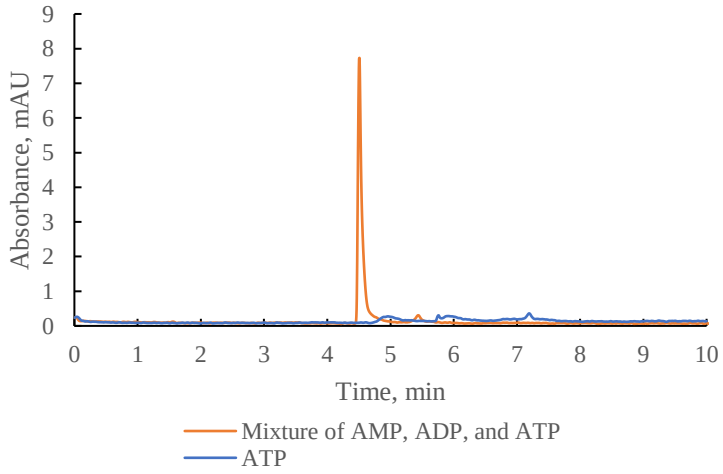

Figure 7.8. Electropherograms obtained following injections of analyte mixture and ATP standard with a low pH BGE. BGE: 15 mM phosphate pH 2.1, 15 mM TTAC. 50 μm ID fused silica capillary, 55.0/63.5 cm long, –27.5 kV. Capillary temperature 25 °C. Detection wavelength – 254 nm.

7.3.3.2. Chelation with Mg^{2+}

The next approach was based on the idea that the overall negative charge of ATP could be lowered by introducing its interaction with Mg^{2+} ions present in the BGE (Figure 7.7). This should have a minimal effect on the EOF present in the system if the amounts of added metal ions are kept low and do not change the BGE pH or ionic strength. Magnesium chloride was used to introduce Mg^{2+} ions into the BGE, and concentrations ranging from 0.5 mM to 10 mM were tested. As can be seen in Figure 7.9, addition of at least 1 mM magnesium was necessary to shift the peak of ATP before the negative system peak serving as marker of EOF mobility. Further increase of its concentration lead to eventual comigration of ATP and ADP at 10 mM. While the ADP peak appears to also be affected by the increased concentrations of Mg^{2+}, AMP mobility remains unchanged throughout the experiment as AMP is unable to complex with the metal ion.

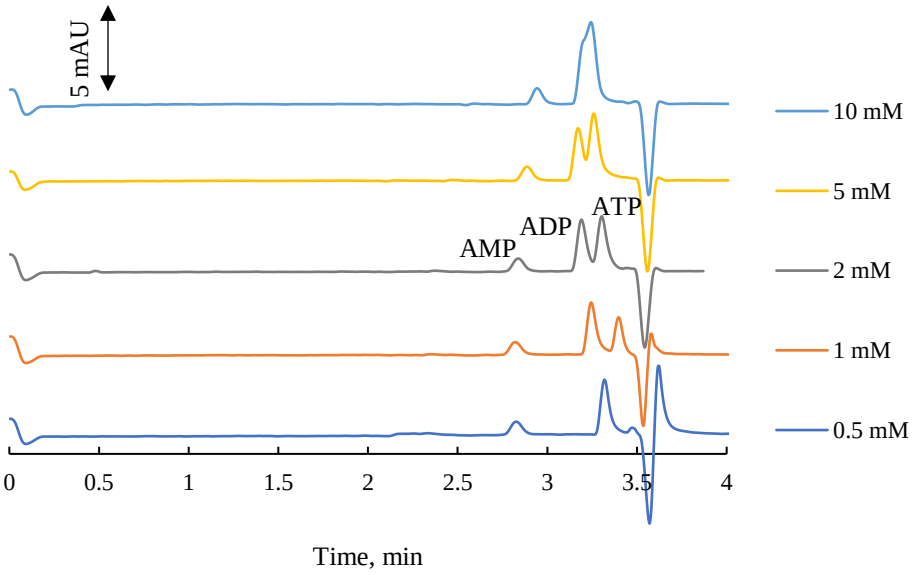

Figure 7.9. Optimization of $MgCl_2$ concentration in the background electrolyte. BGE: 100 mM Tris·HCl pH 7.4, 15 mM TTAC, $MgCl_2$ concentration in legend. 50 µm ID fused silica capillary, 55.0/63.5 cm long, –27.5 kV. Capillary temperature 25 °C. Detection wavelength – 254 nm.

7.3.3.3. Addition of SBE-β-CD

The last approach to altering ATP migration involved an addition of a complexing agent SBE-β-CD to the background electrolyte in order to minimize the interaction between ATP and micelles of TTAC. Concentration of CD additive was varied from 2 mM to 7 mM (Figure 7.10). Addition of 2 mM SBE-β-CD caused comigration of ATP and ADP, with AMP partially resolved from the mixed peak of these compounds. It should be noted that the interaction with CD causes a migration order reversal with ATP migrating before ADP and AMP. Increasing the additive concentration to 5 mM resulted in complete resolution of AMP from the partially comigrating peaks of ATP and ADP. While further increase of additive concentration resulted in improvement of resolution between the first two peaks, such high concentrations of a charged cyclodextrin caused baseline fluctuations and produced significantly lower analyte responses. It should also be noted that the capillary temperature during these experiments was maintained at 15 °C in order to combat Joule heating and improve analyte resolution.

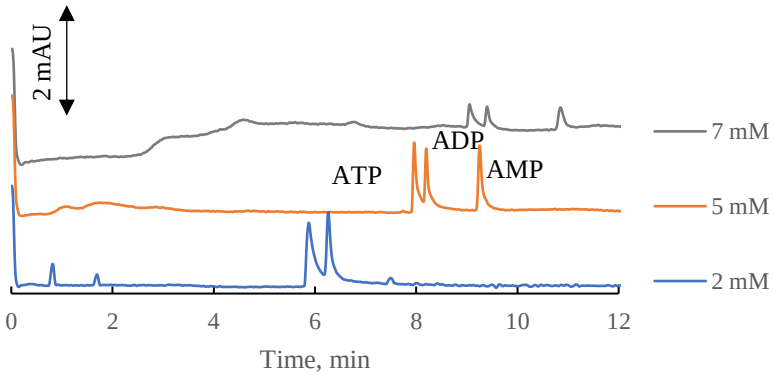

Figure 7.10. Optimization of SBE-β-CD concentration in the background electrolyte. BGE: 100 mM Tris·HCl pH 7.4, 15 mM TTAC, SBE-β-CD concentration in legend. 50 µm ID fused silica capillary, 55.0/63.5 cm long, –27.5 kV. Capillary temperature 15 °C. Detection wavelength – 254 nm.

7.3.3.4. Combining strategies to obtain baseline resolution

Two of the three approaches to altering ATP mobility provided positive results – chelation with magnesium ions and addition of SBE-β-CD. At the same time, neither of them yielded baseline resolution of all three compounds from one another – in the case of Mg^{2+} ADP and ATP began to comigrate at higher concentrations of metal ion additive that reliably placed ATP peak before the EOF marker, and in the case of SBE-β-CD, baseline resolution of AMP and ATP could not be achieved as increased CD concentration resulted in disturbance of baseline and instrument response. Therefore, it was decided to combine the two strategies in one BGE.

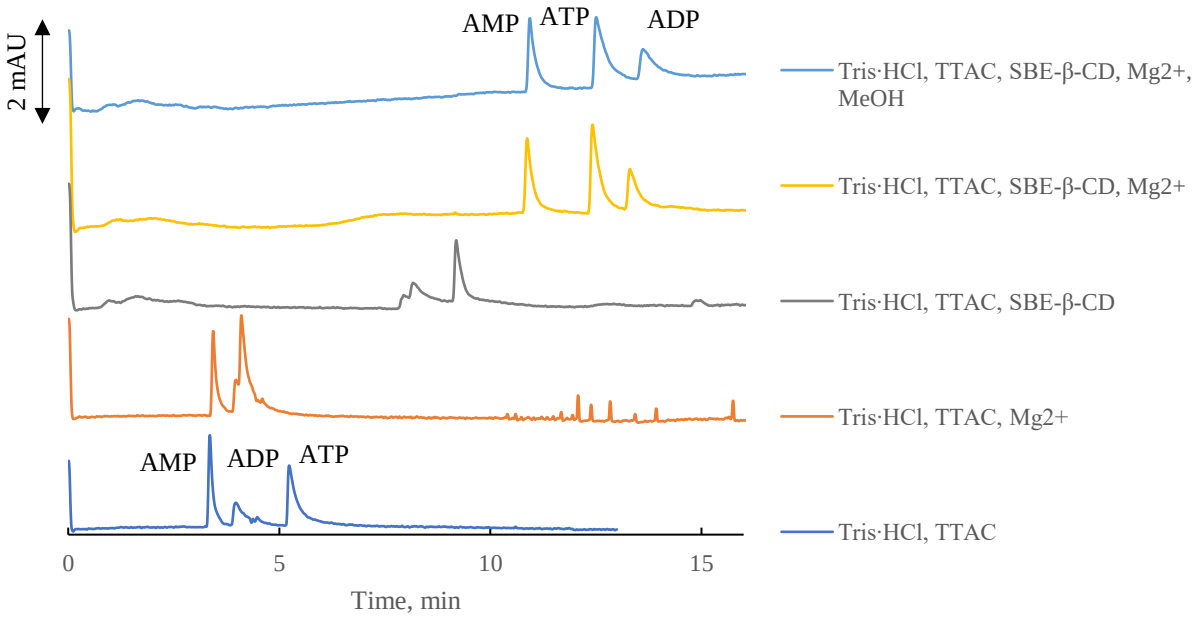

Figure 7.11. Combining two strategies for altering ATP migration – chelation with magnesium ions and complexation with SBE-β-CD. BGE components used for each concentration shown in legend. Component concentrations used: 100 mM Tris·HCl pH 7.4, 15 mM TTAC, 5 mM SBE-β-CD. 1 mM $MgCl_2$, 3% MeOH. 50 µm ID fused silica capillary, 55.0/63.5 cm long, –27.5 kV Capillary temperature 15 °C. Detection wavelength – 254 nm.

Figure 7.11 shows that by combining 2 types of additives and introducing 3% MeOH into the BGE baseline resolution of all analytes could be obtained within a 15 min separation wondow. Notably, the migration order under these conditions is AMP→ATP→ADP. Testing of the tITP preconcentration approach described below was carried out with this optimized BGE: 100 mM Tris·HCl pH 7.4, 15 mM TTAC, 5 mM SBE-β-CD. 1 mM $MgCl_2$, 3% MeOH.

7.3.4. *On-line preconcentration with transient ITP*

The new separation conditions were evaluated for tITP preconcentration with Cl^- as leading electrolyte and β-Ala as trailing electrolyte as described in reference 26[26]. Signal enhancement was observed for all three analytes under these conditions (Figure 7.12). Concentration and time of TE injection were varied to determine the optimal parameters for the preconcentration procedure. As a result, 75 mM β-Ala injected for 100 s at – 5 kV resulted in the greatest peak areas observed (Figure 7.13). Overall, the reoptimized preconcentration procedure resulted in 3–10 times increase of peak height and 6–10 times area increase depending on the analyte of interest. The lowest concentration of analytes that could be detected following preconcentration was 10 μM. While these results may be considered a significant improvement of the CE-UV method sensitivity, further optimization of the preconcentration procedure is necessary to enable detection of the low to mid nanomolar[10,12] physiological extracellular concentrations of ATP.

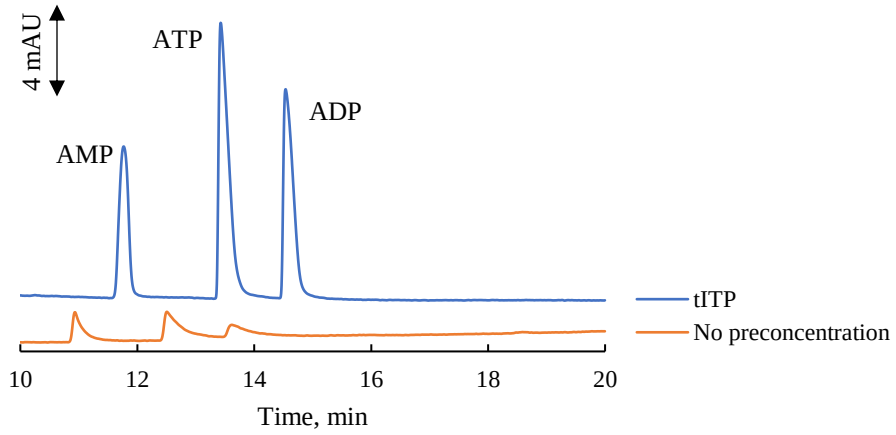

a

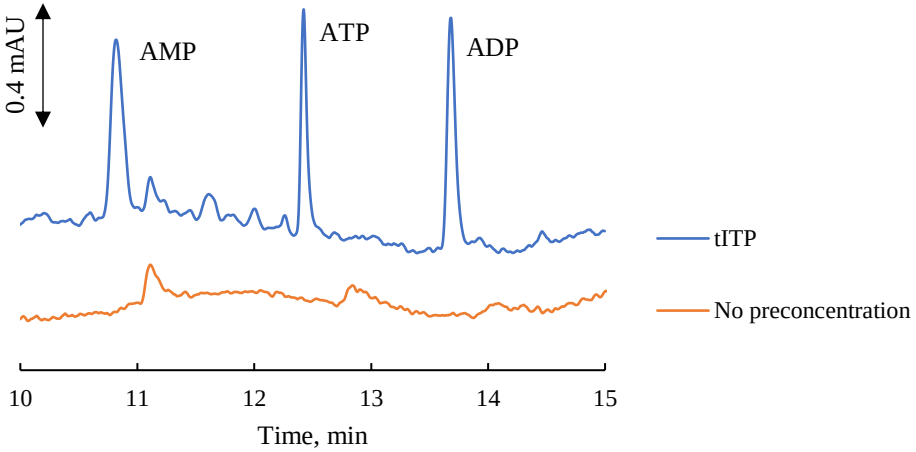

b

Figure 7.12. Implementation of tITP with the new BGE for (*a*) 100 μM and (*b*) 10 μM sample mixes. Sample injection: 20 s, –5 kV. TE (75 mM β-Ala) injection: 100 s, –5 kV. BGE: 100 mM Tris·HCl pH 7.4, 15 mM TTAC, 5 mM SBE-β-CD, 1 mM $MgCl_2$, 3% MeOH. 50 μm ID fused silica capillary, 55.0/63.5 cm long, –27.5 kV. Capillary temperature 15 °C. Detection wavelength – 254 nm.

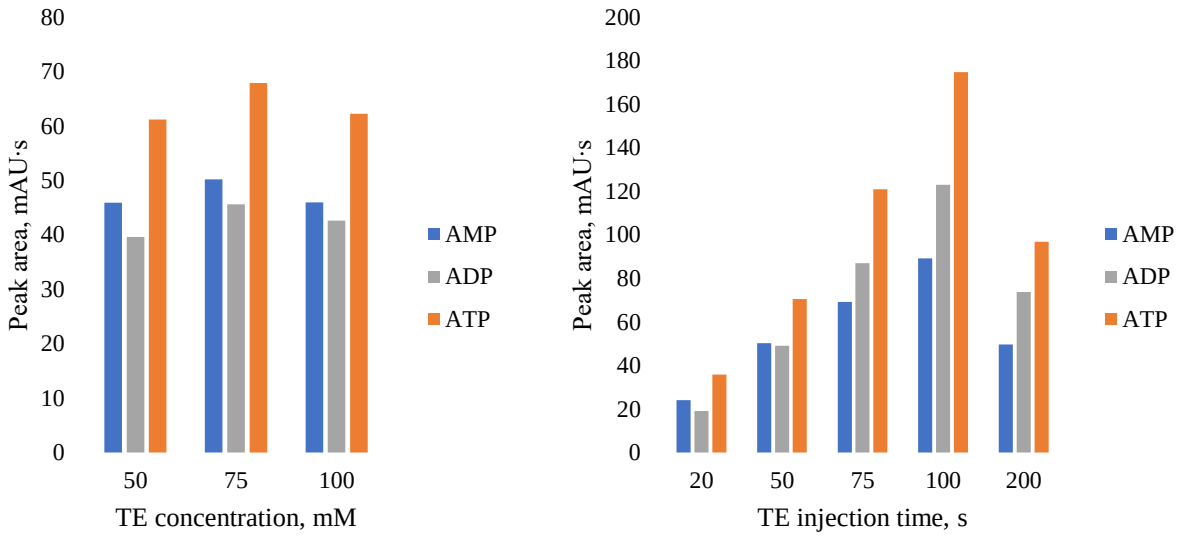

a *b*

Figure 7.13. Optimization of TE concentration (*a*) and injection time (*b*). Sample injection: 20 s, –5 kV. TE injection time for *a* was 75 s at –5 kV. TE concentration in *b* was 75 mM. BGE: 100 mM Tris·HCl pH 7.4, 15 mM TTAC, 5 mM SBE-β-CD, 1 mM $MgCl_2$, 3% MeOH. 50 μm ID fused silica capillary, 55.0/63.5 cm long, –27.5 kV. Capillary temperature 15 °C. Detection wavelength – 254 nm.

7.3.5. *Alternative separation and preconcentration approaches tested*

In the course of the described study, several alternative approaches to separation and preconcentration of AMP, ADP, and AMP in aCSF were evaluated (Table 7.1). While none of the methods yielded satisfactory results, this information could prove useful for future investigations.

Table 7.1. Alternative approaches to analyte separation and sample preconcentration evaluated in the course of this investigation.

Description	Separation polarity	BGE composition	Preconcentration	Result
tITP using hydrodynamic injection of TE	Reverse	100 mM Tris·HCl pH 7.0, 0.5 mM TTAC, 15% ACN	1.5 M β-Ala injected using pressure: 15 mbar for 600 s after sample	Stacking less efficient than traditional tITP, poorly reproducible
Use of polymer-containing BGE for stacking (adapted from Chang *et al.*)	Reverse	100 mM Tris·HCl pH 7.0, 15 mM TTAC, 1.5% PEO	Capillary filled with polymer-containing BGE	Only ATP was stacked
Normal polarity MEKC separation	Normal	100 mM Tris·HCl pH 7.4, 15 mM SDS	N/A	Baseline resolution of analytes within 16 min
tITP using Cl^- as TE and β-Ala as LE	Normal	90 mM Tris·HCl pH 7.4, 15 mM SDS, 200 mM β-Ala	75 mM Cl^- injected for 50 s after sample	Some signal enhancement is observed, but not sufficient for monitoring of biological concentrations
Combination of large volume sample stacking with PEO containing BGE	Normal	100 mM Tris·HCl pH 7.4, 15 mM SDS, 0.5% PEO	Large volume sample stacking	Presence of PEO in BGE does not sufficiently counter sample destacking due to high ionic strength of sample matrix

7.4. Conclusions

CE-UV method for determination of ATP and its metabolites ADP and AMP was developed first as an MEKC separation and then modified to include a magnesium ions and SBE-β-CD for compatibility with tITP preconcentration method developed earlier in our group. The resulting BGE contained 100 mM Tris·HCl pH 7.4, 15 mM TTAC, 5 mM SBE-β-CD, 1 mM $MgCl_2$, and 3% MeOH. Implementation and basic re-optimization of tITP on-line preconcentration approach resulted in significant enhancement of signals for all analytes, although the improved limits of detection were not low enough to enable use of the developed method for analysis of brain microdialysis samples in its current form. Further optimization of the preconcentration procedure including a survey of alternative trailing electrolyte solutions must be carried out to reach biologically relevant LODs. Additionally, capacitively coupled contactless conductivity detection should also be evaluated as the detection method for the developed tITP-CE method.

7.5. References

(1) Erecinska, M.; Silver, I. A. ATP and Brain Function. *J. Cereb. Blood Flow Metab.* **1989**, *9* (1), 2–19.

(2) Du, F.; Zhu, X. H.; Zhang, Y.; Friedman, M.; Zhang, N.; Uğurbil, K.; Chen, W. Tightly Coupled Brain Activity and Cerebral ATP Metabolic Rate. *Proc. Natl. Acad. Sci. U. S. A.* **2008**, *105* (17), 6409–6414.

(3) Rodrigues, R. J.; Tomé, A. R.; Cunha, R. A. ATP as a Multi-Target Danger Signal in the Brain. *Front. Neurosci.* **2015**, *9* (148), 1–11.

(4) Burnstock, G.; B. Fredholm, B.; Verkhratsky, A. Adenosine and ATP Receptors in the Brain. *Curr. Top. Med. Chem.* **2011**, *11* (8), 973–1011.

(5) Liss, B.; Roeper, J. Molecular Physiology of Neuronal K-ATP Channels. *Mol. Membr. Biol.* **2009**, *18* (2), 117–127.

(6) Butt, A. M. ATP: A Ubiquitous Gliotransmitter Integrating Neuron–Glial Networks. *Semin. Cell Dev. Biol.* **2011**, *22* (2), 205–213.

(7) Xu, P.; Xu, Y.; Hu, B.; Wang, J.; Pan, R.; Murugan, M.; Wu, L. J.; Tang, Y. Extracellular ATP Enhances Radiation-Induced Brain Injury through Microglial Activation and Paracrine Signaling via P2X7 Receptor. *Brain. Behav. Immun.* **2015**, *50*, 87–100.

(8) Walz, W.; Ilschner, S.; Ohlemeyer, C.; Banati, R.; Kettenmann, H. Extracellular ATP Activates a Cation Conductance and a K+ Conductance in Cultured Microglial Cells from Mouse Brain. *J. Neurosci.* **1993**, *13* (10), 4403–4411.

(9) Hide, I.; Tanaka, M.; Inoue, A.; Nakajima, K.; Kohsaka, S.; Inoue, K.; Nakata, Y. Extracellular ATP Triggers Tumor Necrosis Factor-α Release from Rat Microglia. *J. Neurochem.* **2000**, *75* (3), 965–972.

(10) Melani, A.; Corti, F.; Stephan, H.; Müller, C. E.; Donati, C.; Bruni, P.; Vannucchi, M. G.; Pedata, F. Ecto-ATPase Inhibition: ATP and Adenosine Release under Physiological and Ischemic in Vivo Conditions in the Rat Striatum. *Exp. Neurol.* **2012**, *233* (1), 193–204.

(11) Doná, F.; Conceição, I. M.; Ulrich, H.; Ribeiro, E. B.; Freitas, T. A.; Nencioni, A. L. A.; da Silva Fernandes, M. J. Variations of ATP and Its Metabolites in the Hippocampus of Rats Subjected to Pilocarpine-Induced Temporal Lobe Epilepsy. *Purinergic Signal.* **2016**, *12* (2), 295–302.

(12) Melani, A.; Turchi, D.; Vannucchi, M. G.; Cipriani, S.; Gianfriddo, M.; Pedata, F. ATP Extracellular Concentrations Are Increased in the Rat Striatum during in Vivo Ischemia. *Neurochem. Int.* **2005**, *47* (6), 442–448.

(13) Llaudet, E.; Hatz, S.; Droniou, M.; Dale, N. Microelectrode Biosensor for Real-Time Measurement

of ATP in Biological Tissue. *Anal. Chem.* **2005**, *77* (10), 3267–3273.

(14) Yao, W.; Wang, L.; Wang, H.; Zhang, X.; Li, L. An Aptamer-Based Electrochemiluminescent Biosensor for ATP Detection. *Biosens. Bioelectron.* **2009**, *24* (11), 3269–3274.

(15) Taylor, A. L.; Kudlow, B. A.; Marrs, K. L.; Gruenert, D. C.; Guggino, W. B.; Schwiebert, E. M. Bioluminescence Detection of ATP Release Mechanisms in Epithelia. *Am. J. Physiol. - Cell Physiol.* **1998**, *275* (5 44-5).

(16) Kitajima, N.; Takikawa, K.; Sekiya, H.; Satoh, K.; Asanuma, D.; Sakamoto, H.; Takahashi, S.; Hanaoka, K.; Urano, Y.; Namiki, S.; Iino, M.; Hirose, K. Real-Time in Vivo Imaging of Extracellular Atp in the Brain with a Hybrid-Type Fluorescent Sensor. *Elife* **2020**, *9*, 1–18.

(17) Marklund, N.; Salci, K.; Ronquist, G.; Hillered, L. Energy Metabolic Changes in the Early Post-Injury Period Following Traumatic Brain Injury in Rats. *Neurochem. Res.* **2006**, *31* (8), 1085–1093.

(18) Lietsche, J.; Imran, I.; Klein, J. Extracellular Levels of ATP and Acetylcholine during Lithium-Pilocarpine Induced Status Epilepticus in Rats. *Neurosci. Lett.* **2016**, *611*, 69–73.

(19) Liu, J. X.; Aerts, J. T.; Rubakhin, S. S.; Zhang, X. X.; Sweedler, J. V. Analysis of Endogenous Nucleotides by Single Cell Capillary Electrophoresis-Mass Spectrometry. *Analyst* **2014**, *139* (22), 5835–5842.

(20) Muroya, S.; Oe, M.; Nakajima, I.; Ojima, K.; Chikuni, K. CE-TOF MS-Based Metabolomic Profiling Revealed Characteristic Metabolic Pathways in Postmortem Porcine Fast and Slow Type Muscles. *Meat Sci.* **2014**, *98* (4), 726–735.

(21) Osbourn, D. M.; Weiss, D. J.; Lunte, C. E. On-Line Preconcentration Methods for Capillary Electrophoresis. *Electrophoresis* **2000**, *21*, 2768–2779.

(22) Britz-McKibbin, P.; Terabe, S. On-Line Preconcentration Strategies for Trace Analysis of Metabolites by Capillary Electrophoresis. *J. Chromatogr. A* **2003**, *1000* (1–2), 917–934.

(23) Kitagawa, F.; Otsuka, K. Recent Applications of On-Line Sample Preconcentration Techniques in Capillary Electrophoresis. *J. Chromatogr. A* **2014**, *1335*, 43–60.

(24) Arnett, S. D.; Lunte, C. E. Investigation of the Mechanism of PH-Mediated Stacking of Anions for the Analysis of Physiological Samples by Capillary Electrophoresis. *Electrophoresis* **2003**, *24* (11), 1745–1752.

(25) Guihen, E.; O'Connor, W. T. Current Separation and Detection Methods in Microdialysis the Drive towards Sensitivity and Speed. *Electrophoresis* **2009**, *30* (12), 2062–2075.

(26) Durayalage Ungawel, S. M. Development Of Microchip Electrophoresis Platforms Coupled With Electrochemical Detection For Continuous On-Line Monitoring Of Neurochemicals In Vivo, University of Kansas, 2019.

(27) Kroflič, A.; Šarac, B.; Bešter-Rogač, M. Influence of the Alkyl Chain Length, Temperature, and Added Salt on the Thermodynamics of Micellization: Alkyltrimethylammonium Chlorides in NaCl Aqueous Solutions. *J. Chem. Thermodyn.* **2011**, *43* (10), 1557–1563.

(28) Stockbridge, R. B.; Wolfenden, R. The Intrinsic Reactivity of ATP and the Catalytic Proficiencies of Kinases Acting on Glucose, N-Acetylgalactosamine, and Homoserine. A Thermodynamic Analysis. *J. Biol. Chem.* **2009**, *284* (34), 22747–22757.

8. Future directions

8.1. Microdialysis sampling with perfusates containing sub-physiological concentrations of NaCl

8.1.1. *Internal standard compatible with liquid chromatography with electrochemical detection (**LC-EC**)*

Use of an internal standard (**IS**) in studies employing microdialysis (**MD**) sampling serves several purposes. When added directly to perfusate, it can provide information on probe recovery and its changes throughout the experiment. If the analytical method needs to be controlled for reproducibility, it may be added to the collected sample immediately prior analysis. In the study described in Chapter 4, 50 μM 3-nitrotyrosine (3-NT) was added to the perfusate for the evaluation of probe performance using undiluted MD samples for capillary electrophoresis (**CE**) analysis. This required collection of additional sample and performance of extra sample runs with long analysis times (> 30 min). Unfortunately, under the conditions of the LC-EC method used for the quantification of neurotransmitter metabolites, 3-NT could not be detected.

Future experiments will survey compounds suitable as internal an standard for both addition to perfusate and collected MD samples. The compounds should be unavailable endogenously, electrochemically active, and fully resolved from the analyte peaks in the LC-EC experiments. If two or more of such compounds are identified, they may be used simultaneously – one in the perfusate and the other as an additive prior to analysis. This would allow to monitor both fluctuations in probe performance and control the LC analysis reproducibility.

8.1.2. *LC-EC method for determination of neurotransmitters*

The LC-EC method used in this study enabled reliable simultaneous determination of 3 neurotransmitter metabolites in MD samples collected *in vivo*. Unfortunately, determination of the

neurotransmitters themselves could not be performed due to their migration with the void peak in the case of norepinephrine and epinephrine, elution close to a large peak of metabolite (dopamine migrated on the tail of DOPAC), and limits of detection which were not sufficiently low. In the future, further optimization of the LC-EC method will be carried out to enable the separation and detection of the neurotransmitters along with their metabolites. Alternative detection methods (*e.g.* mass-spectrometry) may be considered if no improvements are achieved with LC-EC.

8.1.3. *Study of the dependence of neurotransmitter and metabolite recovery on NaCl concentration – experiments with longer post-surgery rest time*

The study described in Chapter 4 determined that to draw definitive conclusions regarding the effects of NaCl content in perfusate on the amount of analytes present in the MD sample, the rest time between probe implantation and off-line collection of sample fractions must be longer than 1 h. A study with rest times of 2 h and above will be carried out to determine under what conditions no time-dependent changes of analyte concentrations for *in vivo* MD sampling occur, making it possible to perform experiments evaluating other parameters that may affect analyte recovery.

Once the appropriate duration of rest is determined, a study of the dependence of metabolite recovery on NaCl concentration will be repeated.

8.1.4. *Determination of neurotransmitter and metabolite recoveries using no-net-flux method for MD calibration*

In order to utilize a perfusate with sub-physiological concentration of NaCl (*e.g.* 20% NaCl aCSF) for studies of animal models, it is critical to determine relative recovery of analytes from tissues in the experiment. No-net-flux approach to calibration of microdialysis sampling[1] will be used to determine basal concentrations of analytes and calculate recovery percentages for each species of

interest. In the future, this information will be used to estimate extracellular concentrations of analytes during experiments performed with animal models of diseases.

8.1.5. *Effects on recovery during multi-hour sampling*

It was shown that beyond the initial equilibration time sampling with a perfusate containing 20% of physiological NaCl concentration did not affect analyte and Na^+ recovery for 1 h. A set of *in vivo* experiments will be performed to determine whether longer sampling times result in changes of basal neurotransmitter, metabolite, and metal ion concentrations in the dialysate when a sub-physiological concentration of sodium is used in the perfusate.

8.2. Microchip electrophoresis separation with electrochemical detection (**ME-EC**) methods for monitoring of monoamine neurotransmitters and related analytes

8.2.1. *Internal standard*

To perform accurate quantification and identification of analytes using the ME-EC methods described in this thesis, an internal standard needs to be added to the separation. This will allow to correct for variation of sample injection both run-to-run and following the switch from the standard mixture to the biological sample, especially during off-line analysis where the electrokinetic injection is heavily dependent on the salinity of the sample matrix. A survey of possible IS will be performed to select candidates that would work with both phosphate and MES buffer based background electrolytes (**BGE**).

8.2.2. *Improving limits of detection – decoupling of separation field from the PPF working electrode*

During the off-line analysis of the homogenate sample detailed in Chapter 3, it was possible to tentatively quantify norepinephrine and dopamine. However, limits of detection of the ME-EC

method using MES-based BGE on a double t chip for on-line analysis are currently not low enough to monitor basal, or possibly even stimulated, concentrations of neurotransmitters in microdialysis samples, which tend to be in the nanomolar range[2]. Therefore, future experiments will focus on improving the sensitivity of the developed ME-EC methods by isolating the carbon pyrolyzed photoresist film (**PPF**) working electrode from the separation field by using a metal decoupler electrode and performing the EC detection off-channel. This approach has been proven successful for the devices using metal[3] and carbon paste[4] working electrodes, and the challenge of its implementation with PPF lies in the fabrication of the electrode plate containing both metal and carbon features very close to each other (Figure 8.1*a*). First attempts at fabricating such plates showed that if the palladium electrode is sputtered into the trench of the quartz plate prior to deposition and pyrolysis of photoresist, the high temperatures in the tube furnace interfere with adherence of the metal feature to the glass, causing it to delaminate when the separation current is grounded through it (Figure 8.1*b*). Therefore, the carbon feature must be fabricated first and protected during metal deposition process.

8.2.1. *Monitoring of negatively charged metabolites*

In the described ME-EC separations negatively charged metabolites of dopamine HVA and DOPAC migrate very closely to the peak of ascorbic acid. As ascorbate is present in the brain tissues at high micromolar–millimolar concentrations[5], its signal during analysis of both MD and homogenate samples is large and obscures peaks of both dopamine metabolites. To enable monitoring of HVA and DOPAC, two strategies will be evaluated: enzymatic degradation of ascorbic acid in homogenate samples prior to their off-line analysis and use of a cyclodextrin (**CD**) BGE additive to increase resolution of metabolites from ascorbate. A preliminary study showed that an addition of 20 mM heptakis-(2,6-di-o-methyl)-β-CD to the BGE containing 15 mM

phosphate buffer at pH 8.5 and 2 mM SDS caused 5-HIAA (negatively charged serotonin metabolite), HVA, and DOPAC to migrate faster than ascorbate (Figure 8.2), making it easier to detect these species in the presence of high concentrations of ascorbic acid.

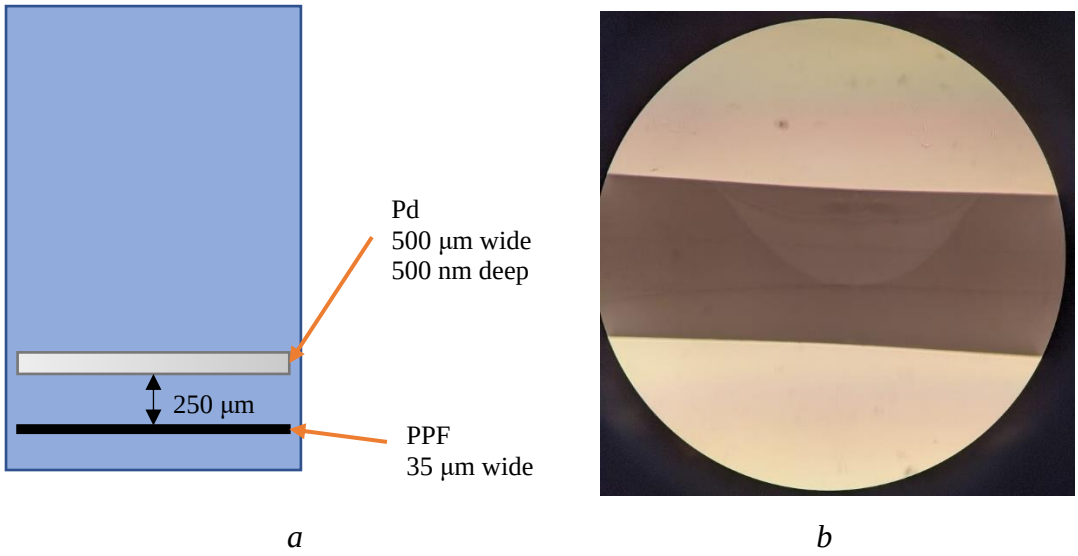

Figure 8.1. (*a*) Decoupler electrode plate design and (*b*) a microscope image of decoupler delaminating from the glass substrate after separation current was grounded through it.

8.3. Application of developed MD and ME-EC methods with animal models (off-line and on-line analysis)

Following optimization and evaluation microdialysis sampling with a low-sodium perfusate, identification of suitable internal standards and improvement of sensitivity for the ME-EC methods, and optimization of strategies for quantification of the negatively charged metabolites, the resulting methods will be implemented with animal models of stroke and neurodegenerative disorders. They will also be used in studies correlating animal behavior with neurotransmitter levels in microdialysates, with the end goal of application for on-animal studies with freely roaming animals.

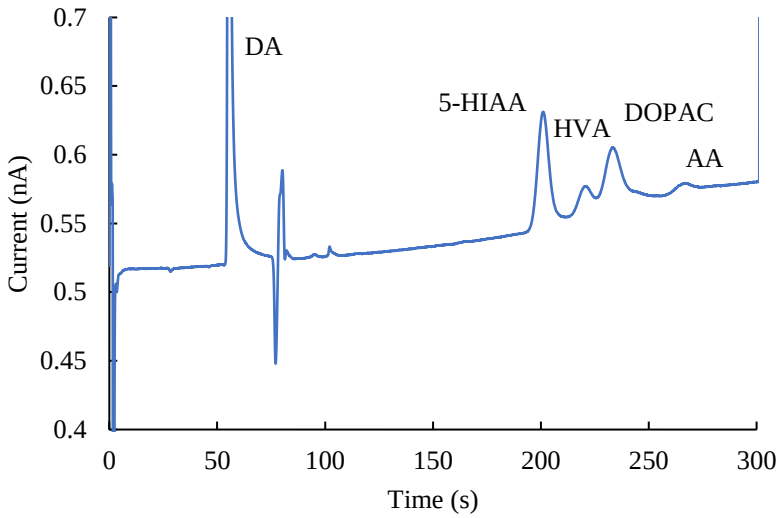

Figure 8.2. Separation of the negatively charged metabolites in a BGE consisting of 15 mM phosphate at pH 8.5, 2 mM SDS, 20 mM heptakis-(2,6-di-o-methyl)-β-CD. 5 cm long separation channel, 220 V/cm. Detection at 0.800 V vs Ag/AgCl.

8.4. Effect of perfusate glutamate of the signal of ascorbic acid

The adverse effects of the presence of glutamate in perfusate on the signal of ascorbic acid described in Chapter 6 were shown to be artifactual. A more recent attempt to evoke ascorbate release by retrodialysis of glutamate at 1 mM showed no increase of the ascorbate signal. Future experiments will be based off a similar study carried out with sampling from rat cortex[6] which utilized a perfusate containing 500 mM monosodium glutamate to induce a 325% increase of ascorbate concentration. The new perfusate will be first evaluated *in vitro* to ensure the absence of non-physiological effects of such high concentration of glutamate on the ascorbate signal.

8.5. CE-UV method for determination of ATP and its metabolites in microdialysis samples

The separation method developed for ATP and its metabolites was shown to be compatible with the previously developed procedure for on-line sample preconcentration using transient

isotachophoresis (tITP). However, the signal improvement obtained with this method was not sufficient to enable detection of basal physiological concentrations of the compounds of interest. Optimization of the on-line preconcentration procedure will be continued to survey alternative trailing electrolyte (**TE**) candidates, TE concentration, duration of injection, and injection method. Once the LODs enabling detection of basal levels of extracellular ATP are achieved, the method will be applied to studies of ATP release in animal models of ischemia and traumatic brain injury.

8.6. References

(1) Kho, C. M.; Enche Ab Rahim, S. K.; Ahmad, Z. A.; Abdullah, N. S. A Review on Microdialysis Calibration Methods: The Theory and Current Related Efforts. *Mol. Neurobiol. 2016 545* **2016**, *54* (5), 3506–3527.

(2) Ngo, K. T.; Varner, E. L.; Michael, A. C.; Weber, S. G. Monitoring Dopamine Responses to Potassium Ion and Nomifensine by in Vivo Microdialysis with Online Liquid Chromatography at One-Minute Resolution. *ACS Chem. Neurosci.* **2017**, *8* (2), 329–338.

(3) Lacher, N. A.; Lunte, S. M.; Martin, R. S. Development of a Microfabricated Palladium Decoupler/Electrochemical Detector for Microchip Capillary Electrophoresis Using a Hybrid Glass/Poly(Dimethylsiloxane) Device. *Anal. Chem.* **2004**, *76* (9), 2482–2491.

(4) Johnson, A. S.; Selimovic, A.; Martin, R. S. Integration of Microchip Electrophoresis with Electrochemical Detection Using an Epoxy-Based Molding Method to Embed Multiple Electrode Materials. *Electrophoresis* **2011**, *32* (22), 3121–3128.

(5) Rice, M. E. Ascorbate Regulation and Its Neuroprotective Role in the Brain. *Trends Neurosci.* **2000**, *23* (5), 209–216.

(6) Alessandri, B.; Landolt, H.; Langemann, H.; Gregorin, J.; Hall, J.; Gratzl, O. Application of Glutamate in the Cortex of Rats: A Microdialysis Study. *Acta Neurochir. Suppl.* **1996**, *1996* (67), 6–12.

Appendix:

CE-UV method for chiral separation of NDA-derivatized glutamate and aspartate

All amino acids except glycine are chiral, and L-isomers make up the majority of those found in animal tissues (both free and as part of proteins and peptides). Nonetheless, since the discovery of D-amino acids in the various tissues of both invertebrate and vertebrate species, the biological function of these "unnatural" amino acids has been a matter of great scientific interest.

In the brain, the most information has been revealed about D-serine (**D-Ser**) and D-aspartate (**D-Asp**). D-Ser was found to be a co-agonist for the N-methyl-D-aspartate (**NMDA**) receptor involved in the L-glutamate (**L-Glu**) excitatory neurotransmission. D-Asp has been shown to participate in neurogenesis, reproduction, and vision. On the other hand, while D-glutamate (**D-Glu**) has been found in various brain regions and peripheral tissues, its function is yet to be identified. Methods enabling quantification of the D-amino acids with high sensitivity are in demand by the researchers who seek to investigate the biochemical functions of these chiral isomers.[1]

During the Summer of 2019 Research Experience of Undergraduates program at the University of Kansas I worked with Samantha Negron – a student from California State University San Marcos – on the development of a separation of glutamate and aspartate chiral isomers following their derivatization for fluorescence detection (**LIF**) with naphthalene-2,3-dicarboxaldehyde (**NDA**) and sodium cyanide (**CN**). The separation of NDA-derivatized amino acids previously developed in our group for microchip electrophoresis (**ME**) coupled with LIF was used as the starting point for the study[2]. To simplify and speed up the survey of the conditions which would enable the chiral separation, optimization of the background electrolyte (**BGE**) composition was carried out using capillary electrophoresis with UV detection (**CE-UV**), as the conventional instrument allowed for automation of the analysis runs.

Instrumentation used for the project included: Agilent 7100 CE-UV system (Santa Clara, CA, USA), 50 µm ID fused silica capillary with 55 cm effective length and 63.5 cm full length (Polymicro Technologies, Phoenix, AZ, USA). Separations were carried out using +30 kV unless specified otherwise, and analyte detection was performed at 254 nm. Derivatization of samples was carried out according to the procedure described by Oborny *et al.*[2] Amino acid standard solutions (Asp, Glu, and arginine (**Arg**)) were prepared in artificial cerebrospinal fluid.

Prior to the development of the chiral separation, parameters of the hydrodynamic sample injection were optimized to ensure reproducibility of the observed peak areas. The following conditions were tested: 50 mbar × 5 s, 30 mbar × 10 s, and 25 mbar × 15 s. As can be seen from Figure A.1, the injection using a lower pressure for a longer time yielded the most reproducible analyte peak areas and was therefore used for the remainder of the study.

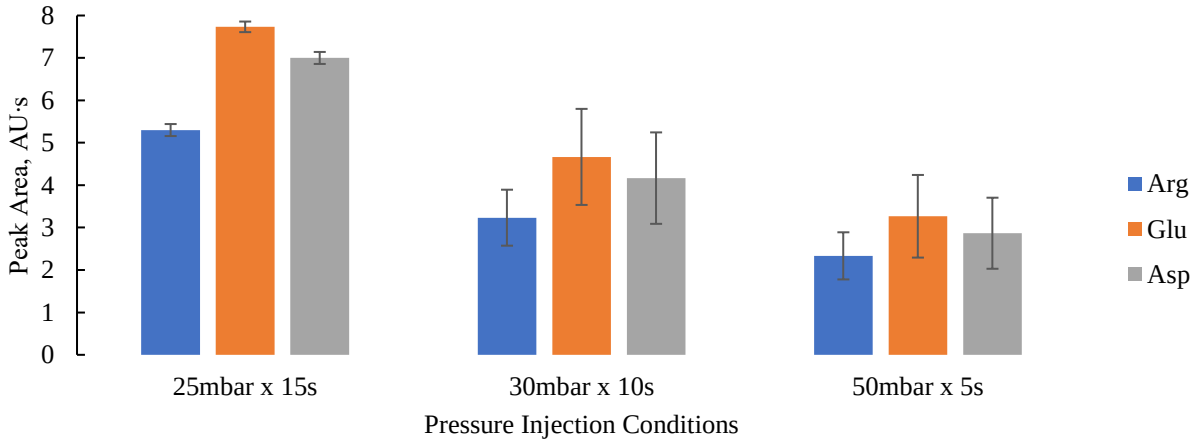

Figure A.1. Comparison of peak areas obtained with various hydrodynamic sample injection parameters. Error bars – standard deviations.

Electrophoretic separations happen based on the differences in the ratio of charge to hydrodynamic radius of the analytes of interest. Furthermore, bulk electroosmotic flow (**EOF**) carries all analytes, independent of their charge, to the detector. As a result, in normal polarity separations the small

positively charged analytes are detected first, followed by larger cations with smaller charge, neutral species, large anions, and small highly charged anions migrating last. However, chiral isomers do not differ from each other in either charge or size. To enable their separation, an optically pure chiral additive – referred to as chiral selector (**CS**) – must be added to the BGE. The CS must interact with each enantiomer of the analyte species differently (form complexes with different stability), changing their effective mobilities and leading to their resolution. Cyclodextrins (**CD**) are cyclic oligosaccharides typically made up from 6–8 glucose units joined by α-1,4 glycosidic bonds. Native and modified cyclodextrins are often used as CS as they are enantiomerically pure, have multiple sites for complexation (through hydrogen bonding or functional groups) and can support host-guest interactions with hydrophobic compounds due to their toroid shape.[3]

The original BGE had the following composition: 15 mM sodium tetraborate pH 9.2, 10% v/v dimethylsulfoxide (**DMSO**), and 1.4 mM sulfobutyl ether-β-cyclodextrin (**SBE-β-CD**).[2] Here the CD was used to improve resolution of different derivatized amino acids, therefore it made sense to explore the selectivity of this CS for the chiral pairs of Glu and Asp before testing any alternatives. To this end, the concentration of SBE-β-CD was varied from 1.4 mM to 12.5 mM, while the other components were kept constant (15 mM sodium tetraborate pH 9.2, 10% v/v DMSO). Resolution of both chiral pairs was observed under these conditions, with the maximum R_s values observed at 12.5 mM of CS (Figure A.2*a*). While the enantioselectivity of this CD was higher for D,L-Glu, neither pair was baseline resolved with the tested conditions.

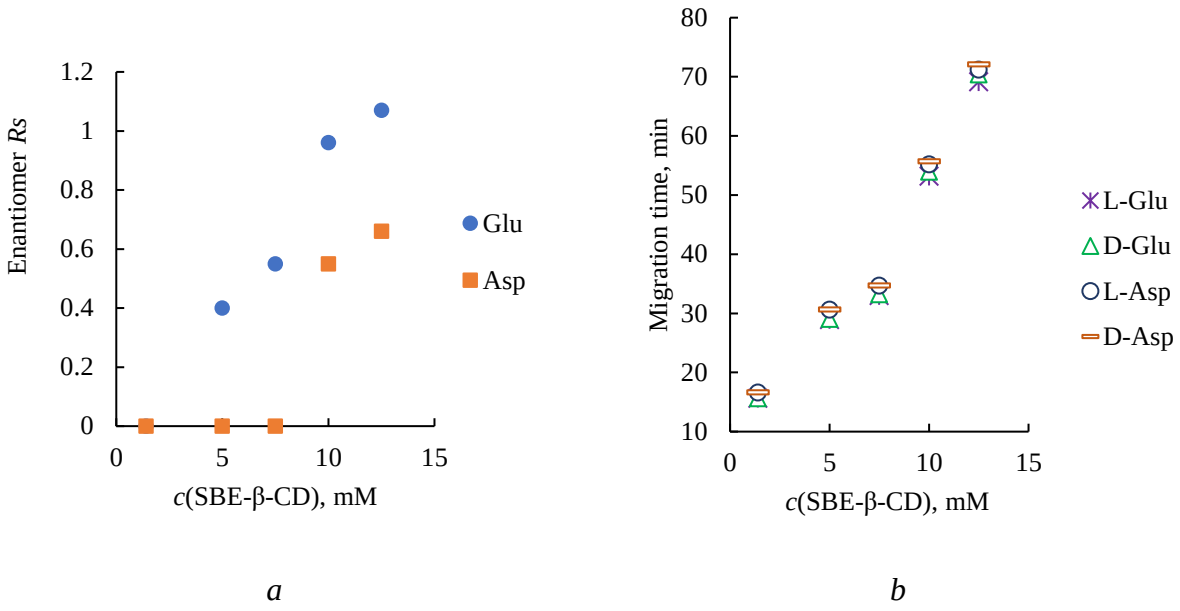

a *b*

Figure A.2. Optimization of the SBE-β-CD concentration in BGE for the chiral separation of D,L-Glu and D,L-Asp. (*a*) Dependence of the chiral isomer resolution on the concentration of CS. (*b*) Dependence of migration time on the concentration of CS.

Increasing the concentration of the CD also caused an increase of analyte migration time. This effect was caused by both the increased ionic strength of the BGE slowing down the EOF and due to complexation of the analytes with the negatively charged CD. As a result, at the highest tested CD concentration the separation took over 1 h, making the second-highest concentration of 10 mM more optimal since the loss of resolution (ΔRs ~ 0.1 compared to 12.5 mM CD) was minimal compared to the nearly 15 min shorter of the separation time.

Next, a neutral β-CD was evaluated as CS. The selector was added to the BGE containing 15 mM sodium tetraborate pH 9.2 and 10% v/v DMSO at concentrations ranging from 0.5 to 7.5 mM Figure A.3). Near-baseline resolution of L- and D-Asp was observed at the lowest concentration of CS tested, and *Rs* values of 3 and above were determined at all other concentrations, with the maximum value of *Rs* = 3.48 at 3.5 mM β-CD. Resolution of the Glu pair followed the same

pattern, however the enantioselectivity was not as strong as for the Asp pair, with the resolution remaining under 1.3 at all concentrations. At the optimal concentration of 3 mM of β-CD the separation took < 21 minutes.

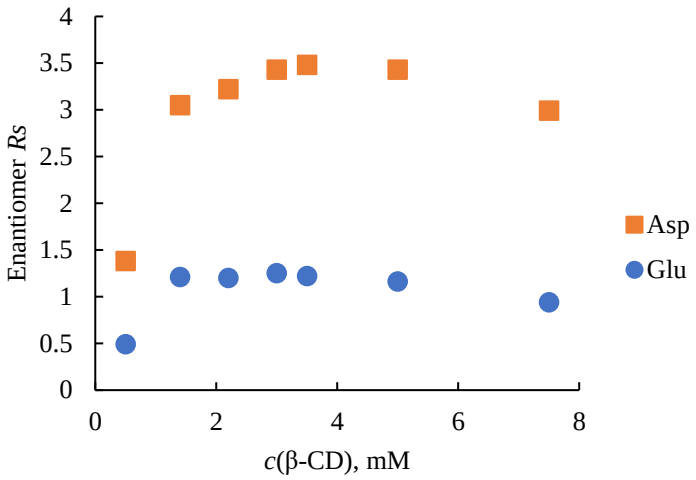

Figure A.3. Dependence of the chiral isomer resolution on the concentration of β-CD.

A positively charged chiral selector the quaternary amine β-CD (**QA-β-CD**) was also tested. A publication by Patel *et al.* described use of this CD as CS for the separation of the NDA-derivatized D,L-Glu and D,L-Asp with a BGE consisting of 110 ppm QA-β-CD, 60 mM MES buffer pH 6.0, 100 mM KBr in reverse polarity with the separation voltage of –30 kV. However, we were unable to replicate their results: when the conditions from the publication were used (Figure A.4). Some chiral selectivity was observed for both pairs, but the peaks were not baseline resolved and had poor shapes. Doubling of the selector concentration to 220 ppm improved analyte resolution but exacerbated the peak shape degradation. When the selector was used with 15 mM sodium tetraborate pH 9.2 and 10% v/v DMSO, no analyte peaks were observed with a normal polarity separation. Switching the BGE to 15 mM citrate pH 6.0 and 10% v/v DMSO with 100 ppm QA-β-CD yielded a separation that was similar to that observed in the MES buffer – with the resolution not reaching baseline and the peaks experiencing significant tailing.

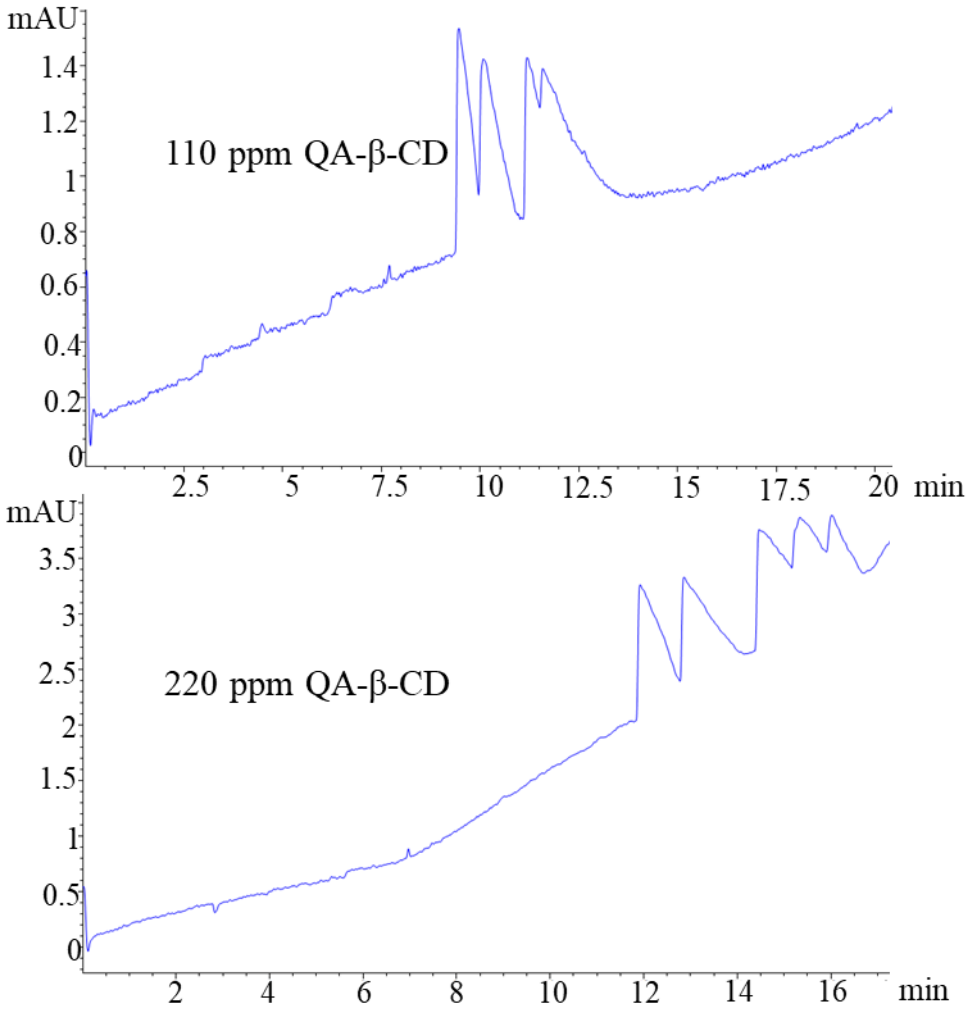

Figure A.4. Separation of chiral isomers of L,D-Glu and L,D-Asp with QA-β-CD as chiral selector using the conditions described in Patel *et al.* BGE: 110 ppm QA-β-CD, 60 mM MES buffer pH 6.0, 100 mM KBr. Separation voltage –30 kV.

While each individual CS failed to enable baseline resolution of both pairs of chiral isomers of interest, it was decided to try using two selectors that showed the best results – native β-CD and SBE-β-CD – simultaneously. Notably, SBE-β-CD was shown to be more selective for the Glu pair and β-CD worked better for resolving D,L-Asp, leading to the assumption that combining the two would yield baseline resolution of analytes. The optimization started by combining the optimal

concentrations of CS in one BGE: 10 mM SBE-β-CD, 3 mM β-CD, and 15 mM sodium tetraborate pH 9.2 with 10% v/v DMSO. Then the ratio of CD concentrations was varied while maintaining the same total concentration of chiral selectors (13 mM). Following variation of the CD ratio, baseline resolution was achieved in a BGE with the following composition: 9.5 mM SBE-β-CD and 3.5 mM β-CD, 15 mM sodium tetraborate pH 9.2, 10 vol% DMSO (Figure A.5).

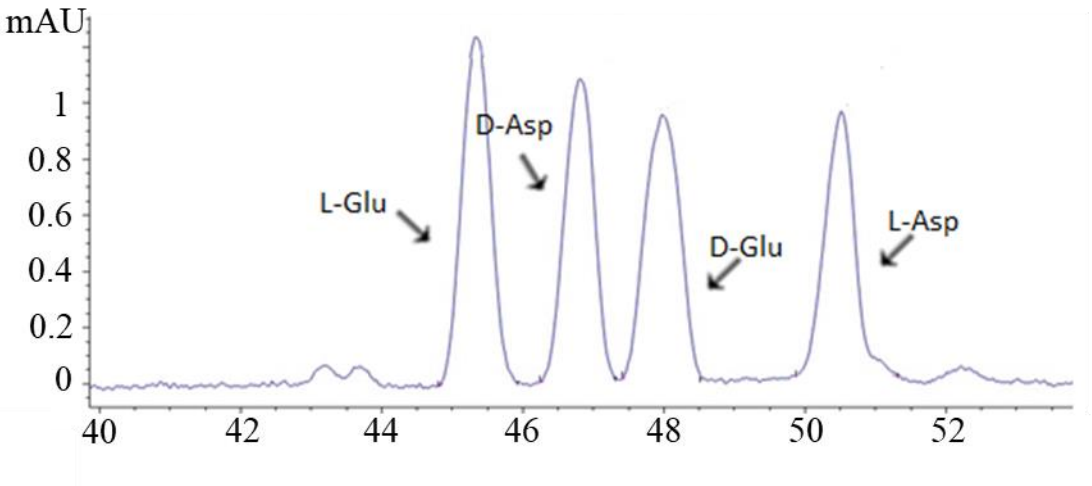

Figure A.5. Baseline resolution of the L- and D- isomers of Glu and Asp using a BGE containing two chiral selectors. BGE: 9.5 mM SBE-β-CD and 3.5 mM β-CD, 15 mM sodium tetraborate pH 9.2, 10 vol% DMSO.

A calibration curve was constructed for the analytes using the optimized BGE (Figure A.6). The lowest concentration that could be detected using CE-UV at 254 nm was 2.5 μM for all analytes. This sensitivity should be sufficient for the detection of basal levels of L-Glu and L-Asp, but not for the D-isomers that are expected to have concentrations in the nanomolar range. A microdialysis sample obtained from rat striatum was derivatized and analyzed using the method, with the unsurprising result of only the L-isomers of the amino acids being detected. To improve sensitivity

and enable detection of the D- chiral isomers, LIF detection must be used instead of UV following analyte separation.

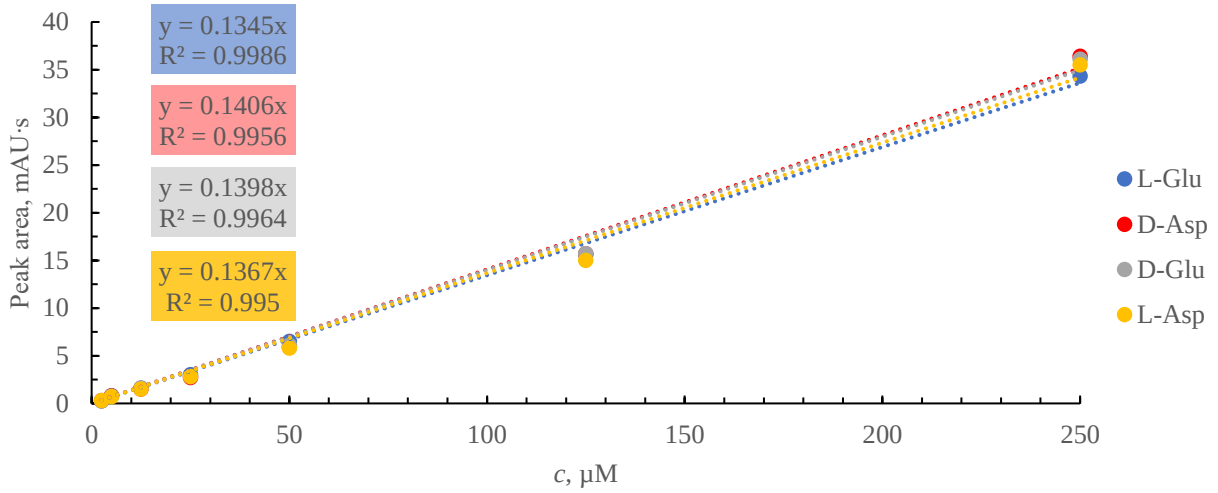

Figure A.6. Calibration curves obtained for the analytes of interest using the optimized BGE.

To conclude, a chiral separation of the chiral isomers of glutamate and aspartate following their derivatization with NDA and CN was developed using a BGE containing two chiral selectors simultaneously – β-CD and SBE-β-CD. Next, the method should be transferred to a ME-LIF platform and evaluated for on-line *in vivo* monitoring of amino acid neurotransmitters and their chiral isomers in the brain using microdialysis sampling.

References

(1) Patel, A. V.; Kawai, T.; Wang, L.; Rubakhin, S. S.; Sweedler, J. V. Chiral Measurement of Aspartate and Glutamate in Single Neurons by Large-Volume Sample Stacking Capillary Electrophoresis. *Anal. Chem.* **2017**, *89* (22), 12375–12382.

(2) Oborny, N. J.; Costa, E. E. M.; Suntornsuk, L.; Abreu, F. C.; Lunte, S. M. Evaluation of a Portable Microchip Electrophoresis Fluorescence Detection System for the Analysis of Amino Acid Neurotransmitters in Brain Dialysis Samples. *Anal. Sci.* **2016**, *32* (1), 35–40.

(3) Řezanka, P.; Navrátilová, K.; Řezanka, M.; Král, V.; Sýkora, D. Application of Cyclodextrins in Chiral Capillary Electrophoresis. *Electrophoresis* **2014**, *35* (19), 2701–2721.